Off-Idle Continuous Descent Operations at Schiphol Airport

Bart Bouwels

Technische Universiteit Delft

TU Delft Delft University of Technology

knowledge & development centre Mainport Schiphol

Challenge the future

This page is intentionally left blank.

Off-Idle Continuous Descent Operations at Schiphol Airport

by

Bart Bouwels

in partial fulfilment of the requirements for the degree of

Master of Science

in Aerospace Engineering at Delft University of Technology

Student Number:	4434560	
Project Duration:	January 4th 2020 - May 3rd 2021	
Thesis Committee:	Prof. Dr. Ir. J.M. (Jacco) Hoekstra	Delft University of Technology, Chair
	Dr. Ir. J. (Joost) Ellerbroek	Delft University of Technology, Supervisor
	F. (Ferdinand) Dijkstra	KDC Mainport Schiphol, Daily Supervisor
	Ir. P.C. (Paul) Roling	Delft University of Technology, Examiner

Version: 1.0
Publication date : April 15, 2021

TU Delft

Preface

The completion of this thesis marks one of my final steps towards obtaining the degree of Master of Science in Aerospace Engineering at Delft University of Technology. When I started this final step, many moons ago, I was given the opportunity to complete it at the Knowledge Development Centre for mainport Schiphol. I would like to start this preface by thanking my daily supervisor from the KDC, Ferdinand Dijkstra, for all of the times he has gone above and beyond what would be expected of a normal daily supervisor. His willingness to share his expertise and spend some extra time to make sure the end result is as good as it can be has been instrumental in the completion of this thesis. I would also like to thank my fellow graduate students at the KDC for their constant support. The importance of their role in my graduation cannot be overstated.

Secondly I would like to express my gratitude to my academic supervisors at TU Delft, Joost Ellerbroek and Jacco Hoekstra, for the many discussions with great ideas and advice, as well as their continued effort in the development of the Open Air Traffic Simulator, BlueSky.

I would also like to thank my parents for both their financial and emotional support throughout my studies. Knowing that no matter what happens, you will always have my back is the greatest present anybody could have every given me. Finally I would like to thank my girlfriend, Claire, for putting up with me these last 5.5 years. I can't believe it's been over half a decade already.

Thank you all,

Bart Bouwels
Oegstgeest, April 2021

Contents

Nomenclature

ACAP	Aircraft Characterstics for Airport Planning
ACMS	Aircraft Condition Monitoring System
AMS	Amsterdam Airport Schiphol
ANP	Aircraft Noise and Performance
ASAS	Airborne Separation Assurance System
ATCo	Air Traffic Controller
ATL	Hartsfield–Jackson Atlanta International Airport
BADA	Base of Aircraft DAta
CAGR	Compound Annual Growth Rate
CAS	Calibrated AirSpeed
Cb	Cumulonimbus
CDA	Continuous Descent Approach
CDO	Continuous Descent Operations
CPA	Closest Point of Approach
DFW	Dallas/Fort Worth International Airport
EAT	Expected Approach Time
ECAC	European Civil Aviation Conference
FMS	Flight Management System
FRA	Flughafen Frankfurt am Main
IAF	Initial Approach Fix
IAS	Indicated Air Speed
ICAO	International Civil Aviation Organisation
ISA	International Standard Atmosphere
JFK	John F Kennedy International Airport
LAX	Los Angeles International Airport
LHR	Heathrow Airport
LoS	Loss of Separation
LTO	Landing Take-Off
LW	Landing Weight
METAR	Meteorological Aerodrome Report
MFW	Maximum Fuel Weight
MLW	Maximum Landing Weight
MTOW	Maximum Take-Off Weight
MVP	Modified Voltage Potential
NOMOS	Noise Measurement System
NoP	Number of Peaks
NRM	Nederlands RekenModel
OEW	Operative Empty Weight
PN	Peak Noise
RMS	Root Mean Square
RNAV	Area Navigation
RTA	Required Time of Arrival
TAS	True AirSpeed
TCu	Towering Cumulus
TMA	Terminal Manoeuvring Area
USA	United States of America

1 Introduction

The Compound Annual Growth Rate (CAGR) of the aviation industry is predicted to be 4.1% from 2015 to 2045 [23]. In recent years, however, increasing public pressure has been put on the industry to further reduce noise and carbon emissions. This can be done by eliminating all horizontal flight segments during the approach phase, reducing the average thrust. Such an approach is called a Continuous Descent Approach (CDA) and has been the subject of many studies. Ideal CDAs are flown with idle thrust, which results in the largest fuel flow reduction but which has a very big drawback; The vertical profiles of ideal CDAs vary greatly between aircraft making it difficult for ground-based systems to predict the exact position of an aircraft ahead of time ([35]). In order to deal with this added uncertainty, additional separation is needed. This greatly reduces the capacity, which means that such a concept can only be used when there is little traffic. ([26]) This greatly limits the benefits since there is very gain during such times. There are other types of CDAs, which take away the need for this added uncertainty, however. These are called a fixed or constant Flight Path Angle (FPA) approaches. Where the FPA during ideal CDAs is optimised by each aircraft's Flight Management System (FMS) for that particular flight, an average is used for this type. This average is then flown with a small, off-idle, amount of thrust. Which means that although in general the noise and emission reductions are decreased when compared to ideal CDAs, ([35], [8]) the capacity is increased ([25]).

In this thesis, fixed-route fixed FPA approach procedures will be designed for the Schiphol TMA and compared to current designs. This will be done by trading off the environmental benefits for capacity under robustness and flexibility constraints. Although only part of the descent occurs inside of the TMA, most of the emission and noise reductions can be achieved here as the inefficient level segments that usually occur here are moved to the upper airspace ([32]).

First, background information is discussed in Chapter 2. This is followed by a literature study in Chapter 3. After this, the research objective and questions are explained. Chapter 5 explains the experiment setup, after which the results will be discussed in Chapter 6. This is followed by a discussion of the results in Chapter 7. Finally, the conclusion and recommendations for future research are described in Chapter 8.

2
Background

In this section the intricacies of Amsterdam Airport Schiphol (AMS) with regards to this research will be explained. First the airport layout and finally the approach procedures are discussed.

2.1. Airport Layout

Most modern large airports have the same runway distribution, which consists of pairs of parallel runways. This is used most in the United States of America (USA), where airports like Hartsfield–Jackson Atlanta International Airport (ATL) and Los Angeles International Airport (LAX) use five and four parallel runways respectively. This is not exclusive to the USA, however. The same concept is used in large European airports like Heathrow Airport (LHR) and Flughafen Frankfurt am Main (FRA), which have two parallel runways each. Amsterdam Airport Schiphol (AMS), on the other hand, has a more dated runway layout. Schiphol has six runways, three of which are parallel. The remaining three cover most other directions. This creates a unique situation where aircraft can almost always land with relatively little crosswind. This is also seen in the Table 5.7, where four of the five most used runways are in different directions. This can also be seen by comparing Figures 2.1 and 2.2, showing Schiphol and LAX, respectively where runways are marked in red. It should be noted that the location of runway 18R was moved downwards in Figure 2.1 to fit inside of the figure.

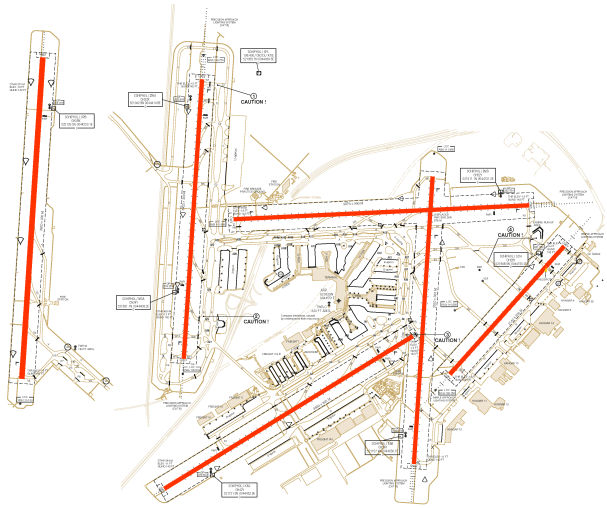

Figure 2.1: Map of Amsterdam Airport Schiphol (AMS) with runways marked in red [27]

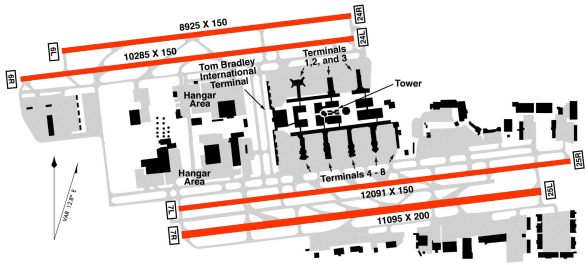

Figure 2.2: Map of Los Angeles International Airport (LAX) with runways marked in red [18]

2.2. Approach Procedures

Schiphol is also different in how it handles its traffic. Where some airports, like Schiphol, use fixed approach routes in some low traffic density situation, this is not the case during peak hours. Area Navigation (RNAV) routes are only used during night-time operations, while during the day, each aircraft is vectored individually by the Air Traffic Controllers (ATCo). The result is that the documented procedures are only used during the night.

The vertical profile of approach procedures is the same at most airports, however. Historically, all aircraft are given an altitude at which to fly until a new command is issued. This can be dictated by the procedure or, as is often the case at Schiphol, by an ATCo. This is called a stepped approach and results in long path segments with relatively high thrust settings at low altitude. This is not the case for Continuous Descent Approaches (CDA), where as much of the descent as possible is done at one time, at the end of the track. The difference in altitude profile and thrust is shown in Figure 2.3. Such CDA procedures have already been implemented at LHR and LAX. It should be noted

that for this research, the stepped or continuous descent approach denomination only specifies the vertical profile, not the horizontal route. Both the continuous descent and stepped approaches in this research use fixed routes, not vectoring.

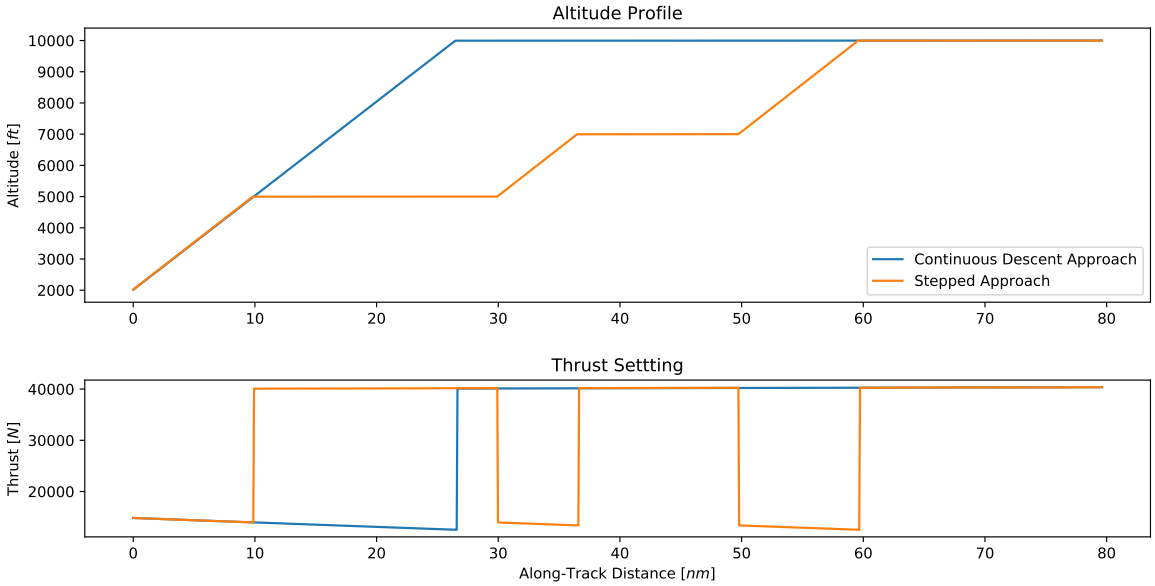

Figure 2.3: Comparison between Continuous Descent and Stepped Approach

3
Motivation

This section starts with different types of constant FPA approaches being discussed, after which the most likely candidate is chosen. Finally, constant geometric FPA approaches are further detailed, showing which questions are currently unanswered.

3.1. Constant FPA Approach Procedure Types

The most basic type of constant FPA approach is a constant geometric FPA throughout the entire approach phase, resulting in what is essentially an extension to the ILS glideslope where all aircraft follow a particular route both horizontally and vertically. There are, however, more types, each of which is shown in Figure 3.1.

One such approach has aircraft follow a certain aerodynamic FPA. While a constant geometric FPA approach is set with respect to the ground, an aerodynamic FPA approach is constant with regards to the air column above the airport. This results in a range of FPAs with regard to the ground, depending on the wind conditions, an example of which can also be seen in Figure 3.1. The result of this is that the approach is aerodynamically optimal for the aircraft and results in a relatively predictable ground speed, eliminating much of added separation needed for idle CDAs. This approach has a large drawback, however: The value of the FPA differs with aircraft type, landing weight, and for different wind and atmospheric conditions, meaning that the exact angle that will be flown varies and needs to be made available to an air traffic controller [26]. This is needed to predict whether or not two or more aircraft will get into a conflict in the future. Due to the fact that the FPA is different for each aircraft, it is almost impossible to ensure separation without a support tool.

Another type of CDA is flown by implementing multiple segments which are flown with a constant geometric FPA. This can be done by assigning a FPA to a velocity window, which is called a Descent-Speed CDA and an example of such a profile is shown in Figure 3.1. One of the main advantages of this type of constant FPA CDA is that it is more fuel efficient than a basic geometric FPA approach and that it can be turned into a procedure much more easily than the aerodynamic flight path angle [38]. It does, however, increase pilot task load as well as traffic complexity since all aircraft decelerate at different rates, causing relatively large variations in the vertical flight path.

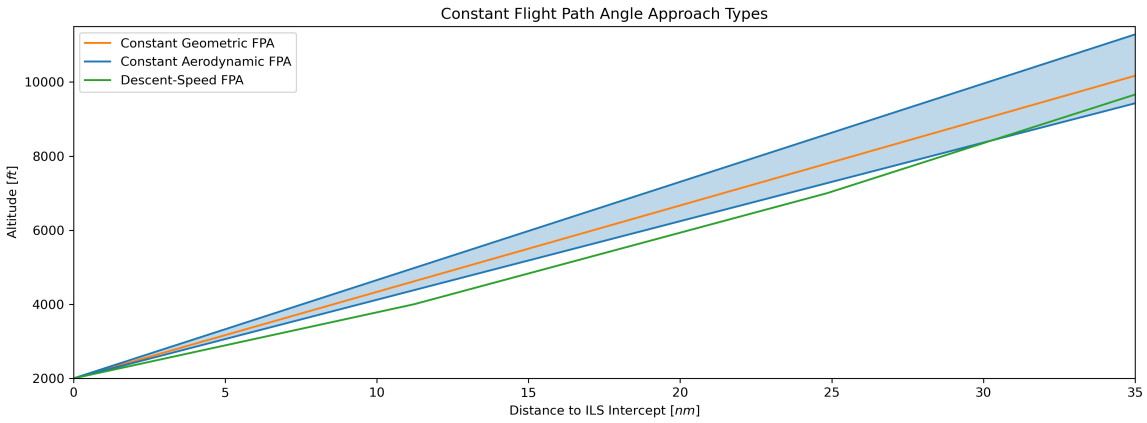

Figure 3.1: Example of a Descent-Speed Continuous Descent Approach

As the scope of this thesis dictates that results can be implemented relatively quickly, the basic geometric FPA approach will be investigated here. This can be easily implemented as a procedure and results in the smallest variation in flight path between aircraft. This makes it ideal for high-density TMAs like that of Schiphol. It should be noted, however, that these types of procedures may result in longer decelerations and higher fuel burn when compared to ideal CDAs. It can also be difficult to find a single feasible FPA that works in all conditions for all aircraft [4].

3.2. Constant Geometric FPA Procedures

Over the years a number of studies have investigated constant geometric FPA approaches, each testing a different aspect of the concept for different types of traffic with different amounts of support tools. The fuel savings outside of the TMA for three different CDA implementations for small jet aircraft like the Bombardier CRJ-700 was investigated by Wu, Green, and Jones [38]. They found that implementing the simplest version of this concept could result in fuel savings within 11, 10, and 6 kg of a fuel-optimal CDA for an average small jet arriving at Dallas/Fort Worth International Airport (DFW), John F Kennedy International Airport (JFK), and Los Angeles International Airport (LAX) respectively. Robinson and Kamgarpour [32] found that implementing ideal CDAs could save up to 80, 125, and 35 kg for each aircraft arriving at these same airports. Comparing the results of Wu, Green, and Jones [38] to those of Robinson and Kamgarpour [32] means that close to 87% of the benefits of ideal CDAs remain when using constant geometric FPA approaches. It should be noted, however, that the 80, 125, and 35 kg of saved fuel is the average for all aircraft types, whereas the losses of 11, 10, and 6 are only for smaller jets. This is in accordance with Turgut et al.'s findings of a maximum fuel saving of 14% [36]. Additionally, Wu, Green and Jones found that up to 70% of the 6 to 11 kg loss caused by the non-ideal vertical routes can be won back by separately calculating the angle of descent for each route and updating this daily with the updated weather information [38].

While Wu, Green and Jones found an ideal universal FPA that varies between 2 and 2.5 °[38], Turgut et al. found 2.5 °to be ideal for A320 and B737 series aircraft operated by Turkish Airlines when taking into account the added time spent in cruise, saving 14%, almost 200 kg, of fuel over the full descent [36]. This is close to the 2.7 °optimum found by Wu and Green [37] to result in better fuel efficiency than idle descents for a Boeing 747. Although it should be noted that the altitude from which the CDAs are initiated has a large influence on the fuel savings, [32] found that the elimination of level segments during the terminal airspace, which is located below FL110, accounts for 62% of the fuel that can be saved during a full descent.

The advantages of such constant geometric FPA approaches were significant enough for Los Angeles International Airport (KLAX) to implement a procedure very similar to it for some of their Instrument Landing System/Localizer (ILS/LOC) approaches. Their simulations found an average fuel burn saving of 70, 30, and 118 kg for their Boeing 737, 757, and 767 aircraft respectively, as well as a decrease in descent time of up to 1 minute and a reduction of the area of the 50 dBA L_{DEN} contour of up to 28% [8]. Additionally, de Muynck et al. found a possible noise decrease of between 3 and 8 dBA for 2°constant FPA approaches [10]. They have simulated the capacity of such a concept at 30 with peaks of up to 33 aircraft per hour per runway. However to accomplish this, a number of support systems were used in each study, including a constant air-to-ground data-link communication and Required Time of Arrival (RTA) capabilities for all aircraft. Since not all aircraft and airports are equipped with these systems, it would take a lot of time and money to upgrade everything to the point where such support systems can be used universally. In order to keep with the scope of this thesis, where the result should be able to be implemented relatively quickly, none of these systems will be oned here.

Although these procedures have already been implemented for some approaches at LAX, these are not generally used when traffic density is high and very little research has been done into their robustness [17]. de Muynck et al., for instance, found that a metering accuracy of ± 30 seconds is needed for such an operation, but this claim is not explained in their paper [10]. de Gelder et al., on the other hand, found that 45 seconds of metering accuracy still results in feasible solutions [9]. These variations could be caused by the fact that different systems are available for each simulation study. The needed metering accuracy has yet to be determined for an airspace without any new airborne systems, like air-to-ground data-link communication. Additionally, the influence of the FPA on operational aspects that aren't the fuel usage and noise production have not yet been thoroughly investigated. This will thus be the focus of this research.

4
Research Objective and Questions

In this chapter, both the research questions and the research objectives will be discussed as well as a number of sub-goals. First, the main research question is stated and further decomposed into smaller, more detailed questions. Then, this is combined with the research objective to form a number of sub-goals.

4.1. Research Questions

The main research question of this thesis is:

> "What is the impact of implementing constant FPA CDA routes without adding new airborne systems at Schiphol airport with regard to the capacity, operation robustness and flexibility, noise production, fuel consumption, and controller task load when compared to a conventional descent profile?"

In order for this comparison to be made both the optimal CDA and the conventional procedures have to be graded on each of the Key Performance Areas (KPAs) mentioned in the main research question. The resulting questions can be found below.

(1) What are the capacity, operation robustness and flexibility, noise production, fuel consumption, and controller task load for conventional, stepped approach procedures?

(2) What are the optimal capacity, operation robustness and flexibility, noise production, fuel consumption, and controller task load for constant FPA CDA procedures?

For conventional procedures most of these questions can be answered based on current data. For CDA procedures, however, a few parameters have to first be optimised, as explained with question 2.1. The required metering accuracy on the Initial Approach Fix is not known for either approach type and will thus be calculated for both.

(2.1) What is the FPA that results in the best trade-off between capacity, operational robustness and flexibility, noise production, and fuel consumption?

(2.2) What is the required metering accuracy on the Initial Approach Fix (IAF) for each type of procedure?

The KPAs that are used in most of these questions can be split into Key Performance Indicators (KPIs). The resulting division is shown below. It should be noted that the level of air traffic controller task load is measured in two ways, as stated below. First, it is determined as the probability that a controller has to issue a command to ensure separation between an aircraft pair. Later, it is defined as the number of actions taken during a simulation. This will be further explained in Chapter 5.

Capacity:

- **Peak capacity**, this is the 99th percentile of the number of aircraft that can be landed on one runway in one hour. The capacity is calculated for each 30 aircraft sequence and converted to aircraft per hour.
- **Average capacity**, this is the 50th percentile of the number of aircraft that can be landed on one runway in one hour. The capacity is calculated for each 30 aircraft sequence and converted to aircraft per hour.
- **Reported capacity**, this is the 10th percentile of the number of aircraft that can be landed on one runway in one hour. The capacity is calculated for each 30 aircraft sequence and converted to aircraft per hour.

Robustness and Flexibility:

- **Percentage of aircraft that can abide by all speed restrictions**. This research uses a maximum speed of 250 kts below FL100. Additionally, upon reaching FL70 all aircraft start to decelerate to 220 kts and at FL40 to 175 kts. The speed restrictions are then set such that at FL40 all aircraft must have decelerated to 220 kts to start the next deceleration and at 2000 ft, the aircraft must have decelerated to at least 180 kts, a normal ILS interception speed.
- **Speed Authority**, this is the amount to which an air traffic controller can still influence the arrival time of an aircraft while staying within the normal operating envelope. It is calculated as the time difference between the fastest and slowest tracks that abide by all speed restrictions.
- **Needed metering accuracy at the IAF**, this is the accuracy with which the incoming aircraft need to arrive at their Initial Approach Fix. It is used in the Inbound Peak Simulation, where different values are used to simulate its effect on stepped and continuous descent approaches.

Noise Production:

- **Surface area of the L_{24h} contours**, this is the closest relative to the L_{DEN} contour that is available for this study. Since the decrease in arriving aircraft at night is not simulated, it does not make sense to penalise evening and night arrivals. The L_{24h} is the same as the L_{DEN} without these penalties, making it ideal. For this research, the 60 and 70 dBA contours will be used.
- **Surface area of the peak noise level contours**, this is the area within which a certain peak noise level occurs. For this research, threshold values of 80 and 100 dBA are used.
- **Surface area of the contour number of peaks contours**, this is the area within which a certain number of peaks with a noise level of over 70 dBA occur per hour. It is linked to both the capacity and the peak noise level and gives an insight into how often a conversation is disrupted every hour. The thresholds that are used for this research are 10 and 30 aircraft per hour.

Emissions:

- **Average fuel usage**, this is the mean of the fuel each aircraft uses to fly from the IAF to the runway threshold.

Task Load:

- **Air traffic controller taskload**, this is first calculated as the probability that a controller has to issue a command to ensure separation between two aircraft. During the final, inbound peak simulation, it is defined as the number of commands that an air traffic controller has to give per aircraft and calculated by how often a conflict happens.
- **Number of aircraft that require path stretching**, this is a measure of how often serious action has to be taken by air traffic controllers. It will be calculated using the percentage of the time that using only speed to solve conflicts fails and results in a loss of separation.

4.2. Research Objective

The main research objective of this thesis is:

> "The objective of the research problem is to develop and test a set of feasible constant flight path angle arrival routes for Schiphol Airport starting at the initial approach fixes and which can be flown without implementing new airborne systems by finding a flight path angle that provides an optimal trade-off between capacity, and robustness and flexibility while reducing noise and emissions and comparing the results to conventional approaches."

In order to achieve the research objective, a fast-time monte carlo simulation will be used to determine the necessary separation of different aircraft categories for different flight path angles and controller task loads. These will then be used to calculate the capacity, robustness and flexibility, noise production, and the fuel consumption as a function of flight path angle.

Finally, the procedure with the optimal flight path angle will be compared to the current routes in terms of capacity, robustness and flexibility, noise, emissions, and task load based on a number of fast-time simulations of an inbound peak.

5
Experiment Setup

This chapter starts with an explanation of the two simulations that will be done for this research, in Section 5.1. This is followed by a discussion of the main input variables; the landing weight, routes, and wind conditions, in Section 5.2. The penultimate section is the tool validation, where all modifications to the simulation databases and software are explained and validated in Section 5.3. Finally all of the calculations are explained in Section 5.4.

5.1. Simulations

In order to answer the research question, two fast-time simulation are used. First, a flight path, monte-carlo simulation is used to determine the optimal FPA per runway. In order to do this, many of the KPI's in Chapter 4 are used. Then, this FPA and concept are validated through a normal fast-time simulation. Here, a full inbound peak is simulated to ensure that the concept is also feasible in practice. This simulation uses an air traffic controller module, which issues speed and heading commands to ensure that proper separation is maintained for all aircraft. The main difference between the two simulations is the fact that during the flight path simulation, all aircraft are simulated at the same time, on top of one another, without any sequencing, whereas during the inbound peak simulation, the sequencing is done prior to simulating. Each of these is explained in further detail in Sections 5.1.1 and 5.1.2.

5.1.1. Flight Path Simulation

The goal of this simulation is to find the optimal FPA per runway. This is done using a fast-time, monte-carlo simulation of the most relevant aircraft types. The monte-carlo part is needed to take the weight variation of aircraft into account. Winds will not be added as a probabilistic effect. Real-life wind scenarios will be used instead. This choice was made to ensure that local, temporary wind phenomena are also taken into account in the simulation. How this is done will be explained in Section 5.2.4. Furthermore, the weight distributions and route designs are shown in Sections 5.2.1 and 5.2.2 respectively. A block diagram of this simulation can be seen in Figure 5.1. The calculation of the inputs is explained Section 5.2, while that of the outputs is explained in Section 5.4.

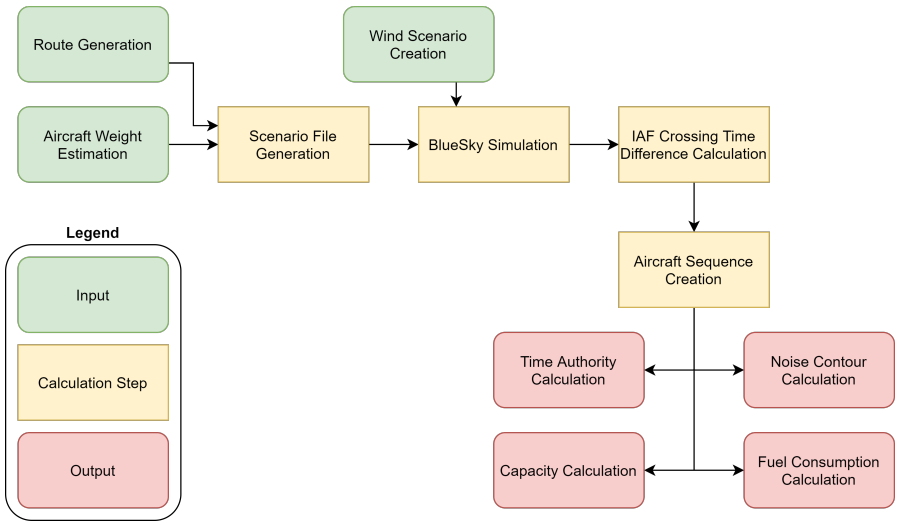

Figure 5.1: Diagram of the Flight Path Simulation

As stated above, sequencing is not added before this simulation. This is because, in accordance with the work of Ren and Clarke [30], this allows for much flexibility in both sequencing and fleet mix. For each aircraft type, the time needed to follow the track is a stochastic variable that, in this study, depends on the aircraft mass and type, the route, as well as the vertical and speed profiles. The distribution of this variable, along with a distance - time plot can then be constructed for each aircraft type. These can be put together as shown in Figure 5.2 [29]. By changing the spacing

at the metering point, all other spacings are also changed. This makes it possible to determine the probability that two aircraft will create a conflict, as a function of the runway capacity.

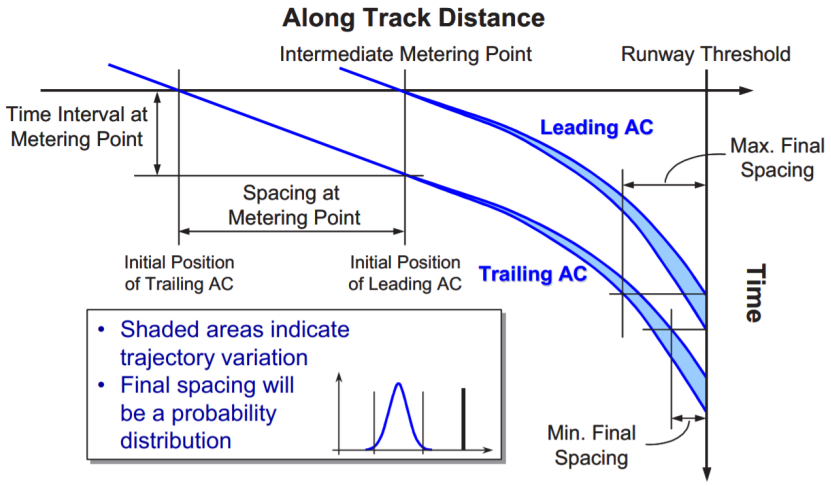

Figure 5.2: Separation Analysis through Distance vs Time Plot [29]

As such, capacity and an indication of controller taskload can be calculated for each FPA. The same is true for the percentage of flights that can perform the descent, giving an indication of robustness. Finally, BlueSky calculates many variables, such as the thrust setting and fuel flow at every position along the path. This also makes it possible to calculate the noise contours and the fuel usage as a function of FPA, finishing off the KPIs listed in Chapter 4. This allows for the optimisation of the FPA per runway based on these criteria which is the goal of the simulation.

5.1.2. Inbound Peak Simulation

While the flight path simulation is relatively abstract and versatile, the inbound peak simulation is much more realistic. It provides some validation that the results of the flight path simulation are feasible. This is needed because during the flight path simulation, it is assumed that all potential conflicts can be solved and that delay does not propagate further through the sequence. This is not the case in this simulation. A real incoming traffic sequence will be simulated in the most challenging wind condition. Then, each of the KPIs in Chapter 4 are calculated for both constant FPA CDAs and conventional, stepped approaches. The fairest comparison can be made between fixed-route, continuous descent and fixed-route, stepped approach procedures, which is why this is done in this study. Though this is not the current situation at Schiphol and thus the results cannot be directly linked to the current situation, which mostly uses vectoring. A diagram showing the general lay-out of this simulation can be seen in Figure 5.3.

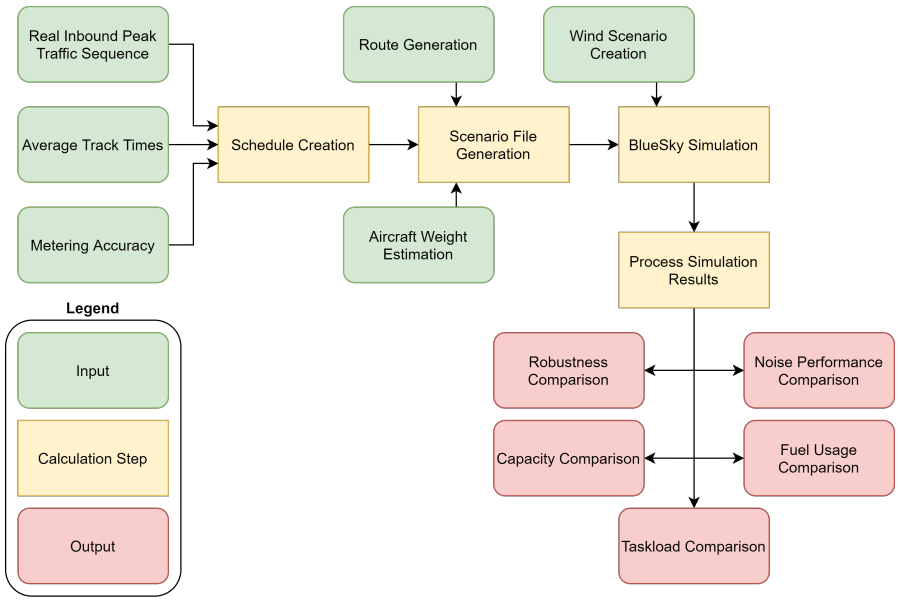

Figure 5.3: Diagram of the Inbound Peak Simulation

The weight distribution and routes will be the same as those used for the Section 5.1.1. At the end of the final flight path simulation, the most critical runway/wind combination will be determined. This is the peak that will be used for this simulation, determining the wind scenario. An actual arrival sequence is then used instead of a randomly generated one to include the effect of upper area controllers modifying the sequence to maximise landing capacity. While this is traditionally done inside of the TMA, using vectoring, this can relatively easily be moved to the upper airspace, resulting in more efficient operations since both the noise and fuel burn impact of overtaking other aircraft is lower when high up.

During this simulation, separation between aircraft has to be assured. To do this, an ATCo is simulated using a variation of the Airborne Separation Assurance System (ASAS) model that is included in BlueSky. This uses state-based conflict detection to determine whether or not two aircraft will be in conflict in the near future. For this detection, the target separation was set to be dependent on the aircraft's speed, essentially changing the conventional distance based separation to time based separation. This was done to mimic the effect of the air traffic controller anticipating that two aircraft will naturally get closer together when they decelerate along the route. The conflicts are then resolved using a Modified Voltage Potential (MVP) algorithm. In order to get an indication of how often the fixed routes can be adhered to and how often additional path stretching is needed, the solutions have been constrained to only use speed control. This means that if a loss of separation occurs, the aircraft pair required path stretching, while the number of conflicts show how often the air traffic controller has to issue commands to the aircraft.

In order to ensure that no aircraft are forced out of their speed envelope by the ASAS, their fastest regular approach is used. This is similar to the fastest track used for the general speed authority in Figure 5.42. To simulate the behaviour of an ATCo instead of a cooperative airborne conflict resolution method, only the trailing aircraft is charged with slowing down to resolve the conflict. Since the base route that all aircraft follow is the fastest they can follow, slowing down still results in the fastest time a particular sequence can be landed.

While the sequence was taken from real operations, the interval between aircraft was not. This was done to ensure that the highest possible capacity can be reached by each route type. Instead of the actual inter-arrival times, for the CDA routes, the time differences found in the flight path simulation are used. This is with the caveat that for the flight path simulation the time differences that correspond to the most challenging wind scenarios are used, while the inbound peak simulation uses the time differences that correspond to the wind scenario that is actually used. Since the time it takes for an aircraft to perform the full track depends heavily on vertical and speed profile, the inter-aircraft arrival time differences that were valid for CDAs cannot be used for the stepped approaches. To account for this, the planned IAF crossing time difference is scaled based on the track time difference between continuous descent and stepped approaches. For example if during stepped approaches the leading aircraft is 10 seconds faster, while the trailing aircraft is 10 seconds slower than it was during CDAs, the inter-aircraft arrival time can be reduced by 20 seconds.

In order to take the fact that aircraft don't arrive exactly on schedule into account, the EAT (Expected Approach Time) adherence is modelled as a normally distributed error on top of the schedule. For this research, the EAT adherence will be specified as the value that is three standard deviations away from the mean and the mean is assumed to be 0. Once this EAT error has been added to the schedule, it's possible for two aircraft that cross the same IAF in sequence to be created within minimum separation of each other. To solve this, the time it takes each aircraft type to fly the first 5 nm of its track was calculated through simulation. Each pair of aircraft that arrive at the same IAF is then checked to ensure that this $5nm$ separation minimum is adhered to. $5nm$ was chosen here because this is the minimum separation that area control works with and thus also the minimum separation at which they can allow aircraft to enter the TMA.

5.2. Input Variables

The most important input variables are discussed in this section. First, the landing weight distribution will be discussed in Section 5.2.1. This is followed by Section 5.2.2, where the route definitions are discussed. Finally, in Section 5.2.4, the wind is discussed.

5.2.1. Landing Weight Distribution

In order to accurately simulate the performance of the aircraft, their weight has to be known. Therefore, the following five different methods for estimating the aircraft landing weight were compared: BADA landing speed, ANP landing speed, ECAC weight, CDA speed, and literature based estimation. Each of these will be explained separately below. This is followed by the final comparison, which results in the chosen method. It's assumed that the landing weight is

normally distributed, as is the case in literature [30, 36]. As this allows for significantly literature data to be used. The estimation thus needs to calculate both a mean and a standard deviation.

Turgut et al. [36] published the landing weight distribution of over 5000 Turkish Airways A320 and Boeing 737 family flights. Ren and Clarke [30] used both UPS and Delta Boeing B757-200 and B767-300 aircraft for their research, also publishing their landing weight distributions. These will be assumed to be the true distributions and the result of each method will be compared to these.

BADA LANDING SPEED

The velocity with which an aircraft lands is governed by Equation (5.1). Here, the headwind correction is only used when there's a headwind of over 10 knots.

$$V_{Land} = 1.3 \cdot V_{Stall} + 5 + \frac{V_{HeadWind}}{2} + V_{Gust} \tag{5.1}$$

Each aircraft's landing speed is logged using radar data. In order to reduce any landing speed variations due to the flare, the landing speed is calculated at 70 ft, approximately the altitude at which aircraft cross the runway threshold. Additionally, surface wind data is logged for each active runway. This is correlated with each landing speed based on the flight number and time.

Finally, Eurocontrol's Base of Aircraft Data (BADA) database contains a reference stall speed for each configuration assuming the aircraft is at its reference weight. Based on these, the landing speed can be calculated according to Equation (5.2).

$$m_{Land} = m_{Ref} \cdot \left(\frac{V_{Stall}}{V_{Stall_{Ref}}} \right)^2 \tag{5.2}$$

The resulting mass distribution is shown in Figure 5.4. Although the mean comes reasonably close to that in literature, the standard deviation is much larger.

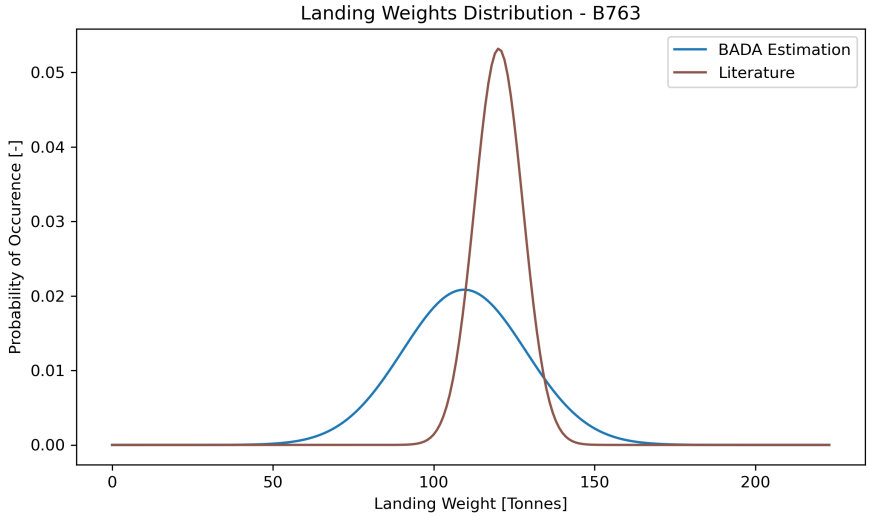

Figure 5.4: Mass Distribution Calculated through BADA

ANP LANDING SPEED

Eurocontrol's Aircraft Noise and Performance (ANP) database contains an operational coefficient D for many aircraft types. This parameter directly relates aircraft landing weight to its landing speed. It's calculated by the manufacturer of each aircraft, but not validated further. The conversion from landing speed to weight is done according to Equation (5.3) [11].

$$m_{Land} = \left(\frac{V_{Land}}{D} \right)^2 \tag{5.3}$$

It should be noted that D is not in the ANP for the Boeing 737-800 series. Since this aircraft type is part of the validation set explained in Literature Based Estimation, the D value is assumed to be the same as that for the Boeing 737-700.

Figure 5.5 shows the resulting landing weight distribution. Again, the mean is relatively close to that in literature, but the standard deviation is much larger.

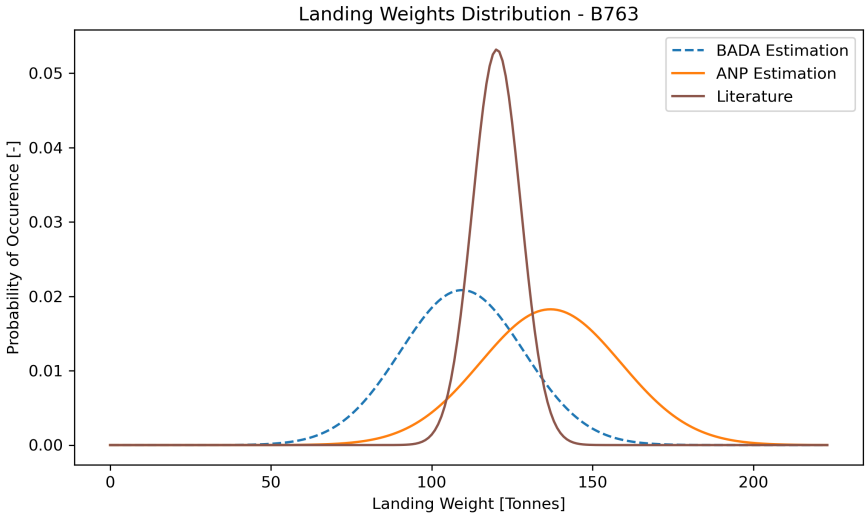

Figure 5.5: Mass Distribution Calculated through ANP

CDA SPEED

Currently, nighttime operations at Schiphol dictate that all aircraft perform Continuous Descent Operations (CDO). At high altitudes, two assumptions have been made: All aircraft are in their clean configuration and all aircraft perform this descent at descent thrust. Additionally, the horizontal and vertical speed, the acceleration, and the altitude are known from radar data and the aircraft performance is known from BADA 3. This leaves only the aircraft mass in Equation (5.4). [13]

$$m = \frac{(T - D) \cdot V}{g\frac{dh}{dt} + V\frac{dV}{dt}} \tag{5.4}$$

The resulting distribution can be seen in Figure 5.6. Both the mean and the standard deviation are extremely far away from what literature suggests. It is expected that this is caused by a mismatch between the assumed and the used thrust.

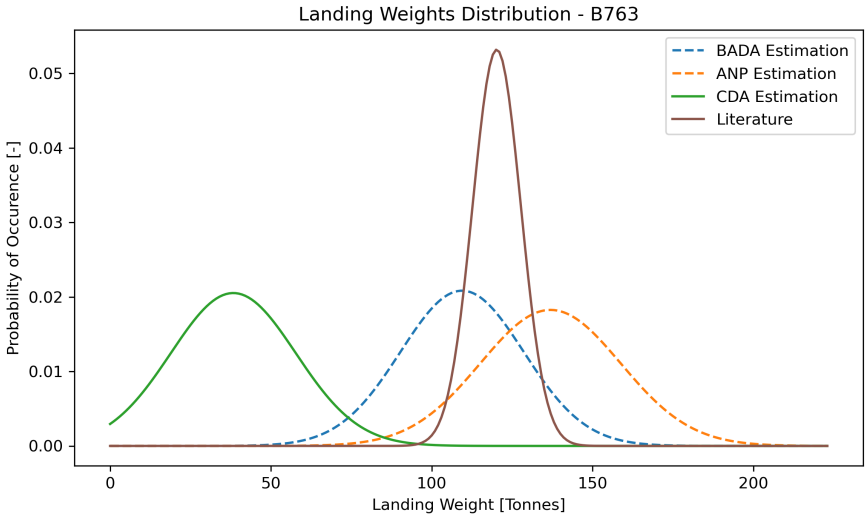

Figure 5.6: Mass Distribution Calculated from CDAs

LITERATURE BASED MASS FRACTIONS

The final estimator is based on literature. Based on these landing weights, the landing fuel and its distribution are calculated using Equations 5.5 and 5.6. This is then calculated as a percentage of the Operating Empty Weight (OEW), Maximum Take-Off Weight (MTOW), Maximum Landing Weight (MLW), and Maximum Fuel Weight (MFW). The average is taken over all aircraft types. The resulting percentages and their uncertainties are shown in Table 5.1 and 5.2. Since the MLW based estimation has the best results, this will be used. It should be noted that the literature for the Airbus A321 and the Boeing 767-300 were not used to calculate the mass fractions. This was done to allow these two aircraft to function as a small validation dataset.

$$\mu_{LW} = OEW + \eta_2 \cdot MLW \tag{5.5}$$

$$\sigma_{LW} = \eta_1 \cdot MLW \tag{5.6}$$

Table 5.1: Literature Based Mean Landing Fuel Estimation

Mean Landing Fuel Percentage of	**Percentage**	**Mean Error** [$Tonnes$]	**Maximum Error** [$Tonnes$]
OEW	39.1%	-0.06	4.08
MTOW	20.1%	-0.04	1.13
MLW	24.4%	0.02	1.1
MFW	72.1%	0.26	3.13

Table 5.2: Literature Based STD Landing Fuel Estimation

STD Landing Fuel Percentage of	**Percentage**	**Mean Error** [$Tonnes$]	**Maximum Error** [$Tonnes$]
OEW	6.8%	-0.09	1.47
MTOW	3.5%	-0.10	0.96
MLW	4.2%	-0.10	0.97
MFW	12.5%	-0.04	1.03

As can be seen in Figure 5.7, this is the most accurate estimation method so far. This is especially the case for the standard deviation, where all other estimation methods result in extreme overestimation. This is to be expected as the estimation is directly based on literature. What this shows, however, is that the maximum landing weight is a good estimator for an aircraft's landing fuel weight. Additionally, the fact that the estimator is very good for the Boeing 767-300, which was not used to calculate the mass fraction, shows that it can be used to accurately extrapolate the landing weights of even much heavier aircraft. This can be seen by the OEWs on which the mass fraction was calculated, the heaviest aircraft on which this was done is the Boeing 757-200, with an OEW of 58.4 tonnes. The Boeing 767-300, which is shown in Figure 5.7, has an OEW of 86.1 tonnes, almost 50% more.

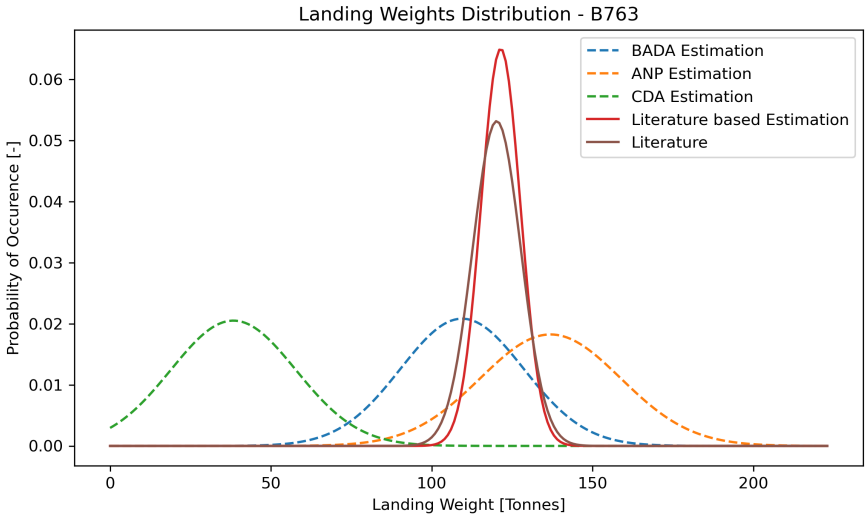

Figure 5.7: Mass Distribution Calculated from Literature

ECAC WEIGHT

Document 29 of the European Civil Aviation Conference (ECAC) [11] states that on average, the weight of a landing aircraft is 90% of its Maximum Landing Weight (MLW). The document does not include a measure for the standard deviation, however, and can thus only be used to estimate the mean. This can also be seen in Figure 5.8, where only the mean is shown. This seems to be a relatively accurate estimation.

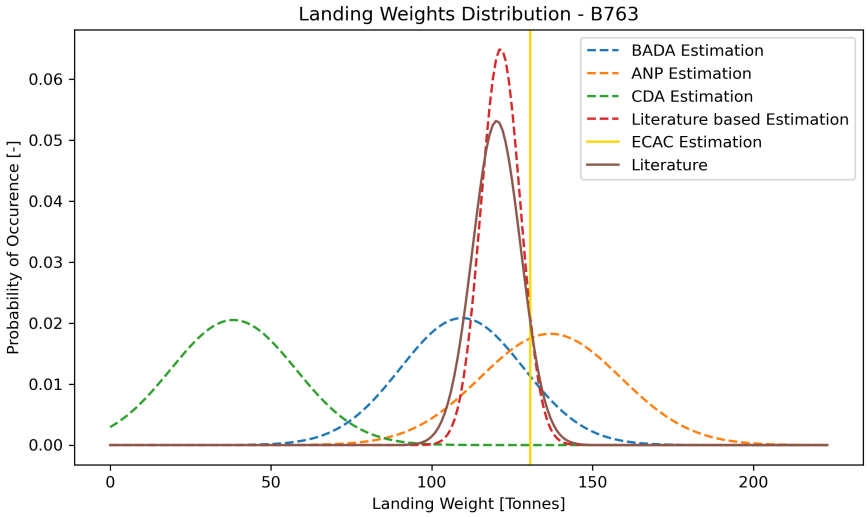

Figure 5.8: Mass Distribution Calculated through ECAC's Mass Fraction

FINAL WEIGHT ESTIMATION

In order to assess which estimation method is the best, the estimation error for each method is shown in Figures 5.9 and 5.10.

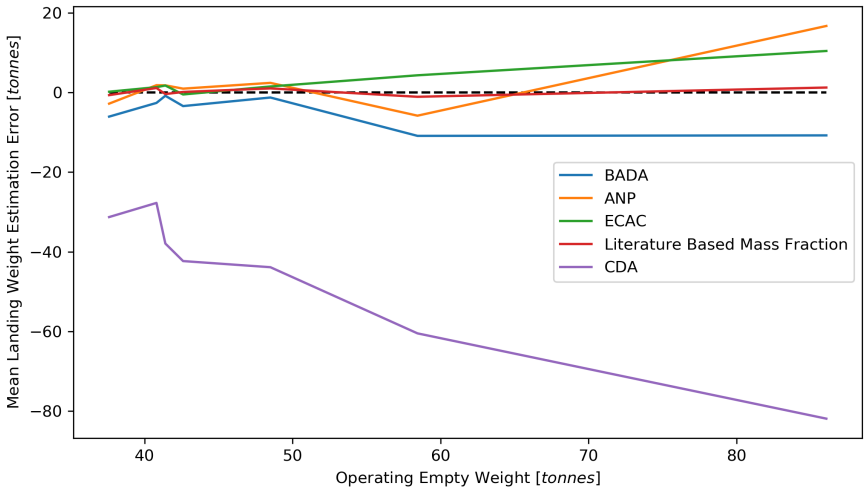

Figure 5.9: Mean Landing Weight Estimation Error as a Function of OEW

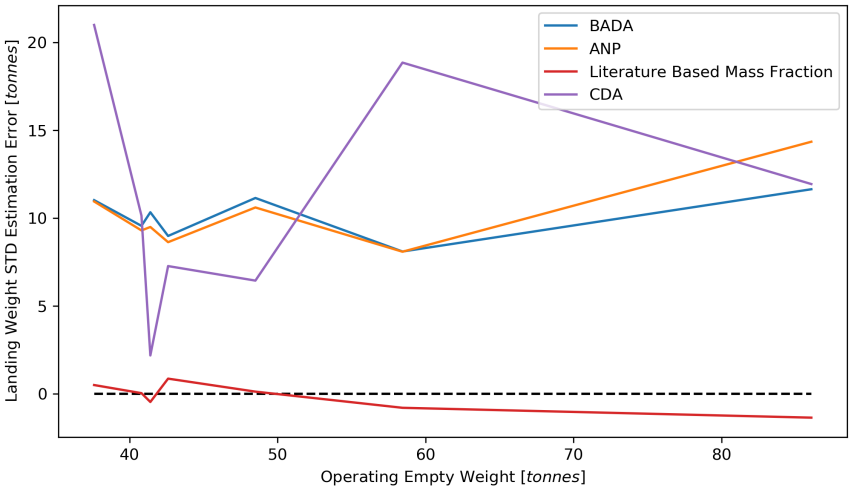

Figure 5.10: Landing Weight STD Estimation Error as a Function of OEW

Since CDA based estimation results in a very large, non-constant bias in all mean landing weight estimates, this method is disregarded. Ignoring this, Figure 5.11 shows the remaining mean landing weight estimates.

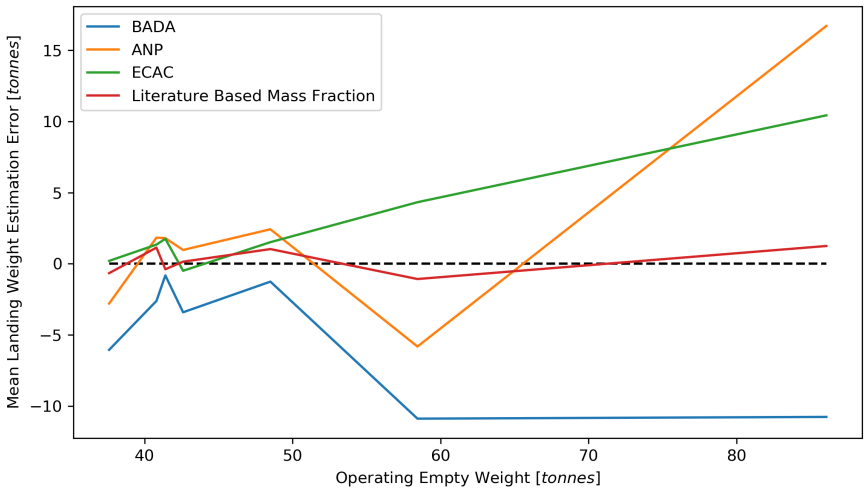

Figure 5.11: Mean Landing Weight Estimation Error as a Function of OEW without CDA

Figure 5.11 shows that for each aircraft type, the literature based mass fraction results in the best estimation. The same is true for the standard deviation in Figure 5.10. This will thus be used for the full weight estimation.

WEIGHT ESTIMATION SUMMARY

To recap; In order to simplify the weight estimation, a normal distribution is assumed. This allows for the mean and the standard deviation to be calculated independently. For the mean landing weight, five different estimation methods were used, while only four were available to estimate the standard deviation. Out of these, the MLW literature based mass fractions result in the best approximation of the landing weight and will thus be used.

VALIDATION

In order to ensure that all aircraft weights are within the bounds of reality, each estimated landing weight is compared to that aircraft type's OEW and MLW. For simulation purposes, the Embraer 175L (E75L) was replaced by an Embraer E170 as the E75L is not included in BADA 3.12. The same is true for the Airbus A320Neo, which is replaced by its predecessor, the A320. The aircraft types and their respective weights are shown in Table 5.3.

Table 5.3: Relevant Weights for the most used Aircraft

Aircraft Type	**OEW** [*Tonnes*]	**MLW** [*Tonnes*]
B738	41.4	65.7
E190	27.1	44.0
A320	42.2	64.5
B737	37.6	58.2
A319	39.9	61.9
E75L	21.9	34.0
A333	122.1	184.4
A321	48.0	75.1
E170	20.2	33.3
B744	176.7	284.7
B77W	167.8	251.3
B772	135.6	203.9
B739	42.9	66.6
B789	128.8	192.8
B763	85.3	136.1
A332	120.4	181.3
B77L	145.2	223.2
DH8D	16.6	27.8
F100	24.5	36.7
B788	120.0	172.4
CRJ9	21.7	33.3
A20N	42.2	66.8
B748	208.6	312.1
B733	32.6	52.1
E195	27.1	45.8

All maximum landing weights are published in each manufacturer's Aircraft Characteristics for Airport Planning (ACAP) [6], [1] or Airport Planning Manual (APM) [12], [7], [19] documentation. The operating empty weight is not as well documented, however, as this varies between different operators and even between aircraft of the same type. Boeing is the exception to this. They publish the design OEW in their ACAPs. [6] The remaining OEWs are estimated in The International Directory of Civil Aircraft [20].

As explained above, the chosen weight estimation method is based on literature. The estimated mean weight and standard deviation are a function of the OEW and the MLW. The resulting estimates, as well as the probability that they are outside of the bounds of reality are shown in Table 5.4

Table 5.4: Estimated Landing Weights and Probability of Infeasible Estimations for the most used Aircraft

Aircraft Type	**Estimated Mean Weight** [*Tonnes*]	**Estimated Weight STD** [*Tonnes*]	**P(LW < OEW)**	**P(LW > MLW)**
B738	57.4	2.8	4e-09	0.001
E190	37.8	1.9	4e-09	0.000
A320	57.9	2.7	4e-09	0.008
B737	51.8	2.5	4e-09	0.005
A319	55.0	2.6	4e-09	0.004
E75L	30.2	1.4	4e-09	0.004
A333	167.0	7.8	4e-09	0.013
A321	66.3	3.2	4e-09	0.003
E170	28.3	1.4	4e-09	0.000
B744	246.1	12.0	4e-09	0.001
B77W	229.1	10.6	4e-09	0.018
B772	185.4	8.6	4e-09	0.016
B739	59.1	2.8	4e-09	0.004
B789	175.8	8.1	4e-09	0.019
B763	118.5	5.7	4e-09	0.001
A332	164.6	7.7	4e-09	0.014
B77L	199.5	9.4	4e-09	0.006
DH8D	23.4	1.2	4e-09	0.000
F100	33.4	1.6	4e-09	0.016
B788	162.0	7.3	4e-09	0.077
CRJ9	29.8	1.4	4e-09	0.006
A20N	58.5	2.8	4e-09	0.002
B748	284.7	13.2	4e-09	0.019
B733	45.3	2.2	4e-09	0.001
E195	38.3	1.9	4e-09	0.000

In Table 5.4, the final two columns give the probability that the Landing Weight (LW) is outside of the bounds set by the aircraft design. The penultimate column (P(LW < OEW)) shows the probability that the estimated landing weight is smaller than the operating empty weight. This value is the same for every aircraft type as the ratio between the weight difference between the LW and the OEW, and the standard deviation is the same for each aircraft type due to the estimation method. The final columns (P(LW > MLW)) shows the probability that the estimated landing weight is larger than the maximum landing weight. This is different for each aircraft type. This is on average 0.95% with a maximum of 7.7% for the Boeing 787-800. This seems to be an outlier, since the the Boeing 787-900, which is essentially the same aircraft only has a 1.9% chance. Additionally, the Airbus A330-200, which has an extremely similar OEW, also only has a 1.4% chance of exceeding the maximum landing weight. This is further supported by comparing the OEW and MLW of each aircraft to each other, the result of which is shown in Figure 5.12, where the outlier at around 69.5% represents the Boeing 787-800. As the estimated weight distribution depends on the combination of the OEW and MLW, this figure shows that an aircraft can only be between 69.5% and 100% of MLW. This is relatively narrow when compared to the other aircraft, which, on average, allow for landing weights between 64% and 100% of MLW. As a result of this, the probability that the estimated landing weight exceeds maximum landing weight is larger than for the other aircraft types.

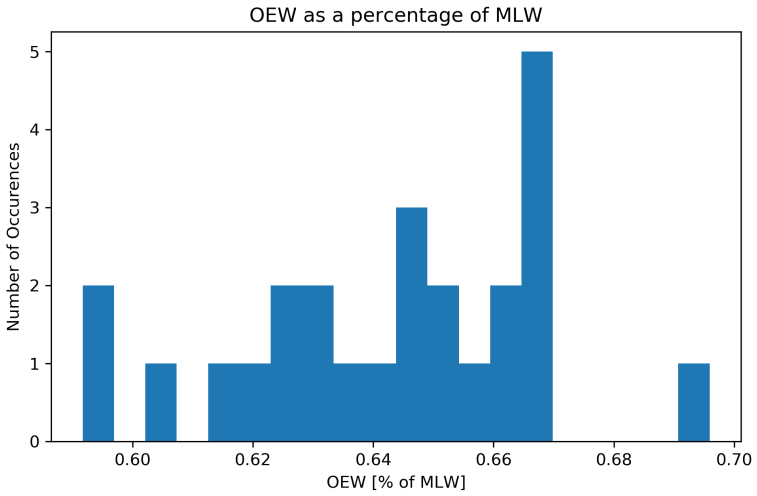

Figure 5.12: OEW as a percentage of MLW

In order to ensure that no aircraft in the simulation exceeds the MLW, this will serve as a cut-off. Although this results in probability spikes at the boundaries, these should be small for nearly all aircraft types.

Finally, the effect of mass estimation error needs to be tested. In order to do this, the capacity, fuel consumption, and noise contours will be compared for three scenarios. Each of these scenarios consists of equally distributed Boeing 737-800 series, Bombardier CRJ-900 series, and Airbus A330-300 series aircraft arriving to land on runway 27 from RIVER. The difference between the three scenarios is the weight. The first is at the estimated mean (or average) landing weight (ALW), while the other two are 10% higher and 10% lower.

All simulations were completed with sequences of length 100,000. Over 10 iterations, the calculated capacity varies by 0.1 AC/hr, while the mean fuel usage varies by 1.3 kg and the noise areas by 0.1%.
The simulated capacities and mean fuel usage are shown in Table 5.5. The reported capacity is the capacity that can be attained 90% of the time in the simulation, while the peak capacity can only be attained 1% of the time. This will be explained in detail Section 5.4.1. The reason the capacities are so high is the fact that all aircraft are stacked behind each other perfectly, removing all cutting losses. If the minimum separation is 3 nm, the aircraft will maintain 3.01 nm minimum separation, while in real life this would be more to the order of 3.3 nm.

It's interesting to note that if the calculated mean landing weight is higher than the actual landing weight, the capacity is still accurately calculated, while the mean fuel usage is slightly underestimated. If the calculated mean landing weight is lower than the actual landing weight, however, the capacity is slightly underestimated while the fuel usage remains representative.

Table 5.5: Capacity and Fuel Usage Comparison at different Landing Weights

Weight	**Reported Cap.** $[AC/hr]$	**Mean Cap.** $[AC/hr]$	**Peak Cap.** $[AC/hr]$	**Mean Fuel Usage** $[kg]$
ALW + 10%	43.2	44.9	48.7	403
ALW	42.7	44.4	48.1	405
ALW - 10%	42.7	44.4	48.1	414

Table 5.6: Comparison of Noise Performance at different Landing Weights

	Threshold	**ALW + 10%**	**ALW**	**ALW - 10%**
L_{24h} Contour Area $[km^2]$	60 dB	2506	2512	2515
	70 dB	1072	1072	1076
Peak Noise Contour Area $[km^2]$	80 dB	907	908	913
	100 dB	23	23	23
Nr. of Peaks Contour Area $[km^2]$	10 AC/hr	1973	1971	1971
	30 AC/hr	1035	1035	1036

Comparing the noise performance numbers shown in Table 5.6 shows only extremely small differences between the different aircraft weights. This is corroborated by Figure 5.13, where there are only 2 gridpoints with an absolute error of the L_{24h} map of over 0.2 dB. The actual flown routes are shown in magenta in this figure. For the number of peaks, there can be a more significant difference, however, where comparing the average landing weight to the light scenario results in a small underestimation, as seen in Figure 5.14. This is not accounted for in Table 5.6 since the difference is a constant 0.6 aircraft per hour, which still leaves the same area above 10 and 30 aircraft per hour.

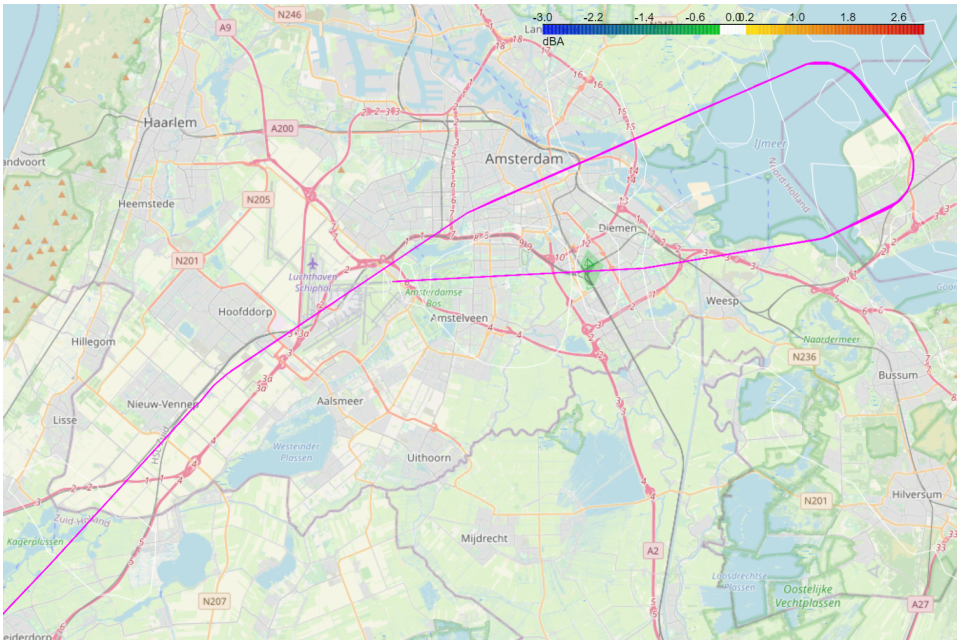

Figure 5.13: L_{24h} Error between Average Landing Weight and Average Landing Weight - 10%

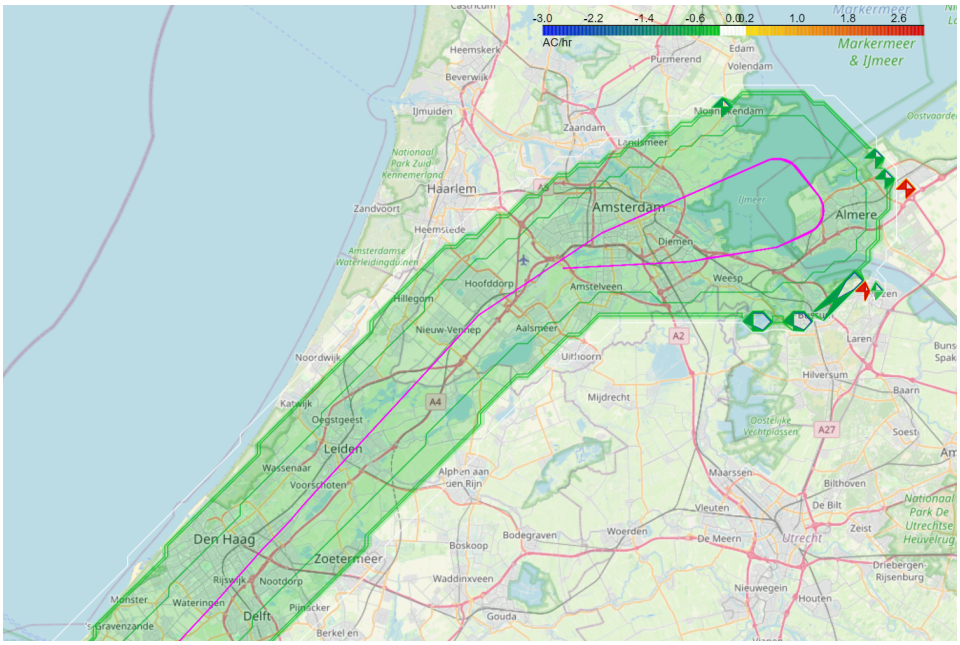

Figure 5.14: Number of Peaks Error between Average Landing Weight and Average Landing Weight + 10%

5.2.2. Route Definition

The route concept used in this study is different from that currently used at Schiphol. This study employs fixed routes, whereas the current operation relies on manually vectoring each aircraft. In order to ensure that all routes are still representative for their current counterparts, the route definitions are based on RADAR tracks. How this is done is explained below. Before this, however, the runway selection and the trimming of the flight tracks is explained.

Finally, the vertical component of the stepped approaches for the inbound peak simulation are explained.

RUNWAY SELECTION

In order to efficiently assess the impact and feasibility of implementing Continuous Descent Operations (CDO) at Schiphol, the most used runways will be investigated. This highlights one of the more unique aspects of Schiphol: The configuration of its runways. Where most modern airports have a limited number of parallel runways, Schiphol also has three non-parallel runways (04/22, 06/24, and 09/27). The result of this is that aircraft land in every direction, making it important to not only investigate CDAs for the parallel runways, but also for the rest. Table 5.7 [2] shows the runway usage for the five most used runways.

Table 5.7: Landing Runway Usage Distribution

Runway	Number of Landings	Percentage of Landings
18R	91200	39.6%
06	48000	20.8%
18C	31800	13.8%
36R	30000	13.0%
27	29400	12.7%

As can be seen in Table 5.7 [2], runways in each direction are used regularly. Since the wind field is not expected to change significantly between different parallel runways, 18C will not be included. The remaining four will be included in the flight path simulation, as together they represent nearly all landing traffic from each possible direction. Since the inbound peak simulation is much more specific, the most common runway (18R) will be used.

FLIGHT TRACK TRIMMING

Calculating the average track can only be done for each route separately. This requires, for instance, that doglegging manoeuvres and aircraft not flying by their Initial Approach Fix (IAF) are filtered out of the data set. This is done by specifying forbidden areas, if any flight track has a data point inside one of these areas, it's discarded. The result of this can be seen in Figures 5.15 and 5.16.

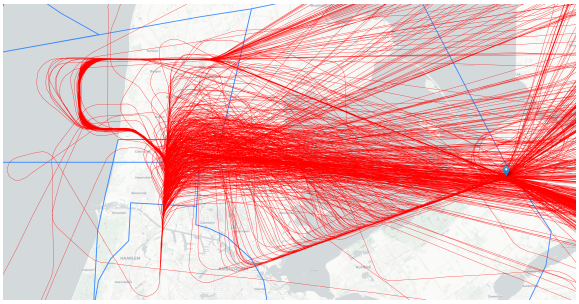

Figure 5.15: Untrimmed Flights from ARTIP to Runway 18R

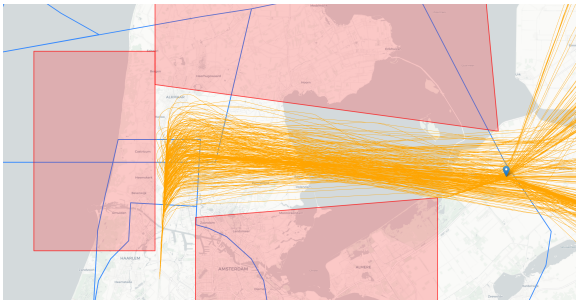

Figure 5.16: Trimmed Flights from ARTIP to Runway 18R

ROUTE AVERAGING

Since Area Navigation (RNAV) routes mostly consist of a limited number of waypoints, taking the average track does not result in a realistic route definition. What it can be used for, however, is ensuring that the calculated route definition is close to what is currently flown.

Since routes are generally defined as a number of straight lines between waypoints, a least-squares solution was used to estimate the average route. In order to ensure that only relevant datapoints are used, this was done per segment of the approach for only the relevant points. Filtering for relevant points was done by checking whether or not each point is within the relevant area and removing all irrelevant ones from the dataset.

The distance to the end of that particular track is then calculated for each relevant point. This ensures that all aircraft count equally towards the solution. If this was not done, slow flying aircraft would be counted more heavily since they create more datapoints close to each other (as the position is measured once every 4 seconds). Finally, Numpy's least-squares estimation is used to independently calculate the latitude and the longitude as a function of along-track distance. The result of the trimming and the selection of relevant points are shown in orange and green in Figure 5.17. Figure 5.18 again shows the relevant points and the result of the least-squares estimation. It should be

noted that the angled cut-off at the end of the route in Figure 5.17 was made to ensure that as little of the turn towards the final approach segment is included as this would influence the the route.

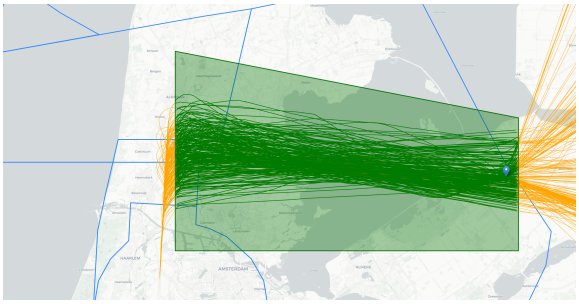

Figure 5.17: Trimmed Flights from ARTIP to Runway 18R and their Relevant Datapoints

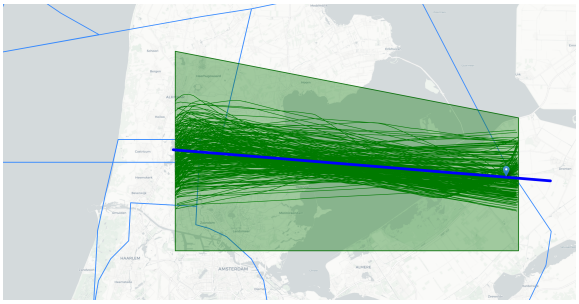

Figure 5.18: Relevant Datapoints and Calculated Least-Squares Route from ARTIP to Runway 36R

WAYPOINT PLACEMENT

In order to calculate the average track mentioned above, the along-track distance was calculated for each datapoint of each flight. This was then used to calculate the distance each aircraft had left to fly at the time each datapoint was created. The coordinates of the datapoint were then put into bins based on the distance each had left. Finally, the average coordinates of each bin was calculated and linked together to create the purple track in Figure 5.19.

Comparing this average tracks to the least-squares routes for runway 18R results in Figure 5.19. The blue markers in this figure represent the IAFs: ARTIP, RIVER, and SUGOL from east to west.

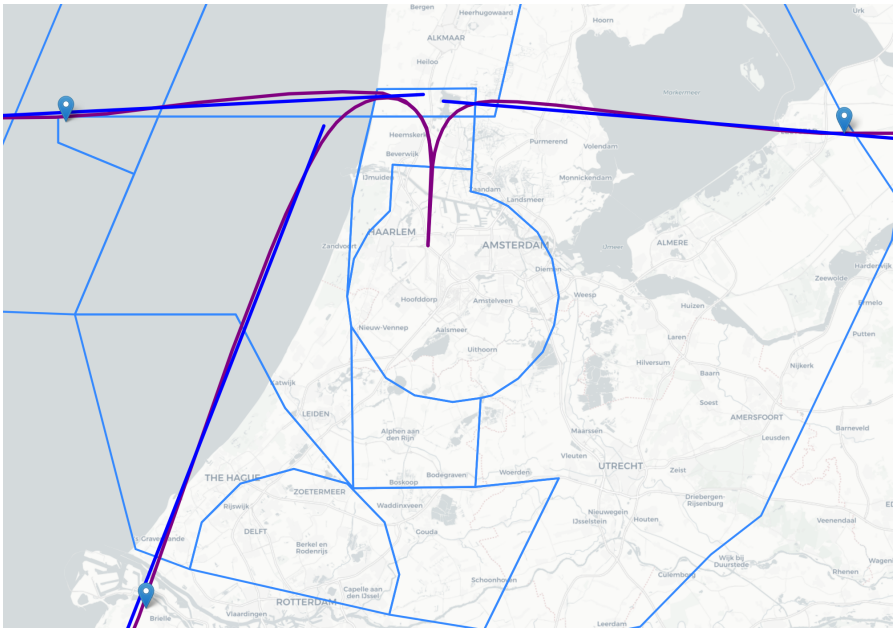

Figure 5.19: Comparison of Average Route to Least-Squares Route

The actual waypoints that aircraft will follow are placed on the least-squares routes. These waypoints are represented by the grey markers in Figure 5.20, which shows the track of a simulated Boeing 737-800 arriving from each IAF. As can be seen below, these tracks follow the average routes fairly well. The software used for this simulation is BlueSky Open Source Air Traffic Simulator, with BADA 3.12 used for performance calculation. Each aircraft completes the entire track at 250 knots and starts at BADA 3.12 reference mass, which is then reduced due to fuel usage.

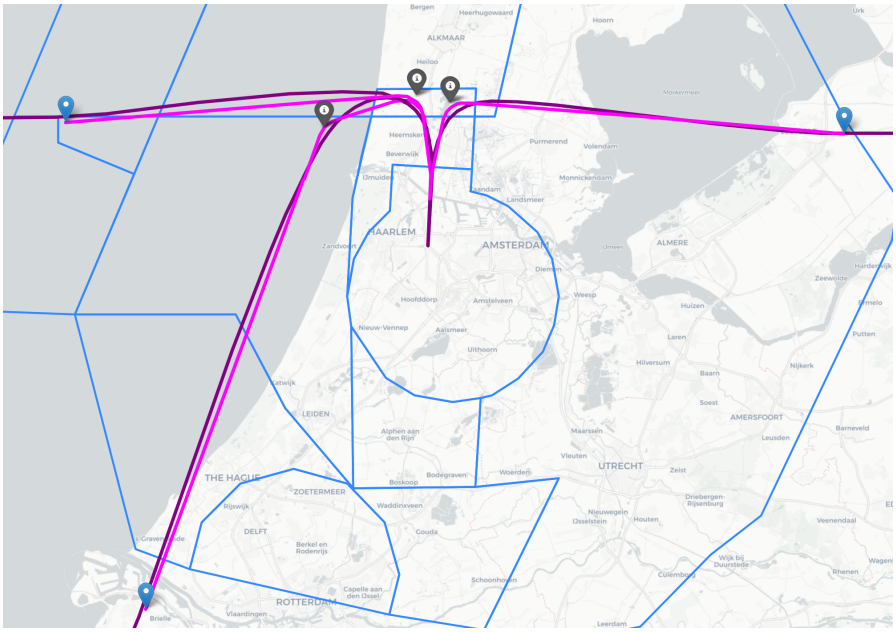

Figure 5.20: Comparison of Average Route to Simulated Flight Tracks

The Boeing 737-800 was chosen because it's a medium, middle of the line aircraft and because it's the aircraft that most frequently lands at Schiphol airport, with 21.6% of all movements in 2018, according to Schiphol's Noise Monitoring System (NOMOS) [33].

ROUTE SUMMARY

In conclusion: Since the exact horizontal route of the aircraft is not the focus of the research, they are kept relatively simple. Since most routes tend to consist of two segments: the final approach and a straight segment that leads there, only one waypoint is needed to define them. In order to ensure that the location of this waypoint matches the average turn-in point, a least-squares estimation of the initial segment was made. The final location on the waypoint was then visually placed on this line to match the average track as well as possible.

STEPPED APPROACH VERTICAL PATH

As stated above, the inbound peak simulation is only done for the most used runway (18R). This reduces the total number of routes to 3, once from each IAF. While the vertical continuous descent routes are very simple, those for the stepped routes are more complex. Since fuel usage is one of the key performance indicators, the number of track miles has to be the same for both types of approaches. As such, every route starts at the IAF. After this, the stepped approaches have a number of horizontal segments. The altitudes at which these are generally located can be seen in Figure 5.21.

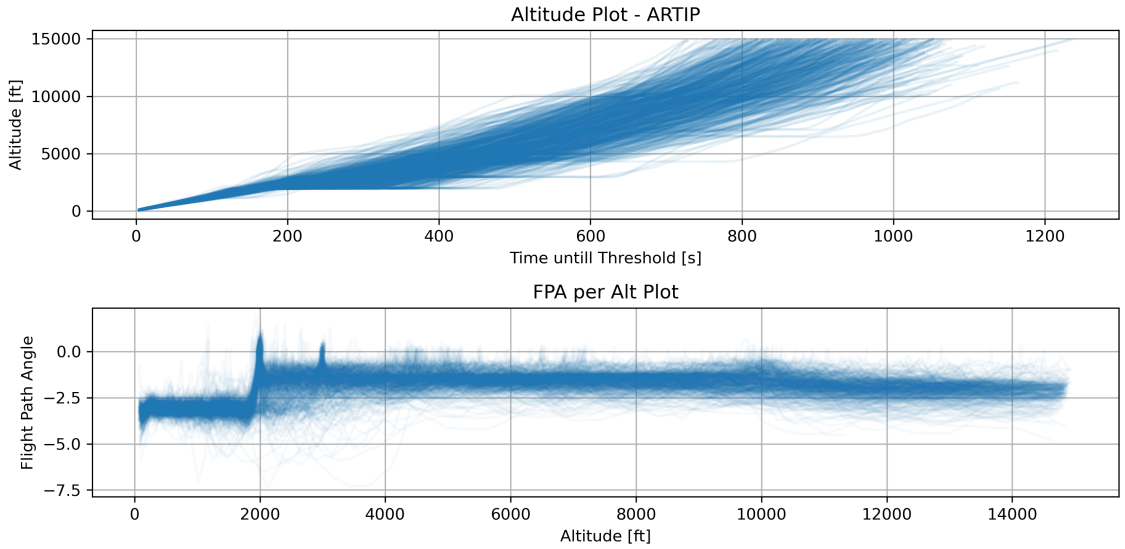

Figure 5.21: Vertical Profile of Real Stepped Approaches from ARTIP to Runway 18R

As shown in Figure 5.21, the most common step altitudes are at FL100, FL70, FL50, 3000 ft, and at 2000 ft. However, since steps at FL50 are often used by air traffic controllers to solve conflicts, it is not used as often and the actual altitude at which the step is done is not a precise as it is at some of the other altitudes.

The next step is then to calculate the average length of each step. To do this, the average distance each aircraft flies within 5% of the step altitude was calculated. The result of this calculation can be seen in Table 5.8, and the total vertical profile this creates for the SUGOL route is shown in Figure 5.22.

Table 5.8: Length of each Altitude Step for each Route

Step Altitude	**Length of Step**		
	ARTIP	RIVER	SUGOL
FL100	4.24	5.14	4.35
FL70	2.90	3.45	2.59
3000 ft	1.85	3.23	1.31
2000 ft	3.79	11.46	6.72

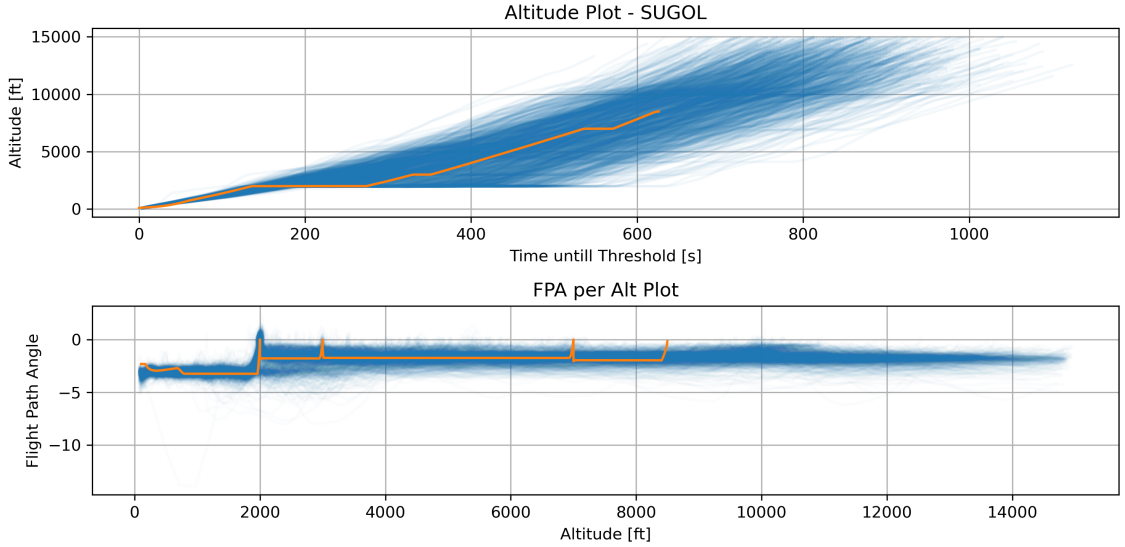

Figure 5.22: Vertical Profile of Real and Simulated Stepped Approaches from SUGOL to Runway 18R

5.2.3. Impact of Weather on Capacity

Before implementing the relevant weather into the simulation, it's important to know the impact that each weather type has on airport operations. Eurocontrol found 5 types of weather that have an influence on airport capacity [3]. These 5 types are the wind, visibility, percipitation, and freezing, and dangerous conditions.

The severity of this impact is then rated on an integer scale: A coefficient of 0 means no impact, while 1 is a small impact that is still manageable and anything over that shows actual bad weather. An example of the scoring for the wind is shown in Figure 5.23.

Wind Code	Wind speed [kt]	Wind coeff	gust
Code 1	≤ 15	0	+ 1
Code 2	between 16 and 20	1	
Code 3	between 21 and 30	2	
Code 4	> 30	4	

Figure 5.23: Severity of the Capacity Impact of Wind Conditions

In order to determine how often each type of weather impacts the capacity at Schiphol, the percentage of time that each coefficient is higher than 1 was calculated using Meteorological Aerodrome Report (METAR) data from 2019. The result of this analysis can be seen in Table 5.9.

Table 5.9: Caption

Weather Type	Percentage of Time above Threshold
Visibility	0.1%
Wind	28.2%
Precipitation	0.1%
Freezing Conditions	0.3%
Dangerous Conditions	5.0%

As Table 5.9 shows, visibility, precipitation, and freezing conditions almost never have an impact on the capacity at Schiphol and will thus be ignored for this research. 4.7 out of the 5.0% of time that dangerous phenomena impact capacity, it is caused by Towering Cumulus (TCu) and Cumulonimbus (Cb) clouds. These are local phenomena that, depending on the conditions, are either ignored or circumnavigated. Since this research focuses on the effects of implementing constant geometric FPA descents, both these and the stepped approach to which they are compared use fixed routes. This means that the impact of having to stretch the path to fly around such phenomena is the same for both continuous and stepped approaches. Therefore, only the wind will be accounted for in this research.

5.2.4. Wind Scenarios

To ensure that the winds used for the flight path simulation are both realistic and limiting, real wind fields will be used, as any type of averaging on these fields would result in a loss of small, local phenomena. The limiting cases that will be used are as close to $\pm 2\sigma$ winds, thus encompassing 95% of all expected wind scenarios. In order to pick a certain high-resolution wind field, the times at which the actual wind was as close to this 2σ wind as possible was calculated from low-resolution data, as doing this for high-resolution data results in computational difficulties. This is done by dividing the wind speed into an along-track and cross-track component with regards to the runway heading. These were chosen because the head- and crosswind are the most important wind parameters when landing and play a large role in the choice of active runway. First the determination of the wind distributions is discussed. This is followed by an explanation of the process through which the best matching wind realisations are found. In order to find which high resolution winds to use in the simulation, low resolution wind data is used. This is made up of one wind vector per sector at five altitudes. As this research is focused on the TMA, only TMA winds are taken into account. Inside of the TMA, this wind vector is given at FL10, FL30, FL50, FL70, and FL90. This entire process is summarised in Figure 5.24.

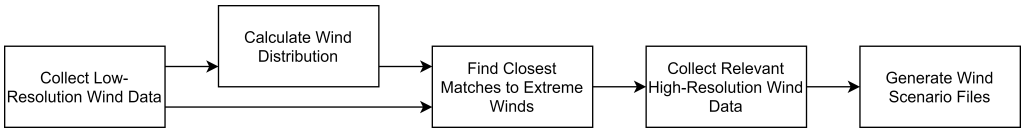

Figure 5.24: Flow Chart of Wind Scenario Setup

WIND DISTRIBUTION

It's important to first filter the winds per runway as they are very different when different runways are in use. This is done for the wind during 2018 and 2019, as active runway data is known for these years. Then, the wind vectors, which are saved as wind speed and direction combinations, need to be converted into along and cross-track components. The distribution of these is shown in Figures 5.25 and 5.26.

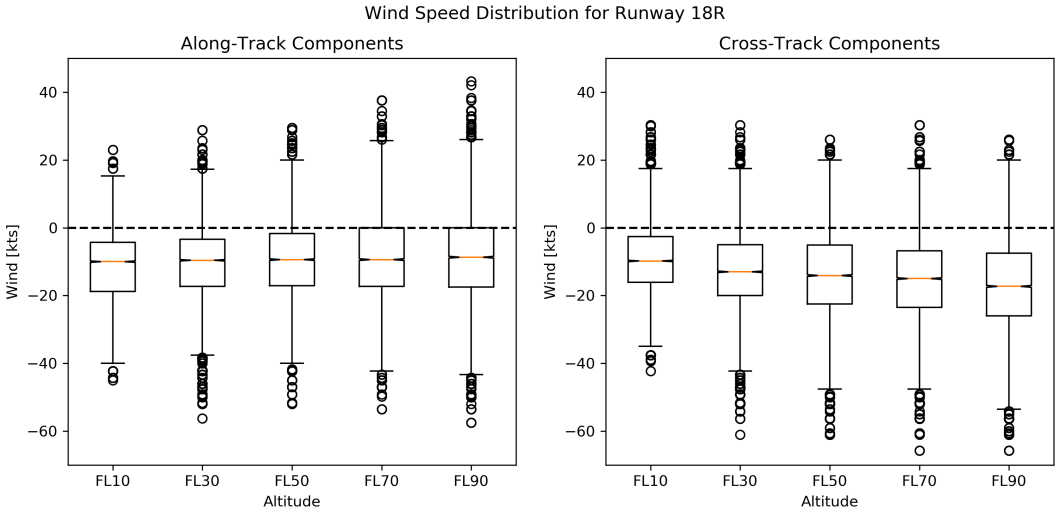

Figure 5.25: Wind Distribution for Runway 18R

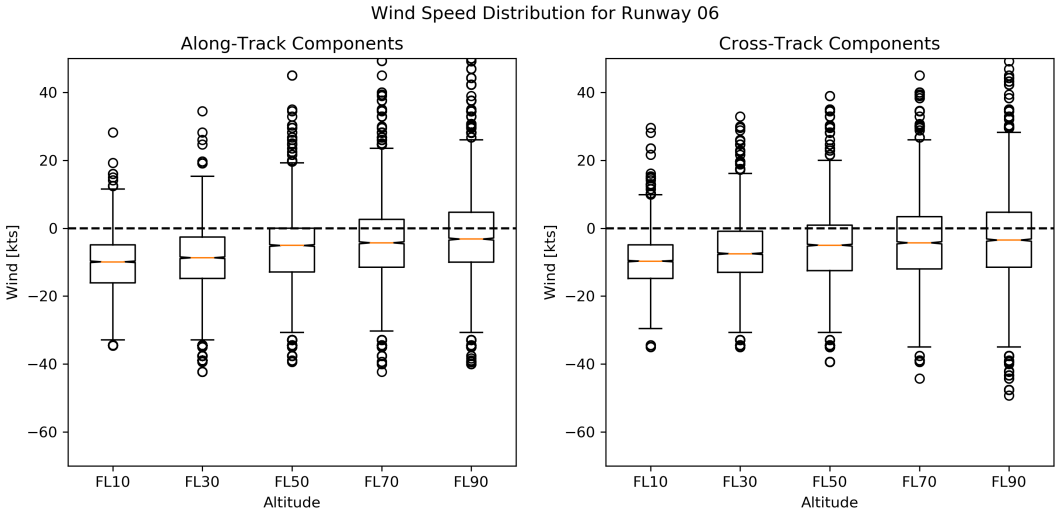

Figure 5.26: Wind Distribution for Runway 06

The negative mean along-track wind velocity for runway 18R in Figure 5.25 indicates a headwind, which is present for all runways. The negative mean cross-track component indicates a cross-wind from the right side of the aircraft. The mean and standard distribution for each component for each runway can then be calculated based Figure 5.25. These allow for the calculation of the 2σ winds.

WIND REALISATIONS

The realisations that will be used in the flight path simulation are all combinations of $\pm 2\sigma_{Along-Track}$ and $\pm 2\sigma_{Cross-Track}$. The closest fit is calculated by minimising the squared error. The average squared error is 271.2 kts^2 per wind scenario, which is mostly caused by the $-2\sigma_{Along-Track}, +2\sigma_{Cross-Track}$ combination, which will be called [-2, 2] from here on out, for runway 06, which has not occurred in 2018 or 2019. This combination is responsible for 1511.0 kts^2 of the total error of 4338.4 kts^2 over all 16 wind/runway combinations. The worst match and the 2σ winds for this are shown in Table 5.10.

Table 5.10: Worst Wind Match, [-2, 2] for Runway 06

Altitude	Real Wind [kts]		2σ Winds [kts]	
	Along-Track	Cross-Track	Along-Track	Cross-Track
FL10	-18.0	-3.6	-27.9	5.2
FL30	-11.5	9.2	-28.8	11.1
FL50	-18.1	2.2	-27.5	14.9
FL70	-18.1	2.2	-27.2	18.0
FL90	-18.1	2.2	-27.7	21.2

Since all real wind speed components in Table 5.10 are much smaller than the prescribed 2σ winds, it is assumed that these are the harshest winds that will be encountered. As this program tries to match 2 full years of wind data and the harshest winds still underestimate the 2σ winds, showing that it's reasonable to use this wind field for simulation.

Ignoring the realisation shown in Table 5.10 results in an average squared error of 188.5 kts^2. The median and best fits are shown in Tables 5.11 and 5.12. The costs for these are 90.1 and 22.6 kts^2 respectively. It should be noted that many of the real winds are the same, this is caused by the prediction accuracy of the real winds, as the wind direction is logged in multiples of 10 and the wind speed in multiples of 5.

Table 5.11: Median Wind Match, [2, -2] for Runway 36R

Altitude	Real Wind [kts]		2σ Winds [kts]	
	Along-Track	Cross-Track	Along-Track	Cross-Track
FL10	9.9	-23.0	6.4	-24.3
FL30	13.7	-20.9	12.9	-27.2
FL50	16.4	-25.1	16.4	-25.9
FL70	19.2	-29.3	18.3	-25.2
FL90	19.2	-29.3	21.2	-25.6

Table 5.12: Best Wind Match, [2, 2] for Runway 18R

Altitude	Real Wind [kts]		2σ Winds [kts]	
	Along-Track	Cross-Track	Along-Track	Cross-Track
FL10	9.0	12.0	9.0	13.2
FL30	9.0	12.0	12.1	12.5
FL50	14.6	13.7	13.8	11.4
FL70	16.7	11.0	15.9	11.2
FL90	16.7	11.0	18.9	11.2

The date and time for the best fitting wind data is shown in Table 5.13. These are the dates and times for which high-resolution weather data will be used to calculate the wind along the routes.

Table 5.13: Best Fitting Winds

Runway	Wind Scenario	Date	Starting Time
06	[2, 2]	27-04-2018	13:45:45
	[-2, 2]	19-11-2018	06:47:46
	[2, -2]	04-01-2018	18:47:45
	[-2, -2]	20-10-2016	09:55:45
18R	[2, 2]	09-06-2016	05:48:45
	[-2, 2]	20-11-2018	08:58:19
	[2, -2]	20-11-2016	17:47:46
	[-2, -2]	20-11-2016	03:47:46
27	[2, 2]	09-12-2018	19:41:51
	[-2, 2]	13-09-2017	05:49:46
	[2, -2]	21-01-2017	12:56:45
	[-2, -2]	27-02-2017	15:50:46
36R	[2, 2]	07-06-2019	15:51:48
	[-2, 2]	27-11-2017	13:59:19
	[2, -2]	19-03-2018	15:46:46
	[-2, -2]	09-12-2019	15:46:50

Each of these wind files contains 3 hours of winds, updated every 10 minutes. This is not long enough for the Inbound Peak Simulation, as this has thousands of aircraft landing sequentially instead of in parallel, like the Flight Path Simulation. In order to still provide the most accurate winds, these 3 hours are used and after this, they are used in reverse order. This process is then repeated untill the end of the simulation.

VERIFICATION

It is assumed that the wind velocity in each direction is normally distributed. Testing the accuracy of this assumption is done visually. QQ plots are used to compare the wind distribution to a normal distribution.

The coefficient of determination (R^2) of the least-squares line is used to rank the QQ plots. The worst fit is 0.977, showing that the distribution is close to normal. The QQ plots of the median and worst fits are shown in Figure 5.27. These represent the east wind component for runway 36R at FL30, and the north wind component for runway 36R at FL10 respectively.

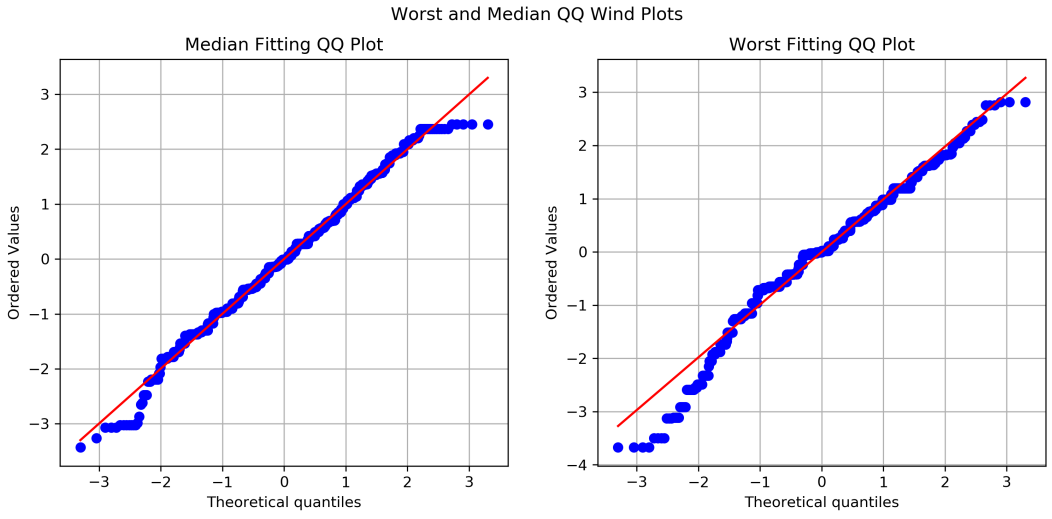

Figure 5.27: Worst and Median QQ Wind Plots

Although Figure 5.27 shows that the tails of the distribution aren't fully normal, this doesn't become relevant until slightly over 2 standard deviations away from the mean. Since only the 2 σ values are used, this is not relevant. Additionally, any error caused by the slight non-normality at 2 σ is expected to be smaller than that caused by the fact that real wind scenarios will be used.

WEATHER SUMMARY

To summarise, as wind is the only weather phenomenon that regularly impacts the capacity of stepped and continuous descent approaches differently at Schiphol airport, this is the only weather type that is included in this thesis. In order to ensure that small-scale wind effects are also included in this study, actual high resolution wind data is used. To do this, no time averaging can be done on the wind scenarios that are used.

First, the $\pm$ 2 σ winds are calculated from low resolution data. These are then used as a goal to determine when the winds were as similar as possible to these $\pm$ 2 σ winds. This gives a list of dates and times, for which the high resolution data was collected and used.

5.3. Tool Validation

The main tools used for the simulations are the performance model, BADA 3.12, and the simulation framework BlueSky. Each of these will be calibrated when needed and validated afterwards. Finally, the impact of an artifact of the BlueSky FMS is investigated in the Deceleration Segment section.

5.3.1. BADA 3.12

Generally the Root Mean Square (RMS) error for the performance and fuel usage of each aircraft in BADA 3 is less than 5% within the normal flight envelope. [28] Since continuous descent approaches are similar to, if not in the normal flight envelope, this 5% error per aircraft type spread over 25 different aircraft types results in approximately 1% RMS error for e.g. the mean fuel usage. This reduction in RMS is due to the square root of n-rule, under the assumption that the mean error is 0.

For this simulation only certain parts of the BADA 3.12 performance model are used. BlueSky assumes that any aircraft can decelerate at 0.5 kts/s at any time, independent of an aircraft's flight path angle. As this is not the case in real life, this needed to be updated before descent performance simulations could be done. Additionally, the problem with this is shown in Figure 5.28, where an Airbus A330-300 is simulated at both OEW and MLW. This shows that according to the base BlueSky build, both of these aircraft would decelerate at the same speed while descending at a 15 deg FPA.

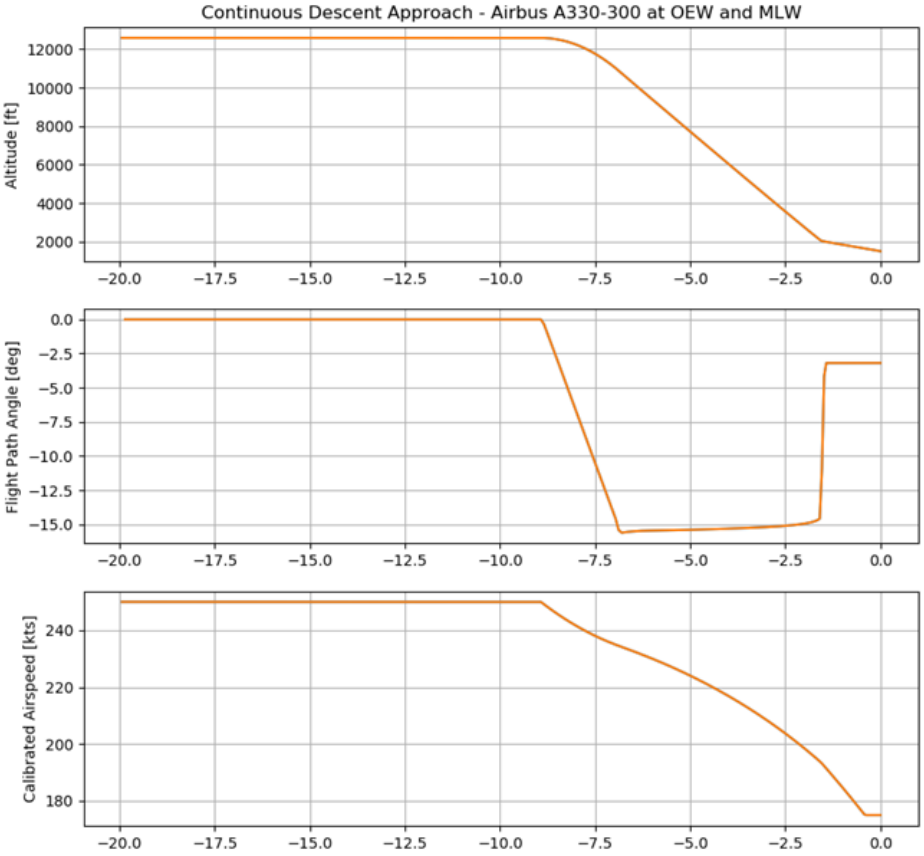

Figure 5.28: Airbus A330-300 Descent Path at OEW and MLW with Original BlueSky Performance

In order to solve this, the basic kinematic equations and sum of forces have to be included in the model. This is done in three steps; First, the thrust force needed to abide by the acceleration command is calculated. Then, this thrust force is capped to realistic limits. Finally, the actual acceleration is calculated using this capped thrust force.

The needed thrust force is calculated using Equation (5.7). In this equations, $a_{x_{Com}}$ is the standard commanded acceleration of 0.5 kts/s that is implemented in BlueSky, m is the mass of the aircraft, D is the drag calculated using BADA 3.12, α is the flight path angle, and g the gravitational acceleration.

$$T_{Needed} = a_{x_{Com}} \cdot m + D + sin(\alpha) \cdot g \cdot m \tag{5.7}$$

The thrust that results from Equation (5.7) can be larger than an aircraft's maximum thrust or even negative. Aircraft cannot produce less thrust than flight idle while in the air, however what this minimal thrust is is not known exactly. As an approximation of this, the 7% thrust that the International Civil Aviation Organisation (ICAO) recommends as the average taxi/ground idle thrust was used [24]. The resulting simulation of the NIRSI transition from ARTIP to 18R is shown in Figure 5.29, where actual RADAR tracks are shown in orange and the simulated tracks in magenta.

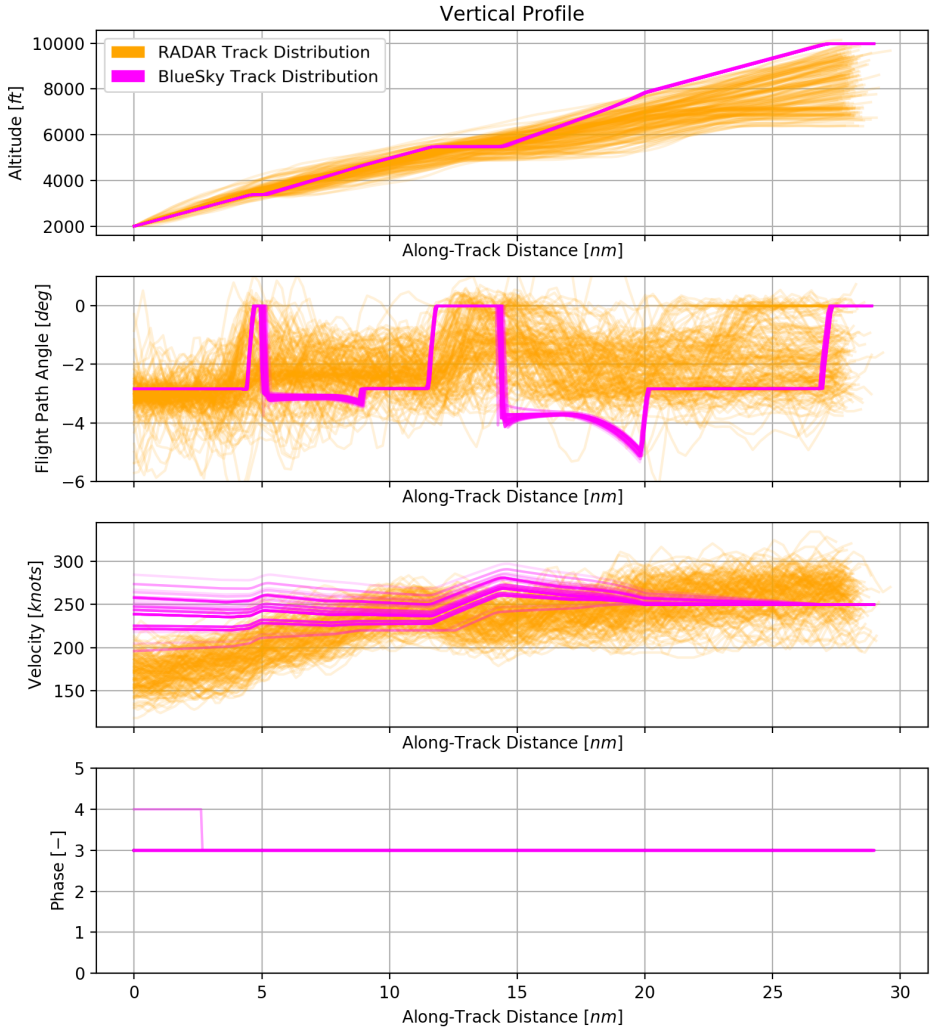

Figure 5.29: Vertical Profile with Standard Performance Values

As Figure 5.29 shows, no aircraft can actually abide by all speed constraints with the base values contained in BlueSky and BADA 3.12. As shown between 20 and 30 nm from the ILS intercept, the standard descent speed that BlueSky employs, which is 300 ft/nm, is too high for many aircraft. This is also shown in the second subplot, where the FPA is shown to be towards to high end of what most aircraft use. Therefore this can be lowered slightly to 250 ft/nm, which results in Figure 5.30.

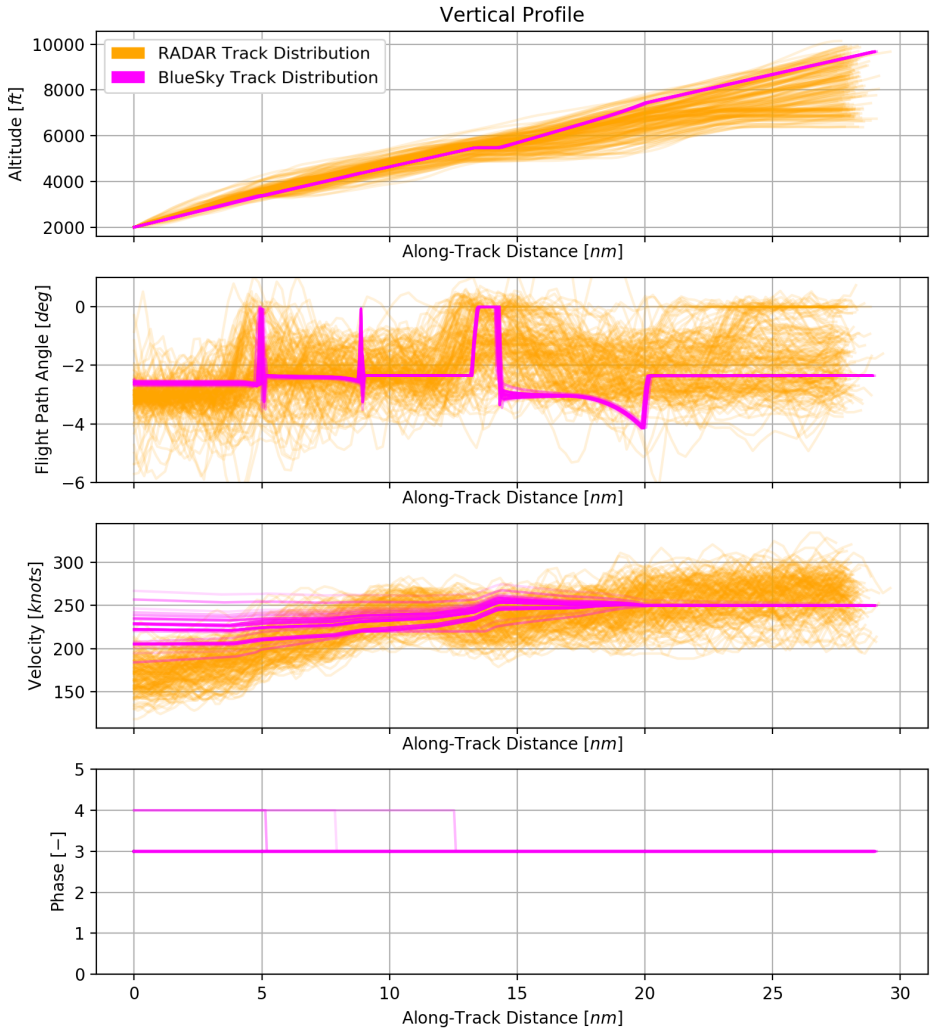

Figure 5.30: Vertical Profile with Reduced Descent Angle

While the reduced FPA helps, it does not fully eliminate the problem. This highlights something that is shown in the bottom subplot of Figure 5.30; The limitations of the configurations contained in BADA 3. BADA 3 only contains five configurations for the entire flight envelope of an aircraft: Take-Off, Initial Climb, Cruise, Approach, and Landing and these correspond to phases 1 through 5 respectively. As shown in this bottom subplot, very few aircraft slow down enough to switch to phase 4, approach configuration. The problem here is that approach configuration corresponds to flaps 2 for Airbus aircraft and flaps 15 for Boeing aircraft, which is generally deployed after the localizer has been captured. During the approach, flaps 1 and 5 are generally used earlier but these are not included as a descent phase in BADA 3.12 [31]. This means that until the end of the vertical profile, a significant portion of the drag that an actual aircraft would experience is not included in the simulation. For example, for a Boeing 737-800, the C_{D_0} term for the flaps 1, 5, and 15 are approximately 5%, 40%, 95% higher than the clean C_{D_0} and the first two are completely omitted in BADA 3.12. Since thrust is roughly equal to drag, the minimum thrust can be lowered in order to account for this. Lowering the minimum thrust from 7% to 0%, assumes that on average a little more than flaps 1 is used over the entire descent. This is reasonable as part of the descent would still be done in the clean configuration, while a significant part is done using flaps 1 and towards the end even flaps 5. The results are shown in Figure 5.31.

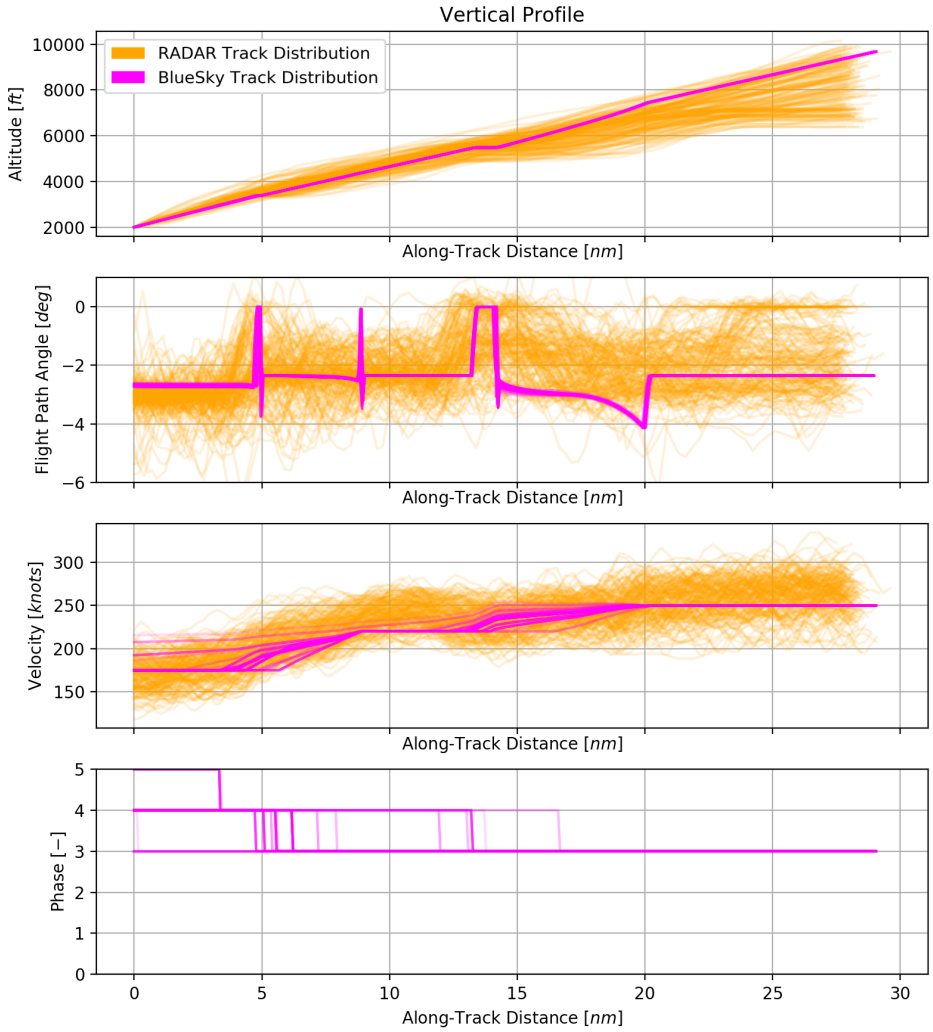

Figure 5.31: Vertical Profile with Reduced Minimum Thrust and Descent Angle

Although Figure 5.31 shows that not all aircraft can abide by all speed constraints, approximately 95% of aircraft can. The final 3 aircraft can be explained by the top subplot. While the altitude profile is within the bounds of what actual aircraft would do, many aircraft start this section lower than FL100. Controllers know that the most aerodynamic aircraft have a tough time following such a steep descent trajectories, this allows them to ask such aircraft to descend earlier. As shown in Figure 5.31, this is done for more than just the most aerodynamic aircraft as a significant portion of aircraft start this segment at FL80. Finally, the commanded deceleration of 0.5 kts/s is close to what the actual aircraft seem to use. This is seen especially well between 5 and 10 nm, where the steepest slope is very similar to how the actual aircraft decelerate.

FLAP SCHEDULE VALIDATION

While RADAR data is useful for providing information on all aircraft arriving at Schiphol, it is not particularly accurate and only provides basic information on the trajectory. In order to get a good understanding of the accuracy of the updated aircraft model used for this research, more detailed information is needed. This is where Aircraft Condition Monitoring System (ACMS) logs come in. A number of these were provided by an airline which operates at Schiphol for 42 flights of their Boeing 737-800 aircraft and 40 flights of their Boeing 777-200 aircraft. These logs provide information on many of the internal systems, however for this validation the most important parts are the fuel usage and flap deployment schedule.

Lowering the minimal thrust is essentially the same as adding additional drag, which is why this was done. However, the fuel usage in BADA 3 consists of two parts: idle fuel consumption and thrust specific fuel consumption. By lowering the minimal thrust, this thrust specific fuel consumption is also lowered. Since the largest value of the two at any time is taken to be the actual fuel usage, lowering the thrust specific fuel consumption means that more often, the fuel consumption is the static, minimal fuel consumption. This means that much of the impact of different flight

path angles is hidden behind the static fuel consumption and as such, the fuel consumption needed to be updated. To do this, instead of taking the maximal value of the two fuel consumption variables, they are added together, since it is assumed that at 0% thrust, the engines are running at idle.

Before getting into the comparison of the simulations and the ACMS logs, there are a few things that need to be noted. For the Boeing 777-200, there are multiple variables that can be used to determine the flap setting. The most important ones are the position of the flap handle and a variable for the flap setting. There is a discontinuity between these two, however. While the flap handle can have 7 different values, which correspond to the 7 flap settings found in literature, the flap setting variable does not include flaps 1 and can thus only have 6 different values. [34] None of the other flap related parameters in the ACMS logs change when the flap handle is set to flaps 1, giving the impression that flaps 1 does not change the configuration of the aircraft. This is strange because according to the OPF file included in BADA 3, the stall speed of a B777-200 is 17% lower with flaps 1 than it is clean. Additionally, the deflection of the flaps at flap setting 1 is less than 1 degree, so it is possible that the variables are not logged accurately enough for this change to show up in the ACMS logs. [34] Because flaps 1 has a significant influence on the stall speed and drag according to BADA, it will be assumed that flaps 1 exists and as such, the flap handle setting will be used for this research.

To determine the accuracy of the flap deployment schedule, the ACMS logs were replicated through simulation in BlueSky. During this simulation, low-resolution wind data was used from the time the actual approaches were performed. The results can be seen in Figure 5.32.

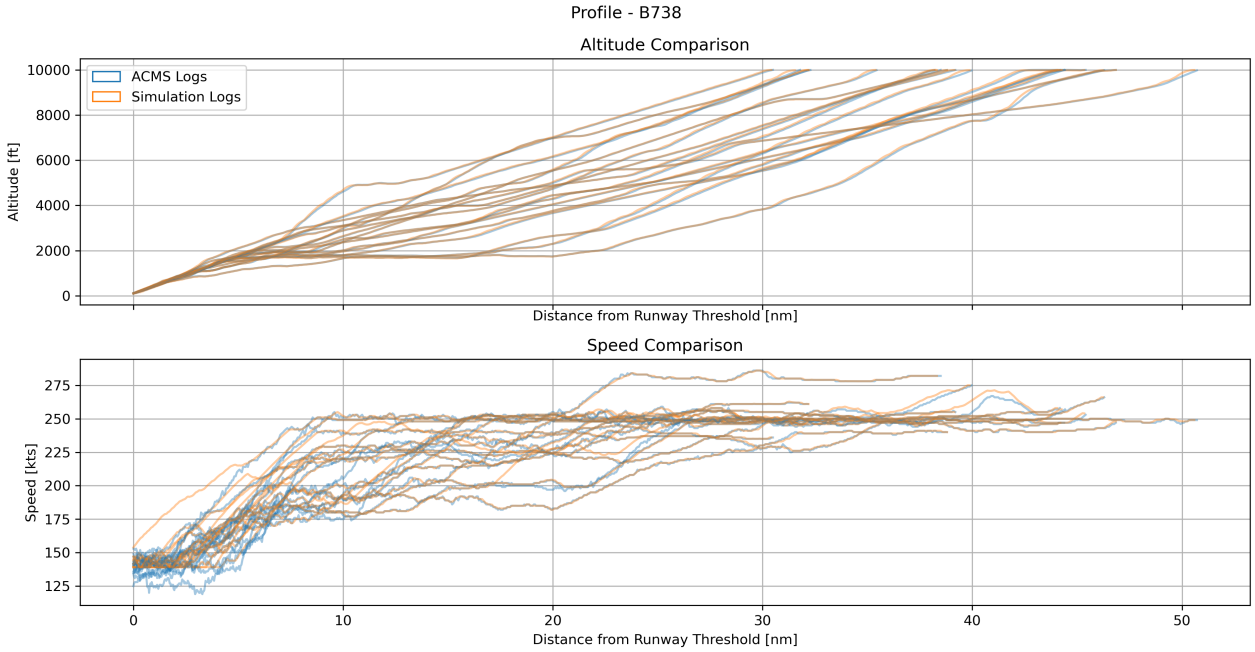

Figure 5.32: Comparison of Speed and Vertical Profile between ACMS and Simulation Logs for all Available Boeing 737-800 Flights Arriving at Schiphol

The flap deployment schedule for the simulations as compared to the ACMS logs can be seen in Figure 5.33.

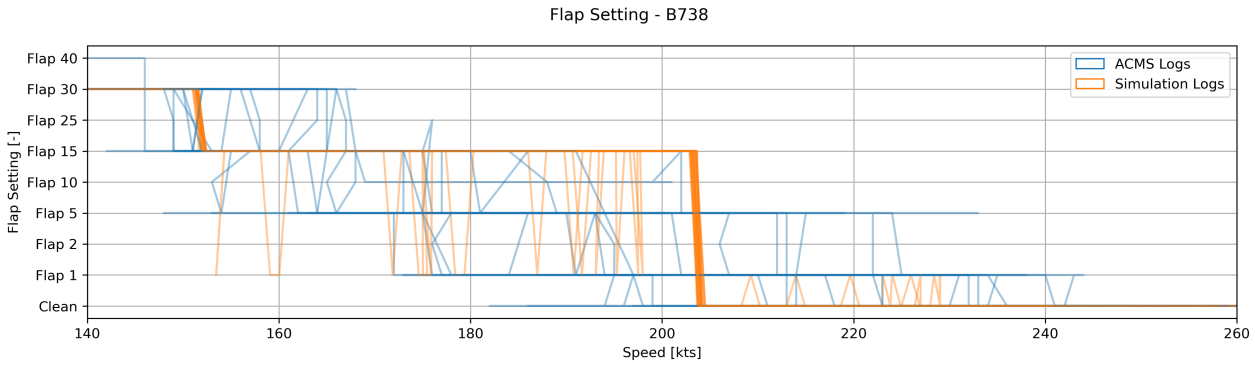

Figure 5.33: Flap Schedule Comparison between ACMS and Simulation Logs for all Available Boeing 737-800 Flight Arriving at Schiphol

As shown in Figure 5.33, the simulated aircraft take a relatively heavy-handed approach to flap scheduling, only using the clean, flaps 15, and flaps 30 settings, omitting the other settings. This hampers the simulated aircraft's ability to decelerate, especially at higher speeds, where real aircraft would deploy flaps 1 and increase their zero-lift drag coefficient by approximately 3% and their lift induced drag coefficient by approximately 25%, significantly increasing the total drag. While these flap settings are included in the BADA database, they are not used during the simulations since they are reserved for the take-off and initial climb phases. To quantify the effect of this, the average drag along the entire approach was calculated using the BADA drag calculation and operational performance data. The results can be seen in Table 5.14.

Table 5.14: BADA Calculated Mean Drag Comparison between ACMS and Simulation Logs

Aircraft Type	**ACMS Log Mean Drag** $[kN]$	**Simulation Log Mean Drag** $[kN]$
Boeing 737-800	438	417
Boeing 777-200	1330	1320

As shown in Table 5.14, the difference between the ACMS and simulation logs is relatively small. As such, the standard phase definitions, together with the updated drag model result in an accurate estimate of the drag that is calculated using real flap settings and thus give an accurate depiction of the decent performance of the aircraft.

5.3.2. FMS Validation

The validation of the Flight Management System (FMS) is done in two parts. The lateral and vertical navigation are tested separately. This is done by comparing actual flight paths over an RNAV route to those simulated in BlueSky. The chosen route is the ARTIP 3B transition to the NIRSI 1B approach for runway 18R, because it is used relatively often, resulting in a large amount of RADAR data.

The lateral navigation control is compared at three locations: at the centre of a turn, on a straight segment between waypoints, and at the end of a turn. The RADAR and BlueSky tracks, shown in orange and magenta respectively, as well as the testing areas (green) and centre of turn (black) are shown in Figure 5.34. The simulated tracks are simulated in BlueSky using BADA 3.12. The aircraft used are of the same distribution as all aircraft landing at Schiphol airport.

While the vertical navigation has already been tuned in Section 5.3.1, a number of aspects with regards to the fidelity of the simulations still need to be discussed.

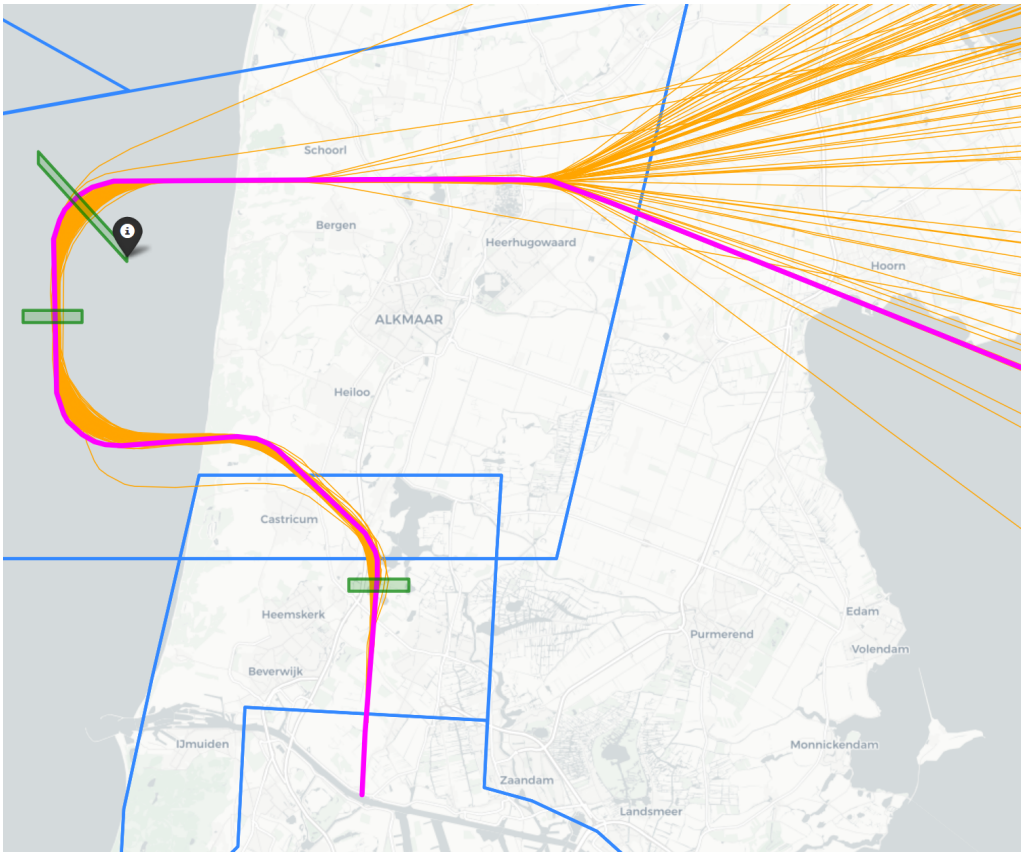

Figure 5.34: Comparison of BlueSky and RADAR Tracks

As shown in Figure 5.34, all simulated aircraft follow almost exactly the same route, showing that aircraft type does not significantly influence the turning performance model. This can also be seen in Figures 5.35 through 5.37.

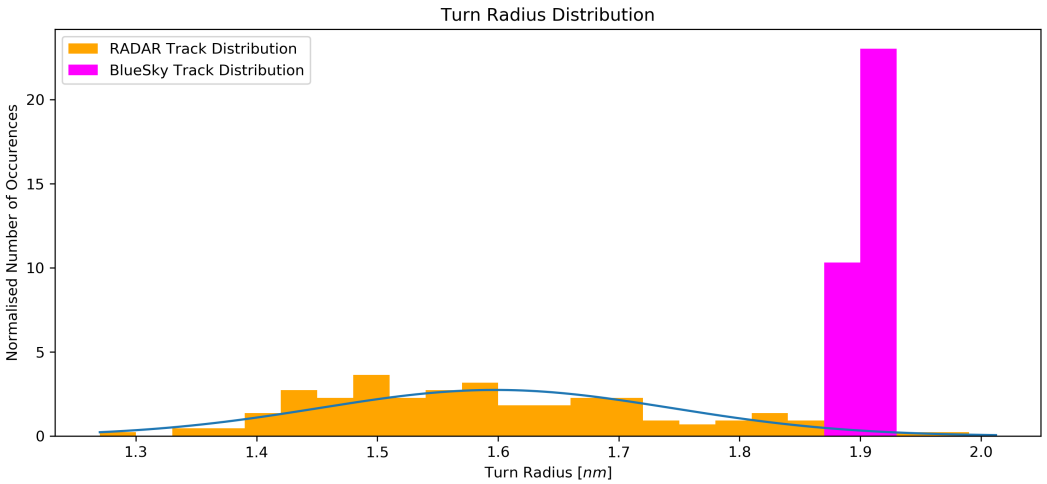

Figure 5.35: Turn Radius Distribution

The turn radius distribution is shown in Figure 5.35, which shows that the turn radius is nearly the same for all aircraft. This is calculated as follows. The centre of all turns was estimated visually and the distance between this and each point within the green area in Figure 5.34 calculated. This means that each flight can have multiple radii, of which the average is taken, the result of which is shown in Figure 5.35 for each flight. The average turn radius in BlueSky is 0.3 nm larger than the real-life average. As the RADAR turn radius is normally distributed, $D(148) = 0.07$, $p = 0.395$, this corresponds to 2.1 standard deviations above the mean. The BlueSky radius is exactly the same for each aircraft, showing that there is a significant difference between the two. For the remaining two sections, the absolute

error is smaller, at approximately 0.12 and 0.04 nm for the straight section and the end of turn checks respectively. This can be seen in Figure 5.36 and 5.37. While the straight section distribution is normal (D(184) = 0.06, p = 0.499), the end of turn route deviation is not (D(184) = 0.14, p < 0.001).

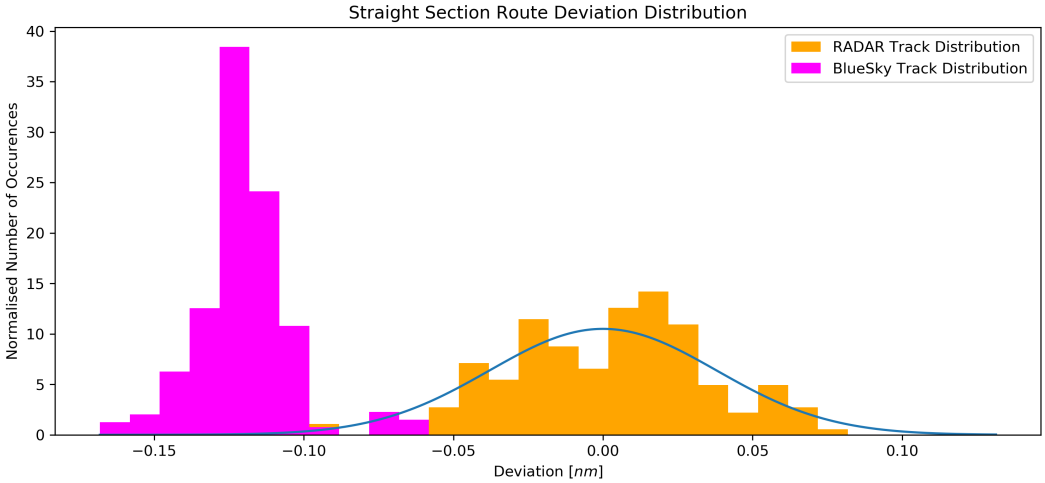

Figure 5.36: Straight Section Route Deviation Distribution

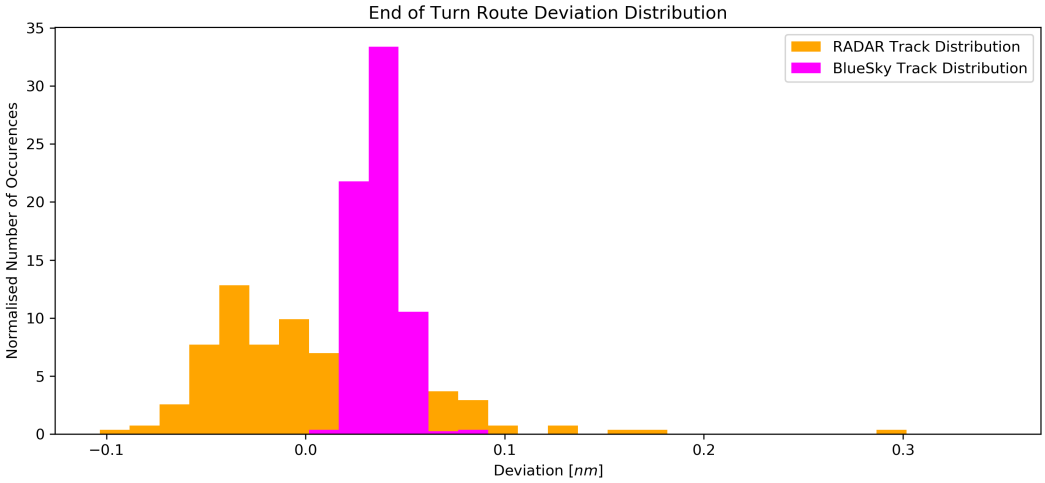

Figure 5.37: End of Turn Route Deviation Distribution

As a result of the constant overestimation of the turn radius, the flight path that is simulated in BlueSky is 315 m longer than what is actually flown on average. What is clearly shown in Figures 5.35 through 5.37 is that navigation accuracy is not modelled in BlueSky.

The vertical navigation consists of two parts, altitude and speed control. The vertical profile of actual aircraft (orange) and their BlueSky simulation counterparts (magenta) are shown in the top two parts of Figure 5.38. Here, a few things should be noted. Firstly, the BlueSky aircraft start at the maximum altitude of FL100, whereas the real aircraft generally start much lower. Secondly, the FMS in BlueSky uses a standard FPA value, which is only deviated from when forced to by altitude constraints. To decide whether or not this is necessary, however, the FMS only looks at the next waypoint. This is what causes the large FPA spike at around 20 nm. Here, the aircraft have passed a waypoint and realise that they suddenly need to descent more quickly to arrive at the prescribed altitude at around 14 nm. Finally, the FMS is programmed to stay as high as possible for as long as possible. This is shown when the aircraft start descending from FL55. Because they stay so high for so long, the standard rate of descent is enough to to directly descent to the ILS intercept. The real aircraft, however, tend to descend a little earlier. At approximately 4 nm, there is a waypoint that has to be crossed at or above 3400 ft. Because these real aircraft are lower than those in BlueSky, their FPA is smaller until they reach this waypoint, after which the FPA drops.

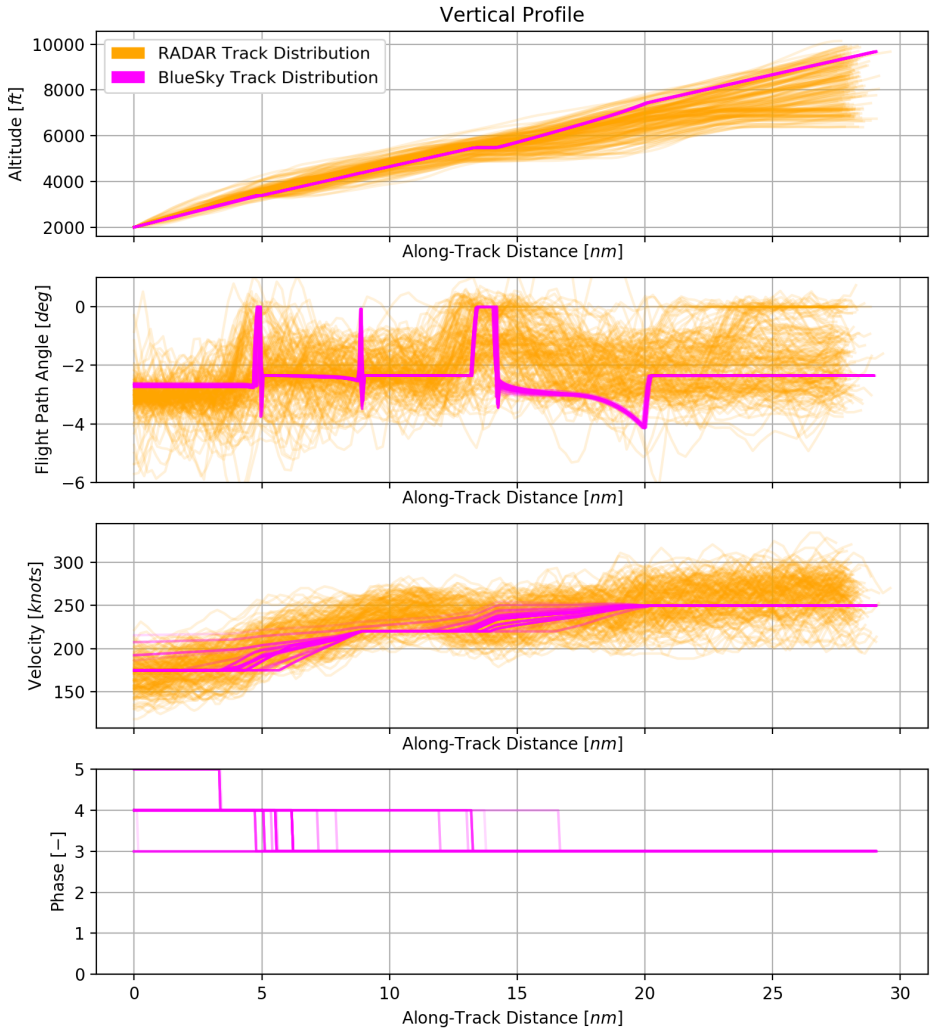

Figure 5.38: Vertical Profile

As shown in Figure 5.38 the overall trend of the BlueSky aircraft is close to what the real aiher aircraft. Additionally, the standard descent speed used in BlueSky seems close to what is used in real life.

The speed control part of vertical navigation is shown in the third subplot from the top in Figure 5.38. The velocity of the BlueSky aircraft is set one waypoint before their location in the actual procedure. This is because speed commands in BlueSky are applied after the waypoint is passed, whereas in real life, they apply at that waypoint. This seems to work very well at the start of the approach, where the procedure is well defined. Towards the end, however, real aircraft slow down gradually. This is not prescribed in any procedures. In order to still allow for a realistic speed profile, a 175 kts constraint was added 5 nm before the ILS intercept. As shown in Figure 5.38, this results in a realistic speed profile.

5.3.3. Deceleration Segment

Finally, it should be noted, however, that aircraft in BlueSky control their speed and altitude at the same time and thus, the deceleration and the descent are combined. In real aircraft, however, the FMS tries to separate these two. This means that a decelerating descent is done in two phases. First, there's a steeper constant speed segment, which connects the initial position to the start of the second segment: the deceleration segment. Here, a reduced vertical speed of approximately 500 fps allows for much faster deceleration. To approximate the length of this segment, a deceleration of 35 kts/min was used.

In order to estimate the impact of this assumption, three aircraft types were simulated to fly from RIVER to runway 27. For this, wind was ignored while all aircraft were flown at their mean estimated landing weight. The simulation was performed at a 2.2 degree FPA and included a Boeing 737-800 series, Bombardier CRJ-900 series, and Airbus A330-300 series aircraft. 2.2 degrees was chosen because this is the FPA where a significant number of aircraft types start

to struggle with speed constraints. The aircraft types were chosen to represent the full spectrum of aircraft arriving at Schiphol. The Boeing 737-800 is the most common aircraft type, accounting for almost 22% of all movements and representing the medium aircraft in for instance the rest of the Boeing 737 series aircraft, as well as the Airbus A320 series. The Airbus A330-300 represents the heavier aircraft like the Boeing 747 series and the Airbus A380 series. The A333 was chosen to represent this group because it is the aircraft type that has the lowest amount of time authority on all approaches and thus stop to comply with all speed constraints at the lowest FPA. Where the A333 is used as an upper bound on the heavy aircraft, the final aircraft type represents the lower bound. While Bombardier CRJ-900 series are classified as medium aircraft according to their wake turbulence category, they are the lightest aircraft type in the 25 most popular aircraft at Schiphol. It also stands in for for instance the Embraer ERJ series.

All simulations were done with sequences of 100,000 aircraft which result in a capacity spread of under 0.1 aircraft per hour. The reported capacity is the capacity that can be attained 90% of the time, while the peak capacity can only be attained 1% of the time. The mean fuel usage meanwhile has a spread of approximately 1.4 kg over 10 iterations. Finally, the noise areas vary by up to 0.2%.

The capacities and fuel usage difference is shown in Figures 5.15 and 5.16. While the capacity difference between the two deceleration types is small, it is significant as all capacity results are within 0.1 aircraft per hour. For the fuel usage, however, this is not the case since the difference is smaller than the spread. As such, by ignoring the deceleration segment in the main simulation, the capacity is only very slightly overestimated, while the fuel usage is not impacted significantly.

Table 5.15: Capacity Comparison with or without Deceleration Segment

Approach Type	**Reported Cap.** $[AC/hr]$	**Mean Cap.** $[AC/hr]$	**Peak Cap.** $[AC/hr]$
With Deceleration Segment	29.6	30.7	33.3
Without Deceleration Segment	29.8	31.1	33.7

Table 5.16: Fuel Usage Comparison with or without Deceleration Segment

Approach Type	**Mean Fuel Usage** $[kg]$
With Decel. Segment	406
Without Decel. Segment	405

An additional advantage of the use of a deceleration segment is that it can allow aircraft to decelerate faster than without it as seen towards the end of the approach in Figure 5.39. However this figure also shows a large disadvantage of deceleration segments however, since the steeper constant speed segments can make it much more difficult to maintain speed, as can be seen between 15 and 12 nm before the runway threshold. It should be noted that an actual FMS would not allow an aircraft to accelerate as seen between 15 and 12 nm before the runway. However, how such an overconstrained problem is solved depends on the exact FMS. Some company's FMSs might reduce speed earlier while others might change the layout of their deceleration segment. Both would require large changes in the FMS included in BlueSky and are thus omitted for this validation.

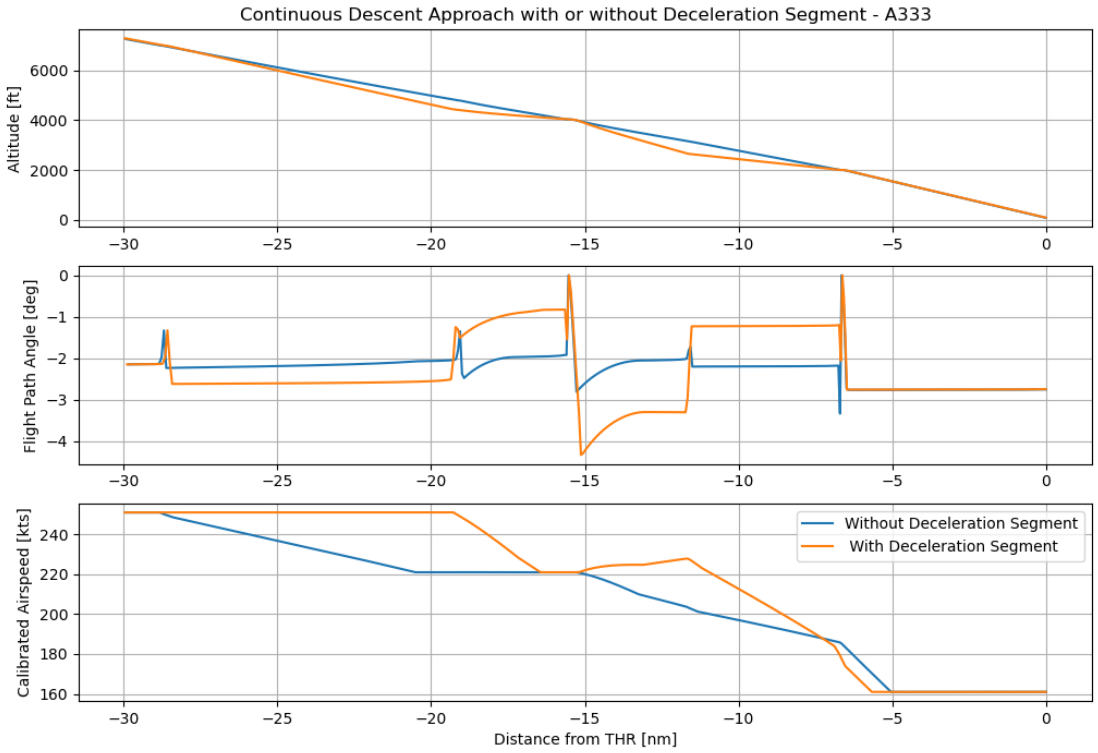

Figure 5.39: Profile Comparison with and without Deceleration Segment

Finally, a comparison of the noise performance of both deceleration types is shown in Figure 5.40. A positive value in this figure means that ignoring the deceleration segment results in an overestimation of the noise. The magenta lines show the flight tracks at a 2.0 degree FPA. This shows that there are only small differences between the two tracks, with a maximum absolute error of 1.6 dB. It is interesting to note that, during the steep decent towards the deceleration segment, the noise is underestimated. While the aircraft approaching the deceleration segment is at lower thrust than the one following the perfect constant FPA approach, it is also significantly lower, resulting in more noise. This changes at the start of the final deceleration segment, however. Almost exactly at the point where the deceleration segment starts, the constant FPA Boeing 737-800 reaches its target speed, meaning that it increases its thrust to stay at that target. On the map, this happens when the aircraft turn from a 240 to a 260 degree course. All other aircraft have not yet reached their target speed and are thus at their minimal thrust, meaning that there is almost no difference between the approach with and without deceleration segments. The end result of this is that at the start of the deceleration segment, the noise is overestimated, as the non-deceleration segment aircraft make more noise on average. A few miles later, this changes when the Boeing 737-800 that did use the deceleration segment also reaches its target speed. At this point, this aircraft starts to emit more noise again as it's following a shallower FPA (that of the deceleration segment) and thus needs more thrust. This shows one of the major limitations of using a one size fits all approach to deceleration segments. For some, like the Boeing 737-800, it will be too long, while for others, like the Airbus A330-300 here, it fits much better.

In conclusion, Figure 5.40 during the steeper decent towards deceleration segment, the noise production is underestimated by ignoring the deceleration segment. During this deceleration segment, however, this difference is much smaller, only showing to the sides of the aircraft, where the directivity of noise results in the largest peaks. This is why, during the straight segments there is no significant change underneath the aircraft while during the turn, where the aircraft has rolled to the side, it is also underneath the aircraft.

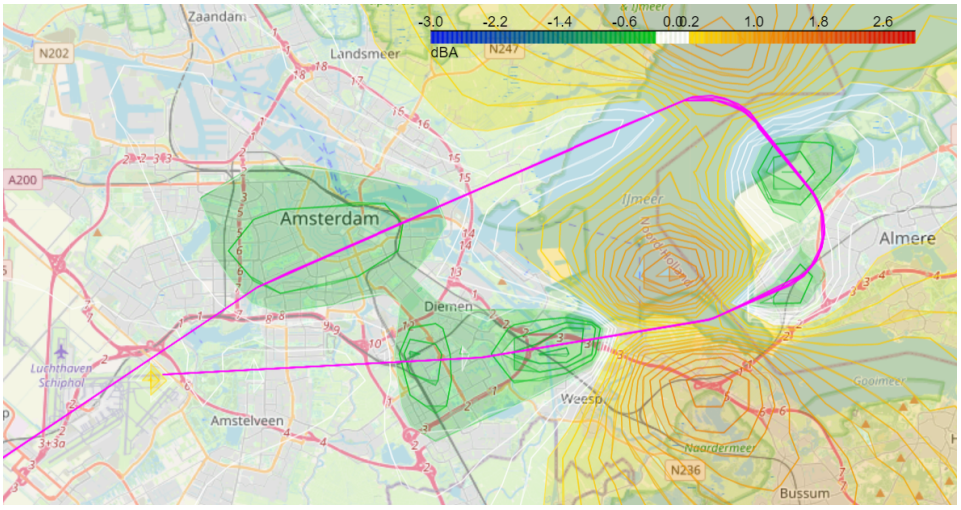

Figure 5.40: L_{24h} Contour Difference with and without Deceleration Segment, Positive Values mean an Overestimation

The areas of the L_{24h}, peak noise, and number of peak contours is shown in Table 5.17. This shows that ignoring the deceleration segment tends to result in an overestimation of especially the L_{24h} contours, as well as the peak noise contours. It should be noted, however, that the overall overestimation of the noise areas does not mean that the contours are always smaller. As stated above, the 100 dB L_{24h} contour is underestimated by ignoring the deceleration segment.

Table 5.17: Comparison of Noise Performance with or Without Deceleration Segment

	Threshold	With Deceleration Segment	Without Deceleration Segment
L_{24h} Contour Area [km^2]	60 dB	2487	2510
	70 dB	1060	1072
Peak Noise Contour Area [km^2]	80 dB	903	908
	100 dB	27	23
Nr. of Peaks Contour Area [km^2]	10 AC/hr	1963	1971
	30 AC/hr	1036	1035

5.4. Calculation Methodology

In this section all calculations needed to perform the flight path simulation are explained. This starts with the way in which the capacity is calculated in Section 5.4.1, followed by the Speed Authority in Section 5.4.2. The final two calculations are the fuel usage calculation in Section 5.4.3 and the noise production calculation in Section 5.4.4.

5.4.1. Capacity

Due to limits on computational power, each aircraft type is only simulated 100 times for each combination of runway, FPA, IAF, and wind scenario at different landing weights.

MINIMUM SEPARATION

When all of the flight tracks have been simulated, the needed time separation on the IAF is calculated. This is done for each combination of aircraft type and IAF. The tracks of the slowest leading aircraft and the fastest following aircraft are plotted in a time-distance diagram like the one shown in Figure 5.41.

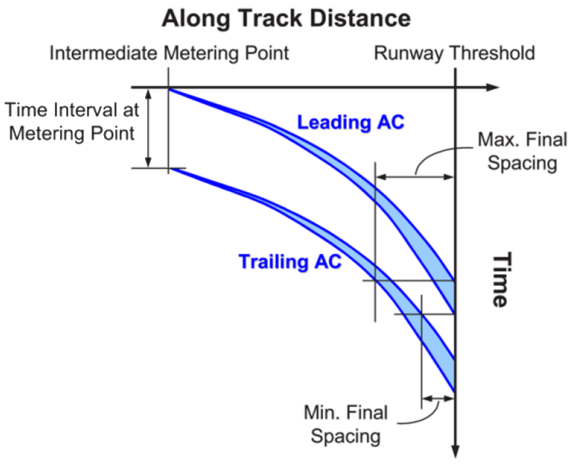

Figure 5.41: Time-Distance Diagram Showing the capacity Impact of translating subsequent Flight Tracks [30] Edited

In order to calculate the needed time separation, the trailing aircraft are translated with regards to the leading ones. This is done by first calculating the distribution of the time it takes a certain aircraft to complete the full track. It should be noted that to limit the computational time and file size, the logging of these track completion times was bounded by the fastest and slowest time such a track is expected to be completed by any aircraft, widened by a further 20 seconds. It is thus possible that some outliers are excluded from further computation. These distribution are assumed to be normal ((D(100) = 0.07, p = 0.685) for a Boeing 737-800 flying from ARTIP to 18R at a 2.2 degree FPA). Then, the average time before landing at which the trailing aircraft get within minimum separation is added to the track time distribution of the leading aircraft. The result of this is the distribution of times at which aircraft are first allowed to land since the minimum separation time has passed since the leading aircraft landed. In order to then calculate the time separation, the amount of overlap the distributions of the leading and trailing aircraft are allowed needs to be set. Since the standard deviation of most aircraft types is relatively small as long as they can abide by all speed restrictions, the value for this only has a very small influence on the resulting sequence. For these simulations 2.5% overlap was used. This means that there's a 5% chance any aircraft needs a command from an air traffic controller to ensure separation, since there's a 2.5% chance that it's too slow and a 2.5% chance that it's too fast.

The calculated time separation is different for each wind scenario. Since flight path simulation is meant to be broadly applicable, the largest separation is taken independent of which wind scenario is actually used. Thus the final result is a matrix containing the initial time separation values for every combination of two aircraft type and IAF combinations which are valid for at least 95% of all expected wind conditions. The inbound peak simulation, however, is much more specific. Here, the time separations which correspond to the wind scenario used for this simulation are used. Here, the final result is one matrix which contains the separation values for just this wind scenario.

SEQUENCE CREATION

Finally, the influence of traffic mix needs to be included. In order to do this, a random sequence of 100,000 aircraft is created. Over 10 runs, these sequences show a variance of less than 0.1 aircraft per hour. The aircraft type and IAF are distributed according to the traffic distribution at Schiphol airport. The twenty-five most used aircraft are used, which span approximately 95% of all aircraft at Schiphol and are shown in Table 5.18. For the IAFs, the distribution in 2018 was used, which means that approximately 42.0% of all aircraft arrive from ARTIP, while 30.3% enter the TMA at SUGOL and the remaining 27.4% fly by RIVER. The average capacity is then the total time needed to land these aircraft divided by the total number of aircraft. For the peak and reported capacities the full sequence is split up into 99,970 sequences of 30 aircraft. The peak capacity is then the capacity that can be attained 1% of the time. Since the reported capacity is used to tell for instance EUROCONTROL how many aircraft Schiphol will be able to land a few hours into the future, this needs to be a capacity that can be maintained most of the time. Therefore, the reported capacity was chosen to be the capacity that 90% of all sequences can exceed.

Table 5.18: Aircraft Type Distribution

Aircraft Type	Percentage of Fleet
B738	21.7
E190	13.7
A320	10.7
B737	8.5
A319	6.4
E75L	5.9
A333	3.1
A321	2.7
E170	2.6
B744	2.5
B77W	2.4
B772	2.1
B739	2.0
B789	1.8
B763	1.6
A332	1.5
B77L	1.3
DH8D	1.2
F100	0.6
B788	0.6
CRJ9	0.5
A20N	0.5
B748	0.5
B733	0.5
E195	0.4

As stated above, the reported capacity is used a few hours in advance when the exact conditions are not know yet. Therefore this capacity is calculated as a function of only the flight path angle for each runway. Since the average and maximal capacity are more related to how the actual aircraft land when they arrive, this is not only calculated for each runway and FPA, but also for each wind scenario.

5.4.2. Speed Authority

While the percentage of the fleet that can abide by all speed restrictions at a certain descent angle gives a reasonably good indication of the operational robustness at this angle, it does not tell the full story. The difficulty of controlling a certain procedure is greatly influenced by the amount of speed authority left for all aircraft. When an aircraft is exactly on the edge of its performance envelope, there is no room left for an ATCo to use speed to solve potential conflicts, greatly harming the efficiency of the operation and mitigating the advantages of RNAV routes. While there are more types of speed authority that could be calculated, only the most general case is used for this research. It is explained below.

Figure 5.42 shows the speed envelope that can be used during a normal approach. The constraints on it are that the aircraft must remain at 250 kts until passing FL70, must reach 220 kts at FL40, and finally pass 180 kts before the ILS intercept at 2000 ft. As stated above, the slowest track is simulated in BlueSky. It is then assumed that, although wind is taken into account, this does not change significantly between the earliest and the latest deceleration. This assumption will be further explained below. If this is assumed, the segment between FL70 and FL40 can be split into two parts: The deceleration and the constant speed part. Since the deceleration part is assumed to be the same, the only difference is in the constant speed section. The length of this constant speed section can be calculated by subtracting the horizontal distance it takes to decelerate from the horizontal distance between FL70 and FL40 (which is only dependent on the FPA). The horizontal distance of the deceleration segment is calculated based the acceleration graph. Once the length of the constant speed segment is calculated, the time difference of that part of the flight track is trivial to calculate based on the two air speeds.

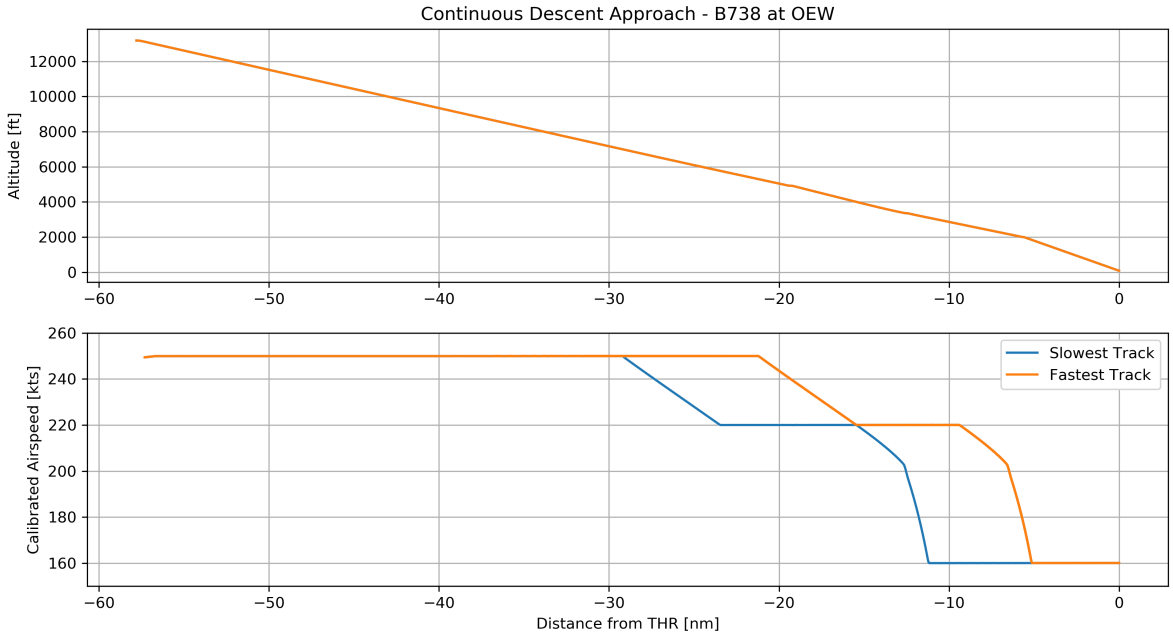

Figure 5.42: General Speed Authority Airspeed Profile

It should be noted that the assumption that the earliest deceleration is the same as the latest deceleration does not hold when an ATCo still has a lot of authority over an aircraft, it is fairly accurate when aircraft reach their performance limits. When there are only a few seconds left during which an aircraft can still maintain a higher speed, this small time difference between the starts of the decelerations does not make a significant difference.

5.4.3. Fuel Usage

The fuel usage is calculated according to BADA 3.12's methodology with one small change. Due to the performance model changes described in Section 5.3.1, the thrust is calculated differently. For all phases of the approach, a minimal fuel consumption is determined in BADA. However, due to the assumption that the part of the drag that is lost due to the missing flap settings, is compensated by lowering the minimal thrust to 0. Since lowering the thrust setting also lowers the calculated fuel consumption, this needs to be compensated. In order to do this, the minimal, idle fuel consumption is added to the thrust based fuel consumption. The average fuel usage is calculated for an entire sequence as used to calculate the average and peak capacity.

5.4.4. Noise Production

In the Netherlands there are currently two models to simulate aircraft noise pollution. The first is the Dutch "Nederlands RekenModel" (NRM), [22] while the second is the (ECAC) Doc. 29 model. [14–16] The ECAC model was implemented to increase the uniformity in the noise calculations of all European airports, which is also why Schiphol has started using it. [5] For these reasons, this research uses the Doc. 29 model created by M.A. Heilig for his Master's Thesis. [21] This model uses ANP version 2.2[1] (released on Feb 22, 2018). For each simulation, standard atmospheric conditions are assumed. Wind is also not taken into account in this model. [21]

When an aircraft type is not contained in the ANP, generally, the parameters of a similar aircraft type are used as a substitution. The only aircraft type for which this is not possible in this research is the Dash 8 Q400 (DH8D). The closest match in the ANP is the Q100 version with the Q200 engines, which is thus what it is substituted by. The problem here is that these engines have a max thrust that is 40% of that of the Q400 engines. This thus greatly overestimates the noise production as the model assumes that the engines are running at 60% thrust instead of the approximately 20% similar aircraft use. The choice was made to ignore this aircraft type for the noise simulations as it only accounts for 1.2% of the total fleet.

The effect of FPA on all metrics is measured as the surface area of certain contours. Since the noise is calculated on a 120 x 110km rectilinear grid with a spatial resolution of 1 x 1km, the surface area is calculated by counting the number of datapoints that exceed a certain threshold. Three metrics will be used to measure the noise impact of different FPA CDAs. Each of these metrics uses two thresholds to ensure that both the impact on low and high noise

[1] Retrieved from www.aircraftnoisemodel.org/home

levels is measured. In real life, one of the most important metrics for measuring noise pollution around an airport is the L_{DEN} contour, which penalises noise produced during the night and evening. However, due to the way in which the sequence is created, the drop in landing slot demand during the evening and night are not simulated, resulting in the exact same capacity at 3:00 am as at 8:30 am. As such, this penalty during the evening and night would not result in a representative contour. As such, the L_{DEN} contour is being approximated by L_{24h}, which is calculated in the same way but without the penalties. The thresholds for the L_{24h} contours are set to 60 and 70dB.
The second metric is the peak noise, this shows the area from which aircraft can be heard. Additionally, this also gives an indication of where people could be disturbed. For the peak noise, the comparison thresholds are set at 80 and 100dB.
Finally, the number of peaks per hour gives an indication of how often conversation volume (70dB) is reached by aircraft flyovers. This also gives an indication of the amount of nuisance that is produced. The threshold here was set to 10 and to 30 aircraft per hour.

For the noise simulations a sequence of 100,000 aircraft is used. Over 25 iterations this results in up to 1.6% spread in the L_{24h} areas. For the peak noise areas this spread is smaller than $1km^2$ and thus 0% and the area within which at least 10 aircraft per hour produce over 70dB varies by 0.3%.

6
Results

The results of both simulations are discussed in this chapter. First, in Section 6.1, the capacity, speed authority, fuel usage, and noise production results during the flight path simulation are discussed. Finally, in Section 6.2, the comparison between constant descent and stepped approaches is done.

6.1. Flight Path Simulation Results

The results of the flight path simulation are explained below. The effect of FPA on capacity, speed authority, fuel usage, and noise perfromance is explained here.

6.1.1. Capacity

The average and peak capacity is calculated for each combination of runway, FPA, and wind scenario. Meanwhile the reported capacity was made independent of the actual wind scenario, as the capacity reported to EUROCONTROL mainly depends on the chosen runway configuration. It should be noted that the calculation results are highly dependent on the methodology. Although these values can be used to give an indication of the impact of different design decisions, the absolute value of the capacity should be taken with a grain of salt. This is caused by the fact that only the separation is only checked at the end of the track. While this is valid for straight routes, where the only manner in which a pair of aircraft can get closer together is due to the deceleration, this is not true when there are turns in the route. When there are turns, the minimum separation is reached during such a turn because then the in-track separation is no longer the actual separation.

The capacity distributions for runways 06 and 27 are shown in stacked histograms in Figures 6.1 and 6.2.

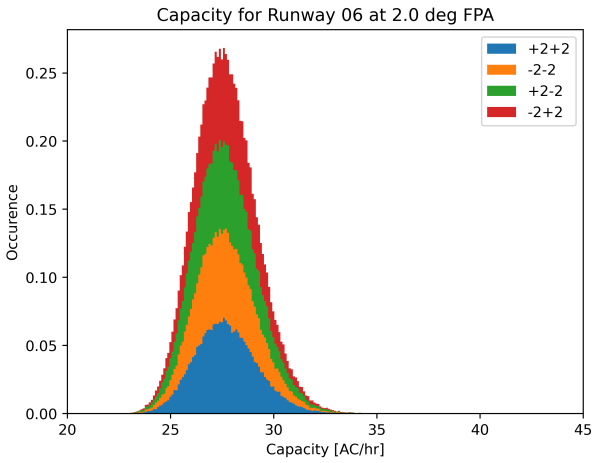

Figure 6.1: Capacity Distribution for Runway 06 at a 2.0 degree FPA

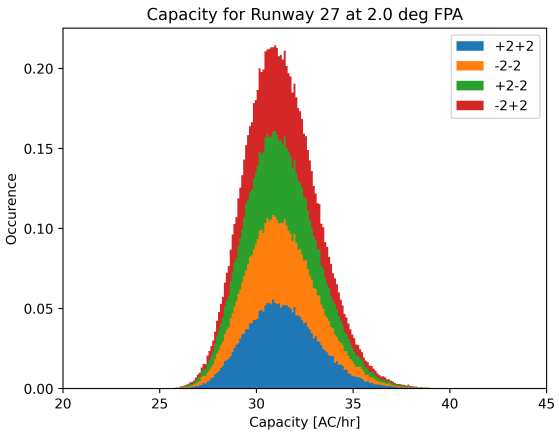

Figure 6.2: Capacity Distribution for Runway 27 at a 2.0 degree FPA

As Figures 6.1 and 6.2 show, there can be a large difference in both the average capacity as well as the possible deviation from this average capacity. The magnitude is mainly determined by the runway choice, not the choice of FPA. This is also shown in the reported capacity in Table 6.1.

Table 6.1: Reported Capacity for Runways 06 and 27

FPA [Deg]	**Reported Capacity for Runway 06** [AC/hr]	**Reported Capacity for Runway 27** [AC/hr]
2.0	25.8	29.0
2.1	25.9	29.1
2.2	26.0	29.2
2.3	26.0	29.0
2.4	25.9	28.8
2.5	25.8	28.3

The reported capacities shown in Table 6.1 are the extremes. Runway 06 has the lowest reported capacity at each FPA while runway 27 has the highest. This shows that much of the capacity is determined by the combination of the wind scenario and the routes, independent of the FPA. For most runways, both the reported and average capacity increase between 2.0 and 2.2 degree FPA and start to decrease for steeper flight path angles. This can also be seen in Figure 6.3.

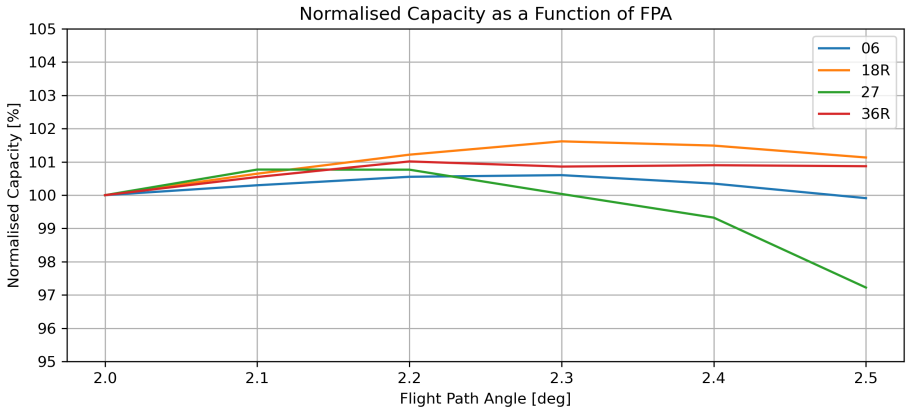

Figure 6.3: Normalised Average Capacity as a Function of Flight Path Angle for each Runway

The slight increase in capacity between 2.0 and 2.2 degrees shown in Figure 6.3 can be explained by the fact that as the FPA increases, the average speed also increases, both due to a decrease in the deceleration performance of all aircraft and due the fact that at higher altitudes, the same calibrated air speed results in a higher true air speed. At higher FPAs, however, a significant portion of the aircraft stop being able to comply with all speed restrictions. This means that some aircraft start to finish the track much more quickly, while others stick to their normal schedule, widening the range times during which aircraft of a certain type can arrive and thus starting to lower the capacity.

The average and peak capacity are calculated for each wind scenario separately. While the reported capacity can be used to inform for instance EUROCONTROL how many aircraft can most likely be landed hours in advance, when the actual winds are not known yet, the average and peak capacity shed more light on the actual day to day operation. The maximal, median, and minimal average capacities, as well as their respective peak capacities are shown in Tables 6.2 through 6.4.

Table 6.2: Highest Reported, Average, and Peak Capacity per FPA for Runway 27, Wind Scenario -2-2

Flight Path Angle [Deg]	**Reported Capacity** [AC/hr]	**Average Capacity** [AC/hr]	**Peak Capacity** [AC/hr]
2.0	29.0	31.2	36.1
2.1	29.1	31.5	36.4
2.2	29.2	31.5	36.4
2.3	29.0	31.2	35.9
2.4	28.8	31.0	35.8
2.5	28.3	30.3	34.9

Table 6.3: Median Reported, Average, and Peak Capacity per FPA for Runway 18R, Wind Scenario -2+2

Flight Path Angle [Deg]	**Reported Capacity** [AC/hr]	**Average Capacity** [AC/hr]	**Peak Capacity** [AC/hr]
2.0	28.4	30.2	34.4
2.1	28.5	30.4	34.8
2.2	28.7	30.6	34.7
2.3	28.8	30.6	34.6
2.4	28.8	30.7	34.6
2.5	28.7	30.6	34.6

Table 6.4: Lowest Average and Peak Capacity per FPA for Runway 06, Wind Scenario +2+2

Flight Path Angle [Deg]	**Reported Capacity** [AC/hr]	**Average Capacity** [AC/hr]	**Peak Capacity** [AC/hr]
2.0	25.8	27.6	31.5
2.1	25.9	27.7	31.5
2.2	26.0	27.8	31.6
2.3	26.0	27.8	31.7
2.4	25.9	27.7	31.7
2.5	25.8	27.6	31.6

Finally, the percentage difference of the reported capacity for all runways as a function of FPA is shown in Table 6.5. This shows that while there is a relation between FPA and capacity, it is not necessarily stronger than that of the choice of runway with certain winds.

Table 6.5: Percentage Difference of Reported Capacity as a Function of FPA for all Runways

Flight Path Angle [Deg]	**Mean Capacity Difference**	**Range of Capacity Differences**
2.0	N.A.	N.A. - N.A.
2.1	0.5%	0.5% - 0.6%
2.2	0.9%	0.8% - 1.2%
2.3	0.9%	0.1% - 1.6%
2.4	0.6%	-0.5% - 1.5%
2.5	-0.1%	-2.5% - 1.3%

6.1.2. Speed Authority

As one might expect, similar routes result in similar amounts of speed authority, as can be seen in Table 6.6, where the routes from RIVER and SUGOL result in extremely similar amounts of speed authority. Most routes are not similar enough to have this effect at all times, however. It greatly depends on the exact wind conditions, as shown in Table 6.7.

Table 6.6: Average General Speed Authority for Runway 27 at a 2.5 deg FPA

Wind Scenario	**Initial Approach Fix**	**Average General Speed Authority** [s]
+2+2	ARTIP	27.7
	RIVER	32.5
	SUGOL	33.3
+2-2	ARTIP	28.9
	RIVER	34.4
	SUGOL	36.0
-2+2	ARTIP	17.8
	RIVER	23.6
	SUGOL	23.5
-2-2	ARTIP	21.8
	RIVER	34.3
	SUGOL	34.7

Table 6.7: Average General Speed Authority for Runway 06 at a 2.0 deg FPA

Wind Scenario	Initial Approach Fix	Average General Speed Authority [s]
+2+2	ARTIP	55.5
	RIVER	43.3
	SUGOL	48.2
+2-2	ARTIP	49.6
	RIVER	62.9
	SUGOL	63.3
-2+2	ARTIP	56.9
	RIVER	37.8
	SUGOL	45.0
-2-2	ARTIP	52.5
	RIVER	40.7
	SUGOL	56.6

Since the speed authority is how much an air traffic controller can still control the arrival time of an aircraft in the TMA, an aircraft that does not comply by all speed restrictions does not have any. Therefore which aircraft are included in the average and minimum speed authorities changes with FPA. While an aircraft may be able to abide by all speed restrictions at 2.0 degrees, this is often not the case at 2.5 degrees. This is not true for the maximal time authority, however, which is why the maximal time authority will be used for comparison between FPAs. The effect of different FPAs on the general authority varies significantly between runways and IAFs as shown in Table 6.8 and Table 6.9.

Table 6.8: Maximal Time Authority Difference Range as a Function of FPA for all Runways starting at SUGOL

Flight Path Angle [Deg]	Time Authority Mean Difference	Range of Time Authority Differences
2.0	N.A.	N.A. - N.A.
2.1	-5.8%	-4.5% - -9.4%
2.2	-11.0%	-8.9% - -16.3%
2.3	-15.0%	-12.6% - -21.2%
2.4	-19.9%	-17.3% - -26.9%
2.5	-24.3%	-20.8% - -33.0%

Table 6.9: Maximal Time Authority Difference Range as a Function of FPA for all IAFs ending at Runway 36R

Flight Path Angle [Deg]	Time Authority Mean Difference	Range of Time Authority Differences
2.0	N.A.	N.A. - N.A.
2.1	-5.8%	-4.4% - -7.3%
2.2	-11.1%	-7.7% - -12.8%
2.3	-16.0%	-13.2% - -18.3%
2.4	-21.0%	-18.4% - -24.1%
2.5	-25.5%	-22.0% - -28.8%

As such, significantly different percentages should be used for each runway and IAF combination. The median case occurs for aircraft flying from SUGOL to 27, which is shown in Table 6.10.

Table 6.10: Maximal Time Authority Difference Range as a Function of FPA for Runway 27 from SUGOL

Flight Path Angle [Deg]	Time Authority Mean Difference	Range of Time Authority Differences
2.0	N.A.	N.A. - N.A.
2.1	-6.6%	-5.0% - -9.4%
2.2	-12.1%	-9.9% - -16.3%
2.3	-16.3%	-13.8% - -21.2%
2.4	-21.2%	-18.3% - -26.9%
2.5	-25.9%	-22.1% - -33.0%

Additionally, the percentage of aircraft that can comply with all speed restrictions varies wildly between routes. While

only 1.3% of aircraft cannot comply with the route from SUGOL to 06 at a 2.5 degree FPA, 76.4% of aircraft could not comply with the ARTIP to 27 route. The median route in this regard is the route from RIVER to 27 with the -2-2 wind scenario, the performance of which is shown with the range of percentages next to it in Table 6.11.

Table 6.11: Percentage of Aircraft that can comply with all Restrictions

Flight Path Angle [Deg]	**Median Route Percentage of Aircraft that Comply**	**Percentage of Aircraft that Comply**
2.0	100%	94.9% - 100%
2.1	100%	92.2% - 100%
2.2	96.8%	86.3% - 100%
2.3	95.4%	82.4% - 100%
2.4	91.4%	46.4% - 100%
2.5	87.5%	23.6% - 99.0%

6.1.3. Fuel Usage

Like the average and peak capacity, the average fuel usage is calculated for a sequence of 100,000 for each runway and wind scenario combination. Generally, there are two situations for the wind. The first case is shown in Table 6.12, where, for most of the approach, aircraft arriving from ARTIP have either a very strong head or a very strong tail wind, resulting in either extremely high or extremely low fuel usage. The second case is shown in Table 6.13, where, at altitude, the head and tail winds are combined with a crosswind. This results in relatively little variance in the fuel consumption.

Table 6.12: Fuel Consumption at Runway 06

Wind Scenario	**Average Fuel Usage at 2.0 deg FPA** [kg/AC]	**Average Fuel Usage at 2.5 deg FPA** [kg/AC]
+2+2	462	356
+2-2	552	448
-2+2	438	333
-2-2	467	360

Table 6.13: Fuel Consumption at Runway 18R

Wind Scenario	**Average Fuel Usage at 2.0 deg FPA** [kg/AC]	**Average Fuel Usage at 2.5 deg FPA** [kg/AC]
+2+2	504	389
+2-2	492	377
-2+2	490	377
-2-2	488	374

On average, the fuel consumption difference between a 2.0 degree FPA and a 2.5 degree FPA is approximately 22%, with the a maximum of 24% and a minimum of 19%. This difference is shown for the median case, runway 06, in Table 6.14.

Table 6.14: Fuel Savings Range as a Function of FPA

Flight Path Angle [Deg]	**Mean Percentage of Fuel Saved**	**Range of Percentage of Fuel Saved**
2.0	N.A.	N.A. - N.A.
2.1	-4.4%	-3.6% - -5.0%
2.2	-8.4%	-7.3% - -9.3%
2.3	-12.7%	-11.1% - -14.0%
2.4	-17.3%	-15.1% - -19.0%
2.5	-21.5%	-19.3% - -23.0%

6.1.4. Noise Production

The size of any noise contour is highly dependent on both the length of a certain track and the wind direction. In general, tail winds result in the best noise performance because when close to the ground, this reduces the thrust setting and thus the noise production as the aircraft still follows the same route. Meanwhile shorter tracks also result in much smaller areas because there is simply less ground to cover. In order to consolidate the results, the areas of

each contour will be averaged over all wind scenarios, while inter-runway comparisons are only done as a percentage change with respect to a 2.0 degree FPA.

L_{24H} CONTOUR

The L_{24h} contours for runway 27 at a 2.0 degree FPA is shown in Figure 6.4. While the difference between this and the 2.5 degree contour is shown in Figure 6.5, where a negative value means a decrease in noise. The magenta lines show the flight tracks at a 2.0 degree FPA. Figure 6.5 shows that, as expected, the noise decreases everywhere between 2.0 and 2.5 degrees. Although the difference between these two FPAs seems rather small, as it is less than 3 dB, the lowest difference that is discernible to the human ear, this still results in a large difference in the area of the contours, as shown in Table 6.16.

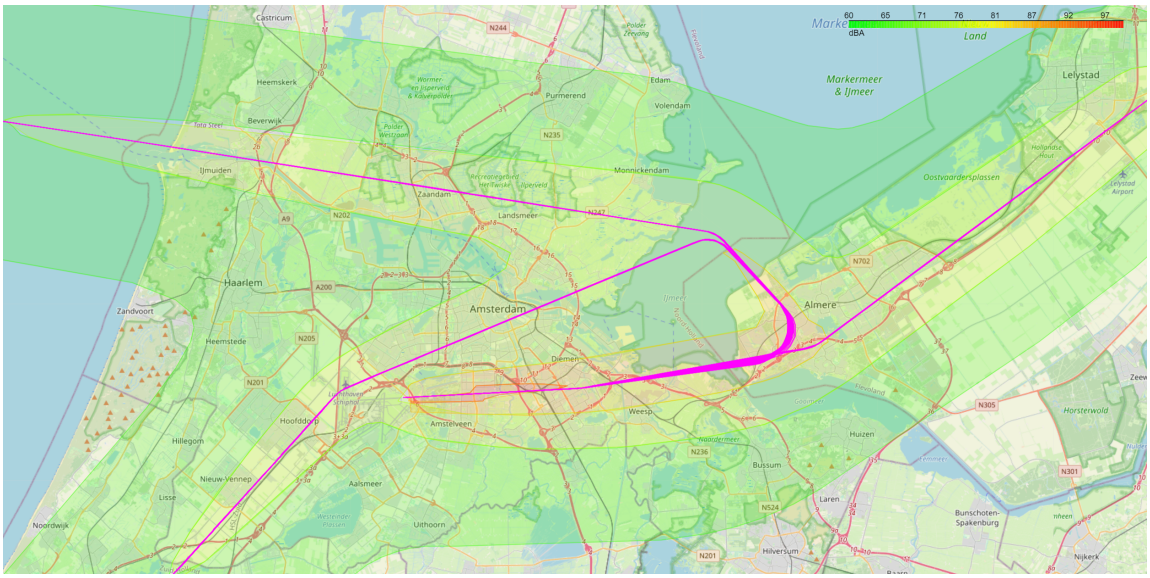

Figure 6.4: L_{24h} Contour for Runway 27 at 2.0 degree FPA

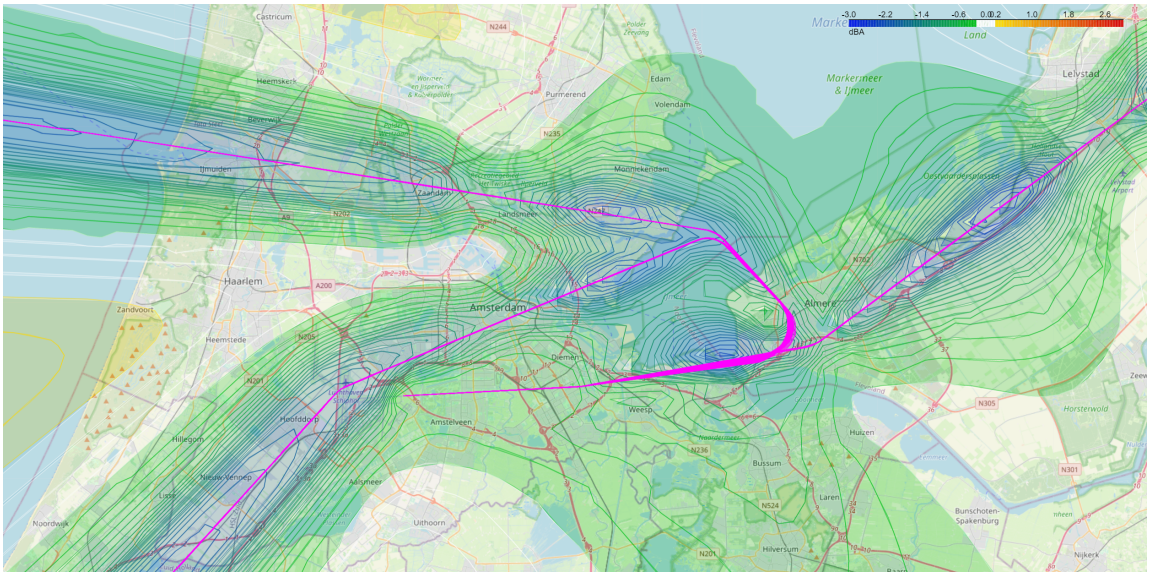

Figure 6.5: Difference between the L_{24h} Contours for Runway 27 at 2.0 and 2.5 degrees

Figure 6.5 shows something counter-intuitive, which can be seen more clearly in Section 6.1.4. Near Zandvoort and Castricum, increasing the FPA from 2.0 to 2.5 degrees actually increase the average noise in these locations. This is caused by the fact that noise attenuation doesn't only depend on distance from the source but also on the elevation angle. This results in the counter-intuitive situation where flying lower can actually increase the size of L_{24h} areas.

This is caused by the directivity of aircraft noise and the roughness of the ground and is thus location and aircraft dependent.

Table 6.15: Area of the L_{24h} Contours for Runway 27 as a Function of FPA

Flight Path Angle [deg]	**L_{24h} Contour Area at 60 dB** [km^2]	**L_{24h} Contour Area at 70 dB** [km^2]
2.0	3516	838
2.1	3518	802
2.2	3526	773
2.3	3499	737
2.4	3477	707
2.5	3419	668

Table 6.16: Normalised Area of the L_{24h} Contours for Runway 27 as a Function of FPA

Flight Path Angle [deg]	**Norm. L_{24h} Contour Area at 60 dB** [km^2]	**Norm. L_{24h} Contour Area at 70 dB** [km^2]
2.0	N.A.	N.A.
2.1	0.5%	-4.5%
2.2	-0.1%	-9.8%
2.3	-1.3%	-16.1%
2.4	-1.5%	-19.7%
2.5	-3.5%	-25.0%

The overall impact of increasing the FPA on the L_{24h} contours is shown in Figures 6.17 and 6.18 below.

Table 6.17: Normalised Areas of the L_{24h} 60dB Contours for all Runways

Flight Path Angle [Deg]	**Mean L_{24h} 60 dB Contour Area Change**	**Range of L_{24h} Contour Area Change**
2.0	N.A.	N.A. - N.A.
2.1	0.1%	0.4% - -0.3%
2.2	0.3%	0.7% - -0.1%
2.3	-0.5%	0.1% - -1.1%
2.4	-1.1%	-0.7% - -1.8%
2.5	-2.8%	-2.1% - -3.4%

Table 6.18: Normalised Areas of the L_{24h} 70dB Contours for all Runways

Flight Path Angle [Deg]	**Mean L_{24h} 70 dB Contour Area Change**	**Range of L_{24h} Contour Area Change**
2.0	N.A.	N.A. - N.A.
2.1	-4.3%	-3.5% - -5.2%
2.2	-7.8%	-6.2% - -8.7%
2.3	-12.0%	-10.4% - -13.4%
2.4	-15.6%	-14.5% - -16.9%
2.5	-20.3%	-18.4% - -22.3%

PEAK NOISE CONTOUR

The peak noise (PN) contours for runway 18R focusing on the ARTIP approach at a 2.0 degree FPA are shown in Figure 6.6, while the difference between the contours at 2.0 and 2.5 degrees is shown in Figure 6.7 with negative values denoting a decrease in noise. The magenta lines show the flight tracks at a 2.0 degree FPA. While the high decibel contours become smaller as FPA increases, as is intuitive, this is not necessarily true for the low decibel contours. Due to the fact that the noise attenuation isn't only a function of the distance from the source, but also elevation angle, it is possible for the attenuation due to elevation angle to outweigh the attenuation due to distance. This means that steeper approaches can result in more noise further out in some locations for some aircraft due to the directivity of noise source as well as the roughness of the ground. This is clearly shown towards the sides of the approach, where up to a 1 dB peak noise difference can be seen on the north and south sides of Figure 6.7.

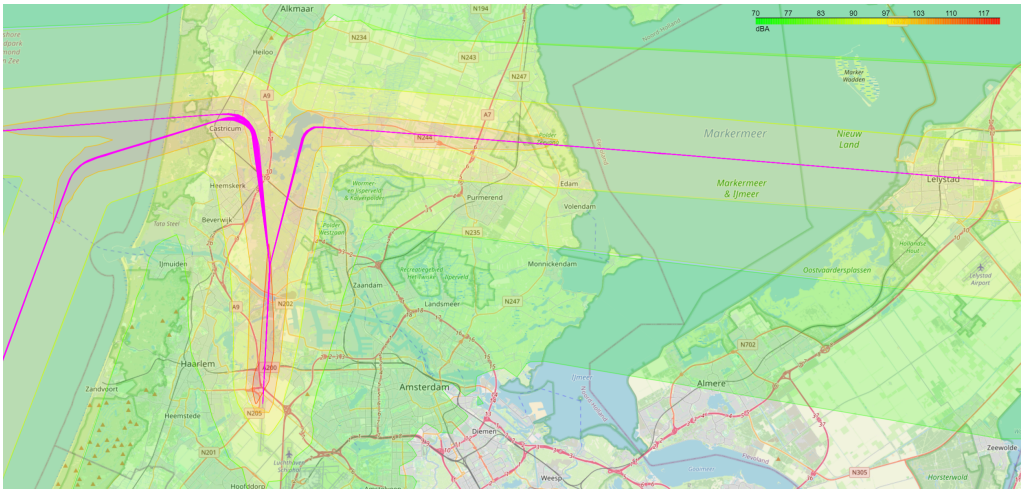

Figure 6.6: Peak Noise Contour for Runway 18R at 2.0 degree FPA focusing on the ARTIP Approach

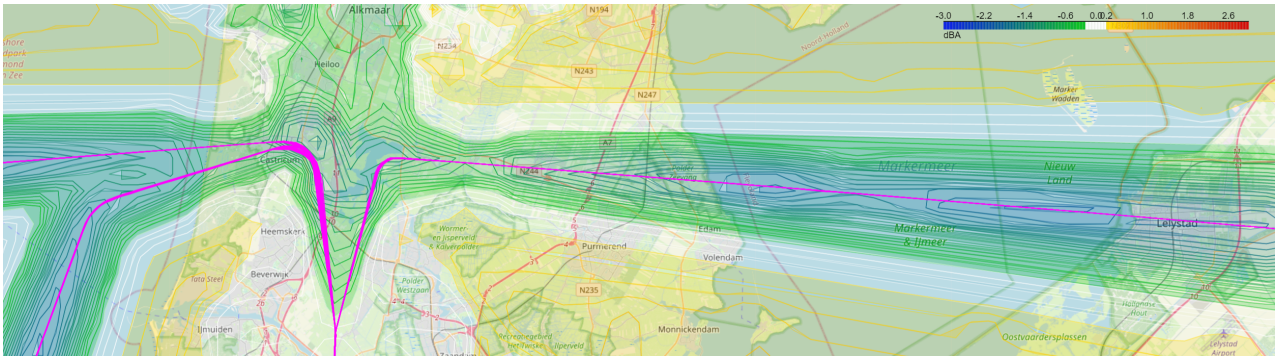

Figure 6.7: Peak Noise Difference between 2.0 and 2.5 degree FPA

The difference between the high and low decibel contours becomes more clear when looking at the actual areas themselves, as seen in Tables 6.19 and 6.20. While the 80 dB noise contour increases by up to about 2% when increasing FPA, the size of the 100 dB noise contour reduces by over 16%.

Table 6.19: Area of the Peak Noise Contours for Runway 18R as a Function of FPA

Flight Path Angle [deg]	**Peak Noise Contour Area at 80** dB [km^2]	**Peak Noise Contour Area at 100** dB [km^2]
2.0	3460	177
2.1	3481	172
2.2	3497	165
2.3	3513	159
2.4	3524	152
2.5	3532	147

Table 6.20: Normalised Area of the Peak Noise Contours for Runway 18R as a Function of FPA

Flight Path Angle [deg]	**Norm. PN Contour Area at 80** dB [km^2]	**Norm. PN Contour Area at 100** dB [km^2]
2.0	N.A.	N.A.
2.1	0.6%	-2.7%
2.2	1.0%	-6.7%
2.3	1.5%	-9.4%
2.4	1.7%	-13.4%
2.5	2.1%	-16.3%

The range of the peak noise area changes as a function of FPA is shown in Tables 6.21 and 6.22.

Table 6.21: Normalised Areas of the PN 80dB Contours for all Runways

Flight Path Angle [Deg]	**Mean PN 80 dB Contour Area Change**	**Range of PN Contour Area Change**
2.0	N.A.	N.A. - N.A.
2.1	0.5%	0.2% - 0.6%
2.2	1.0%	0.9% - 1.1%
2.3	1.4%	1.1% - 1.6%
2.4	1.8%	1.7% - 1.9%
2.5	2.0%	1.8% - 2.2%

Table 6.22: Normalised Areas of the PN 100dB Contours for all Runways

Flight Path Angle [Deg]	**Mean PN 100 dB Contour Area Change**	**Range of PN Contour Area Change**
2.0	N.A.	N.A. - N.A.
2.1	-6.7%	-6.2% - -7.1%
2.2	-11.7%	-10.3% - -13.3%
2.3	-13.7%	-11.9% - -15.6%
2.4	-18.2%	-16.7% - -19.5%
2.5	-21.5%	-18.6% - -24.2%

NUMBER OF PEAKS CONTOUR

The Number of Peaks (NoP) per hour is especially interesting because it is very dissimilar from the other two noise metrics. The number of peaks per hour for runway 18R at a 2.0 FPA can be seen in Figure 6.8 and the difference between that and the 2.5 degree case can be seen in Figure 6.9. Here, a negative value means that the number of peaks per hour has decreased. It should be noted that the difference was smoothed using a convolution filter where all four of the directly adjacent values together account for 50% of the weight, while the central value accounts for the other 50%. This was done to filter out some of the simulation artifacts that can be seen towards the edges of the contours. The magenta lines show the flight tracks at a 2.0 degree FPA.

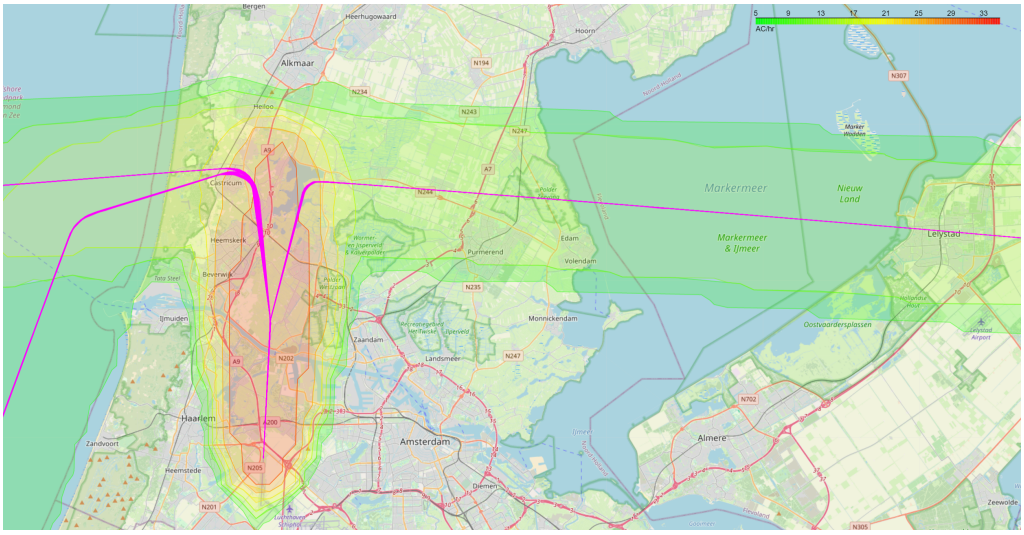

Figure 6.8: Number of Peaks Contour for Runway 06 at 2.0 degree

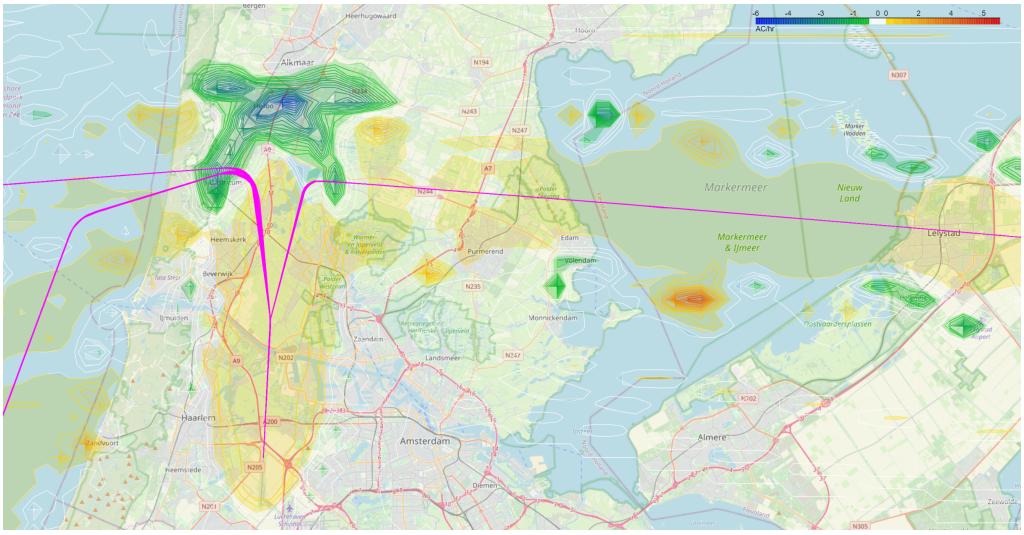

Figure 6.9: Number of Peaks Difference Difference between 2.0 and 2.5 degree FPA

The number of peaks isn't only a function of aircraft noise but also of the capacity. As such, up to a 1% increase at 2.2 degrees and a 3% decrease at 2.5 degrees to the number of peaks is caused by the capacity difference as a function of FPA. This does not explain the full variation seen especially in the 30 AC/hr contours in Tables 6.23 and 6.24. Finally, it should be noted that although the number of peaks underneath the track tends to increase slightly, behind the turn to final there's a big decrease in the number of peaks. Because the threshold for counting the number of peaks is set to 60 dB, when the base L_{24h} value is just above this, it is relatively easy to reduce it underneath this value. This is when happens at the turn for final. Much of the sound of an aircraft propagates towards its rear. This means that when the FPA is increased and the noise is reduced, much of this reduction happens behind where the aircraft would normally fly. This can also be seen in Figure 6.7, where behind and underneath each straight segment there's a reduction in peak noise. However, most of the time, aircraft fly directly over this area, putting the L_{24h} value there over 70 dB. The only place where this is not the case is at the turn for final, where all aircraft need to perform a roughly 90 $degree$ turn, independent of which IAF they arrived from. This means that the L_{24h} value close to the track can actually be close to this 60 dB threshold such that when it is reduced even slightly due to the increase in FPA, it drops below the it.

Table 6.23: Area of the Number of Peaks Contours for Runway 18R as a Function of FPA

Flight Path Angle $[deg]$	**NoP Contour Area at 10** AC/hr $[km^2]$	**NoP Contour Area at 30** AC/hr $[km^2]$
2.0	1114	149
2.1	1147	149
2.2	1115	149
2.3	1144	145
2.4	1143	144
2.5	1138	142

Table 6.24: Normalised Area of the Number of Peaks Contours for Runway 18R as a Function of FPA

FPA $[deg]$	**Norm. NoP Contour Area at 10** AC/hr $[km^2]$	**Norm. NoP Contour Area at 30** AC/hr $[km^2]$
2.0	N.A.	N.A.
2.1	3.0%	0%
2.2	1.0%	0%
2.3	2.7%	-2.7%
2.4	2.6%	-3.4%
2.5	2.2%	-4.7%

The impact of FPA on the peak noise area varies quite significantly between runways, this is largely caused by the altitude at which routes merge. For runway 27, the RIVER and SUGOL routes merge relatively early. This means that from a relatively high altitude approximately 60% of all aircraft are following the same route, which thus results in

a much larger variation in number of peaks contour area than for runway 06, for example, where the aircraft don't merge until their base turn. This variation is also seen in Tables 6.25 and 6.26.

Table 6.25: Normalised Areas of the Number of Peak 10 Aircraft per Hour Contours for all Runways

Flight Path Angle [Deg]	**Mean NoP 10 AC/hr Contour Area Change**	**Range of NoP Contour Area Change**
2.0	N.A.	N.A. - N.A.
2.1	1.6%	0.9% - 2.0%
2.2	2.2%	1.6% - 3.0%
2.3	1.3%	0.6% - 2.3%
2.4	0.2%	-0.7% - 1.0%
2.5	-8.6%	-6.5% - -9.8%

Table 6.26: Normalised Areas of the Number of Peak 30 Aircraft per Hour Contours for all Runways

Flight Path Angle [Deg]	**Mean NoP 30 AC/hr Contour Area Change**	**Range of NoP Contour Area Change**
2.0	N.A.	N.A. - N.A.
2.1	-0.4%	-0.4% - -0.4%
2.2	0.3%	0.0% - 0.9%
2.3	-0.2%	-0.9% - 0.9%
2.4	-1.1%	-2.7% - 0.4%
2.5	-3.5%	-4.7% - -2.6%

6.1.5. Conclusion

Looking at Table 6.11 shows that it is not reasonable to implement any flight path angles over 2.3 degrees. While the median percentage of non-complying aircraft at 2.4 degrees is 8.6%, only 46.4% of aircraft can abide by all speed restrictions during all wind scenarios. This means that depending on the weather conditions, over one in two aircraft would be required to use their speedbrakes or be rerouted to lower the FPA slightly. Between 2.2 and 2.3 $degrees$ the difference in minimal compliance aircraft only drops by 4% to 82.4%. This is happens while on average reducing the fuel consumption by a further 4%, or 22 kg per aircraft and significantly increasing the noise reduction with respect to the 2.0 $degree$ case.

6.2. Inbound Peak Simulation

The main purpose of this simulation is to compare fixed-route continuous descent and stepped approaches. As such, the results are not necessarily directly comparable to real-life. This is for instance caused by the fact that aircraft arriving at Schiphol are currently vectored in rather than using fixed arrival routes. Additionally, as explained in Section 5.1.2, aircraft in this simulation are set to fly the routes as quickly as possible. This allows the air traffic controller module to slow them down as needed to ensure separation without pushing aircraft outside of their speed envelope. If aircraft were allowed to be sped up by the air traffic controller module, it's possible for those aircraft to be sped up so much that they no longer have enough time to slow down and would thus have to go around. Since this is not simulated, this situation should be avoided and as such, aircraft normally fly as quickly as they can and are then slowed down as needed.

6.2.1. Capacity

The capacity distributions as a function of EAT adherence is shown in Figure 6.10.

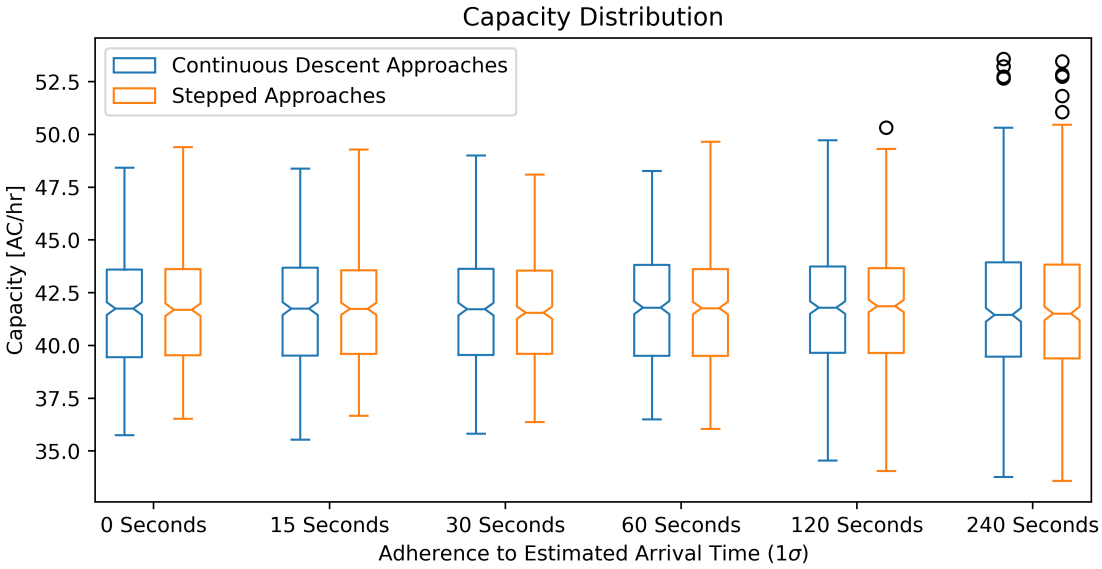

Figure 6.10: Capacity Distribution as a Function of Estimated Arrival Time Accuracy

The main conclusions based on Figure 6.10 is that the average capacity does not change significantly between stepped and continuous descent approaches and between different levels of EAT accuracy. This is to be expected as the air traffic controller module tries to regulate the flow of aircraft to not exceed safe limits. However, with decreasing EAT accuracy, the capacity starts to spread out more. This is also to be expected because if the schedule is followed very accurately, aircraft should slot into a sequence relatively well. However, as the accuracy drops, the size of gaps between aircraft as well as the size of groups of aircraft that arrive at the same time (bunches) increases. These large gaps are what starts to make the reported capacity drop while the large bunches make the peak capacity increase. This is also what causes the increase in outliers at 120 and 240 seconds of EAT inaccuracy, since some conflicts become too complex to solve for the air traffic controller module. This effect can also be seen in Table 6.27. Over 10 runs, the maximum variance of reported, mean, and peak capacity are 0.1, 0.2, and 0.8 aircraft per hour respectively.

Table 6.27: Capacity Distribution Comparison between Continuous Descent and Stepped Approaches for different Estimated Arrival Time Accuracies

EAT Accuracy (1σ) [Sec]	**Reported Capacity** [AC/hr]		**Mean Capacity** [AC/hr]		**Peak Capacity** [AC/hr]	
	CDA	Stepped	CDA	Stepped	CDA	Stepped
0	37.7	37.8	41.7	41.7	47.4	48.4
15	37.8	37.7	41.7	41.7	47.5	47.1
30	37.6	37.7	41.7	41.7	47.8	47.6
60	37.6	37.5	41.7	41.7	47.3	48.0
120	37.0	36.6	41.8	41.8	48.6	48.7
240	36.9	36.8	41.8	41.8	50.3	51.1

The capacities shown in Table 6.27 are much higher than those shown in Table 6.2. This caused by the fact that the spawn time difference between aircraft is different in each simulation. Because the flight path simulation is meant to be broadly applicable and the wind has a significant influence on the time between aircraft, the flight path simulation uses the largest time difference, independent of wind scenario, which greatly reduces the capacity for this simulation. The inbound peak simulation, however, is much more specific and as such uses the time differences that correspond to the wind scenario used for this simulation. This was done because it makes the sequence much more challenging and realistic since in a real-life inbound peak, the aircraft are planned as close together as can be done safely as well.

6.2.2. Fuel Usage

The fuel usage distributions of all aircraft as a function of EAT adherence is shown in Figures 6.11 and 6.12.

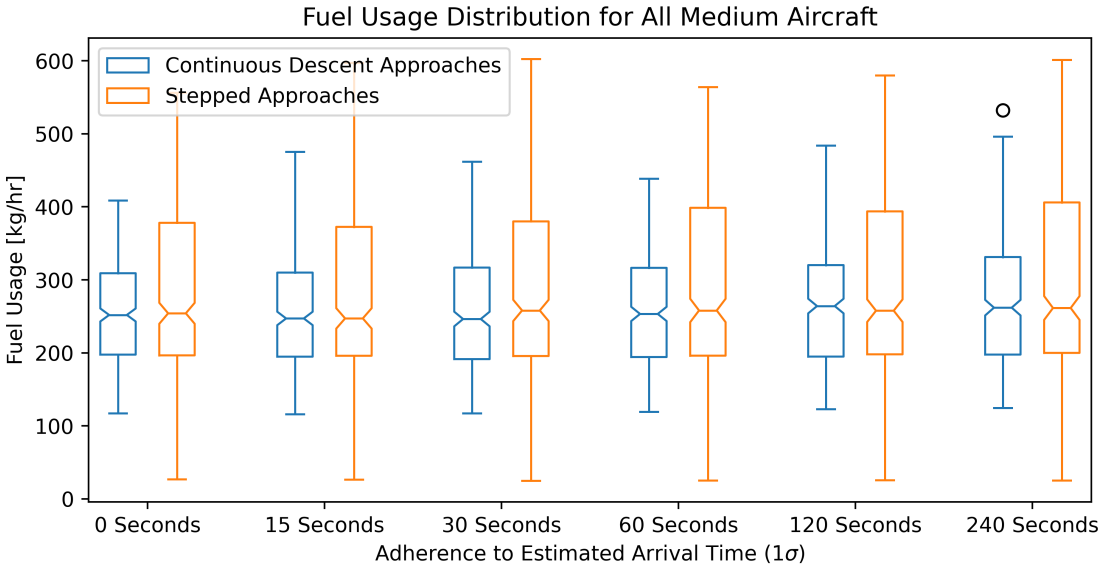

Figure 6.11: Fuel Usage Distribution as a Function of Estimated Arrival Time Accuracy for All Medium Aircraft

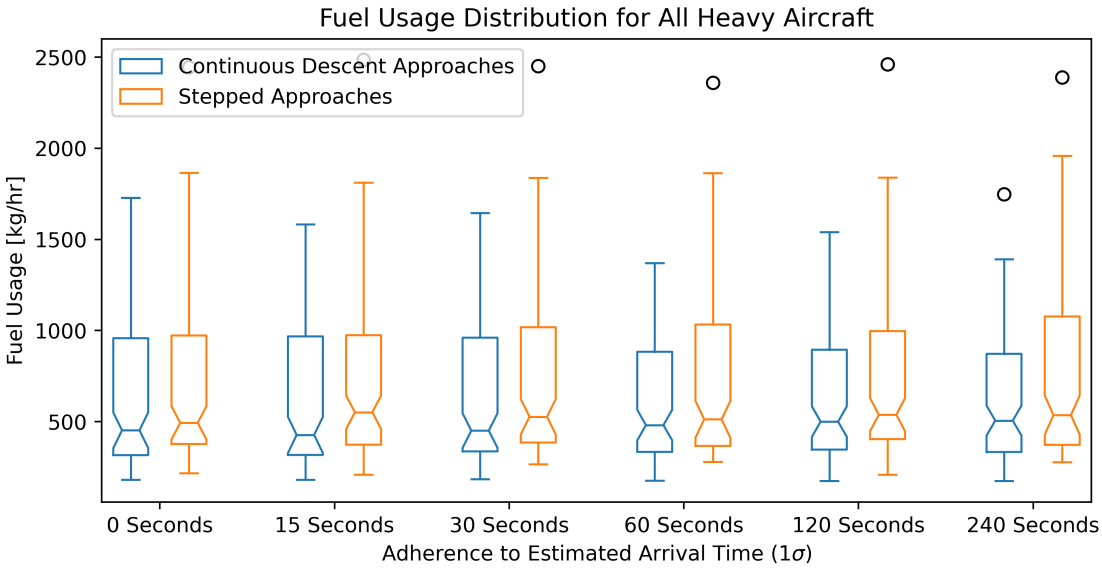

Figure 6.12: Fuel Usage Distribution as a Function of Estimated Arrival Time Accuracy for All Heavy Aircraft

While the spread shown in Figures 6.11 and 6.12 varies between different EAT adherences, overall, the continuous descent approaches have a much lower fuel usage. However, due to the fact that at a 2.3 $degree$ a number of aircraft cannot comply with all speed restrictions, the fuel usage difference is exaggerated. This is because when an aircraft is unable to comply with all speed restrictions, it often spends most of the approach trying to slow down as much as possible and thus at idle thrust, which means that these aircraft use extremely little fuel. This effect is amplified by the fact that these are some of the most fuel hungry aircraft in the simulation. In order to account for this, the aircraft that cannot comply with all speed restrictions are filtered out. The resulting difference is still slightly larger than it would be in real-life because the non-complying aircraft then would require path stretching, which would increase the amount of track miles and thus the fuel usage. While speed brake usage could also be a tool to allow currently non-complying aircraft to comply this is outside of the scope of this research, as those are generally only used in atypical conditions, not as a part of a procedure.

The fuel usage distribution for complying medium and heavy aircraft can be seen in Figures 6.13 and 6.14, while the average fuel usage as for the different EAT adherences is shown in Table 6.28.

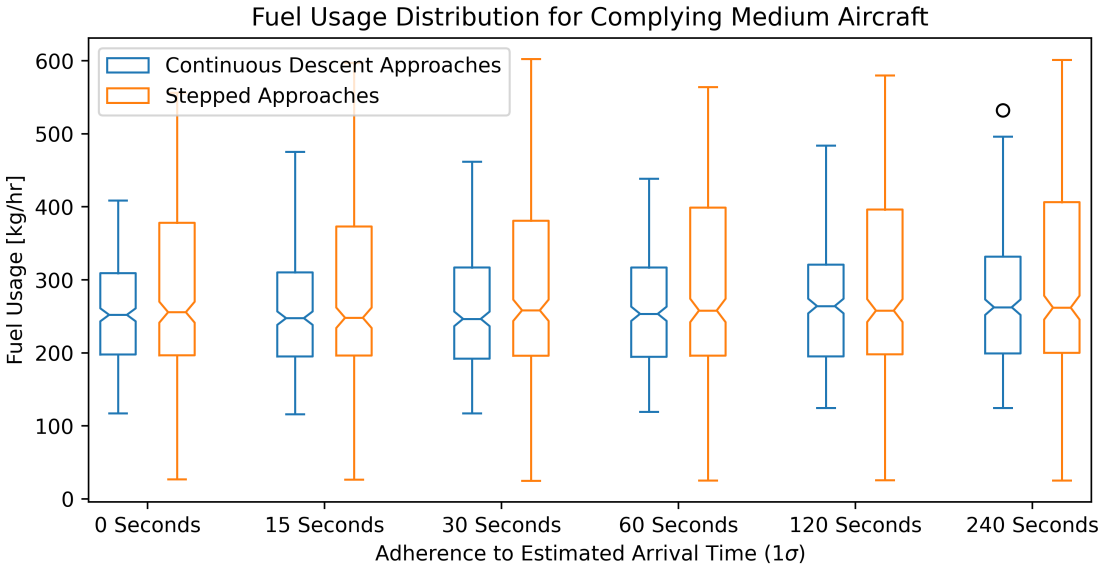

Figure 6.13: Fuel Usage Distribution as a Function of Estimated Arrival Time Accuracy for All Complying Medium Aircraft

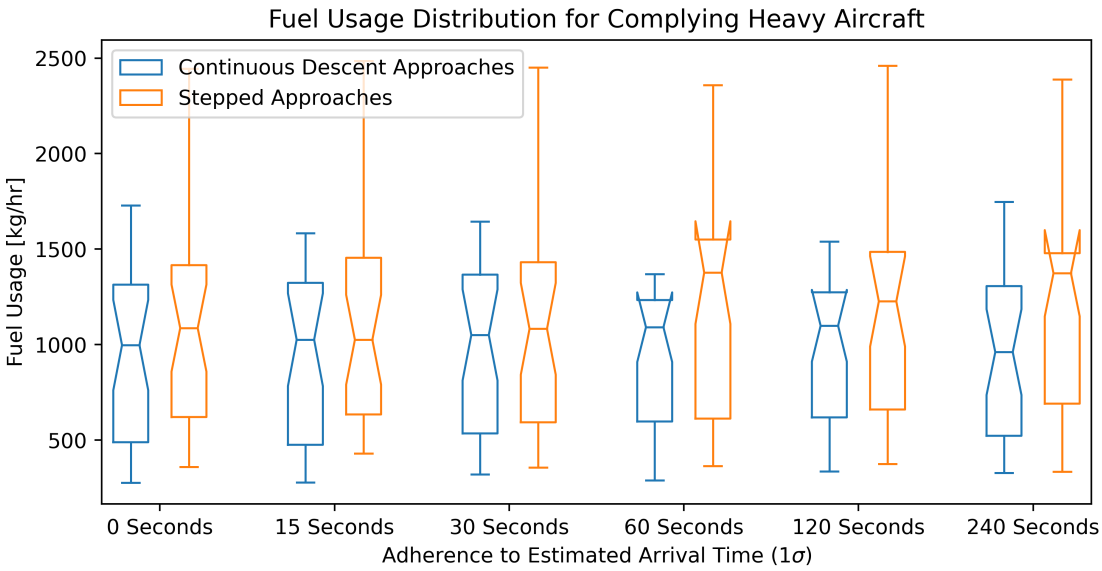

Figure 6.14: Fuel Usage Distribution as a Function of Estimated Arrival Time Accuracy for All Complying Heavy Aircraft

Table 6.28: Mean Fuel Usage for Continuous Descent and Stepped Approaches as a Function of Estimated Arrival Time Accuracy

EAT Accuracy (1σ) [Sec]	**Fuel Usage** [kg/AC]		**Difference** [–]
	Continuous Descent Approaches	**Stepped Approaches**	
0	299	341	13.6%
15	297	340	12.6%
30	299	344	12.9%
60	298	353	15.7%
120	306	351	13.0%
240	308	359	14.1%

The fuel usage shown in Table 6.28 varies relatively significantly. This is caused by the relatively small sequence

length of 500 aircraft. This limit was imposed by a lack computational power. Because the sequence is small, the randomness of aircraft weight and EAT adherence results in varying results for fuel usage. On average, however, switching from stepped to continuous descent approaches results in a fuel usage reduction of almost 14%. The maximal variance of the fuel usage was found to be 15 kg per aircraft over 10 runs.

6.2.3. Noise Production

The penultimate metric in the inbound peak simulation is the noise production. The sizes of the L_{24h}, peak noise, and number of peaks contours will be discussed below.

L24H CONTOUR

The effect of EAT adherence on the L_{24h} contour for stepped approaches is shown in Figure 6.15.

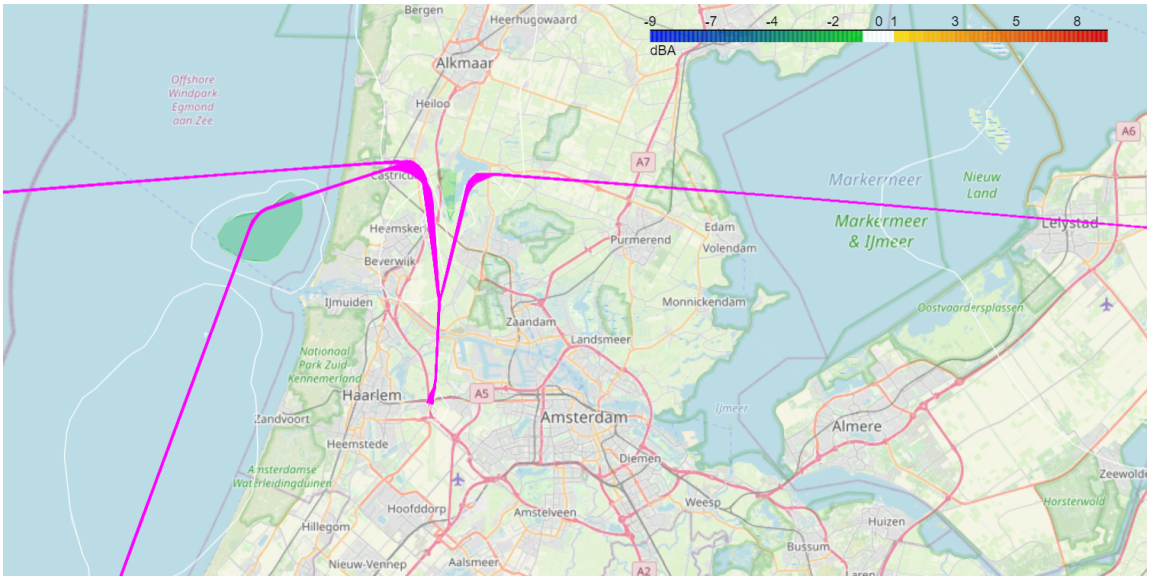

Figure 6.15: Difference between L_{24h} levels with EAT deviations of 0 and 240 seconds (1σ)

As Figure 6.15 shows, there is only a very small difference between the two L_{24h} levels. For CDAs this difference is even smaller. As a result, the impact of EAT adherence on the L_{24h} noise level is assumed to be negligible. Due to this, all further comparisons will be done with the median EAT deviation of 60 seconds.

The L_{24h} contour for continuous descent approaches can be seen in Figure 6.16, while the difference between stepped and continuous descent approaches is shown in Figure 6.17.

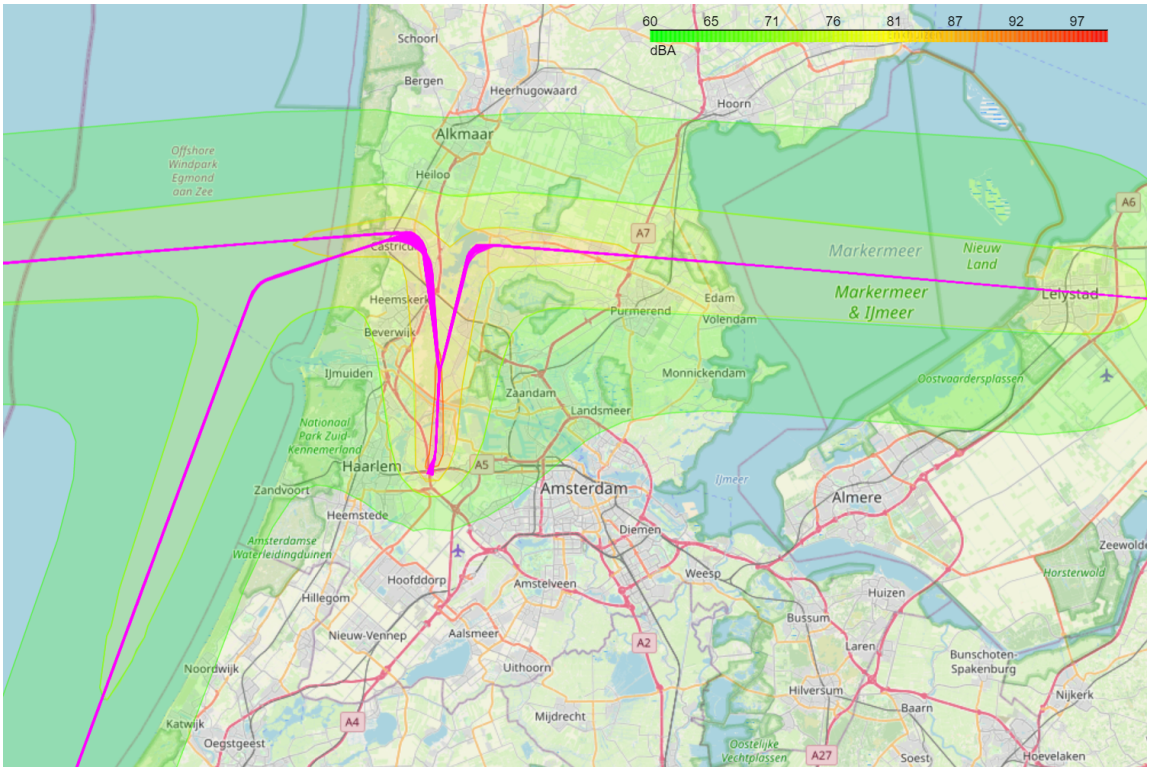

Figure 6.16: L_{24h} Contour for Continuous Descent Approaches with 60 seconds of Estimated Arrival Time Deviation (1σ)

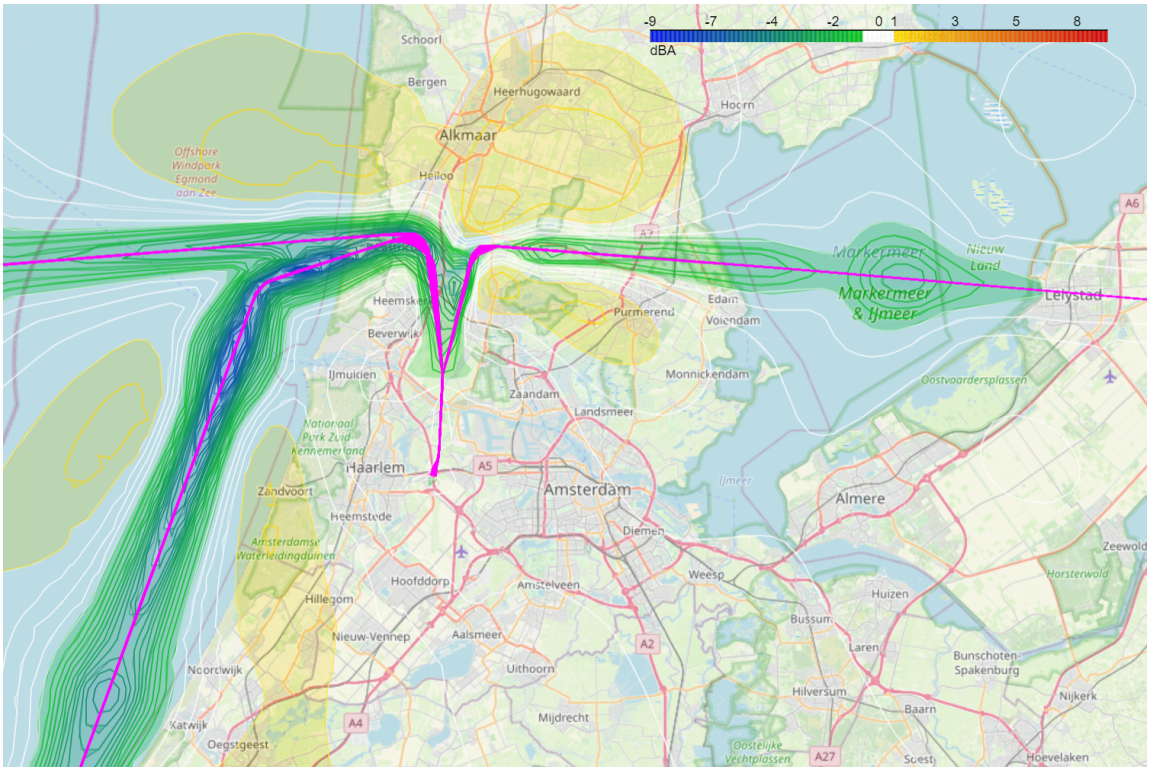

Figure 6.17: Difference between the L_{24h} Contours for Continuous Descent and Stepped Approaches with 60 seconds of Estimated Arrival Time Deviation (1σ)

In Figure 6.17, negative values represent a reduction in noise when switching from stepped to continuous descent approaches. As shown in this figures, underneath the track there is a large noise reduction the magnitude of which differs per initial approach fix. As is the case in Section 6.1.4, when further away from the track, the noise levels

actually increase when further away. This is caused by fact that noise attenuation isn't only a function of distance from the source, but also of the elevation angle. In this case, on average CDAs are significantly steeper than stepped approaches, resulting in aircraft remaining at a higher altitude for longer. As such, the size of the the $60dB$ contour increases slightly when switching to CDAs, while the size of the $70dB$ contour reduces significantly. The actual areas of these contours are shown in Table 6.29.

Table 6.29: L_{24h} Area Comparison for Continuous Descent and Stepped Approaches with 60 seconds of Estimated Arrival Time Deviation (1σ)

	L_{24h} Area $[km^2]$	
Threshold	60 dB	70 dB
Stepped Approaches	3686	1301
Continuous Descent Approaches	3736	1122
Difference [-]	1.4%	-13.8%

PEAK NOISE CONTOUR

The effect of EAT adherence on the peak noise contour for continuous descent approaches is shown in Figure 6.18.

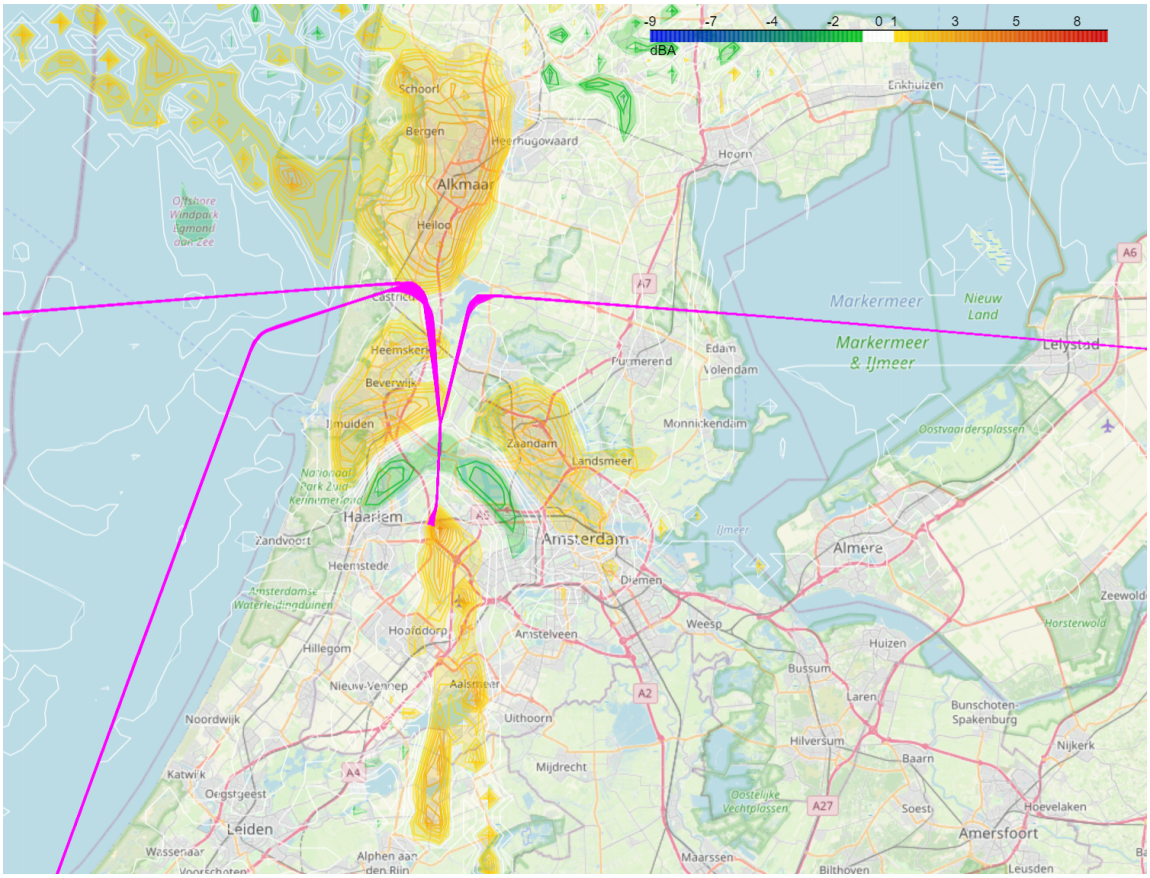

Figure 6.18: Difference between peak noise contours with EAT deviations of 0 and 240 seconds (1σ)

As Figure 6.18 shows, there are very few places where a noticeable change in peak noise level was calculated. For stepped approaches this difference is even smaller. As a result, the impact of EAT adherence on the peak noise level is assumed to be negligible. For this reason, all further comparisons will be done with the median EAT deviation of 60 seconds.

The peak noise contour for CDAs with 60 seconds of EAT deviation is shown in Figure 6.19, while the effect of implementing CDAs over stepped approaches can be seen in Figure 6.20.

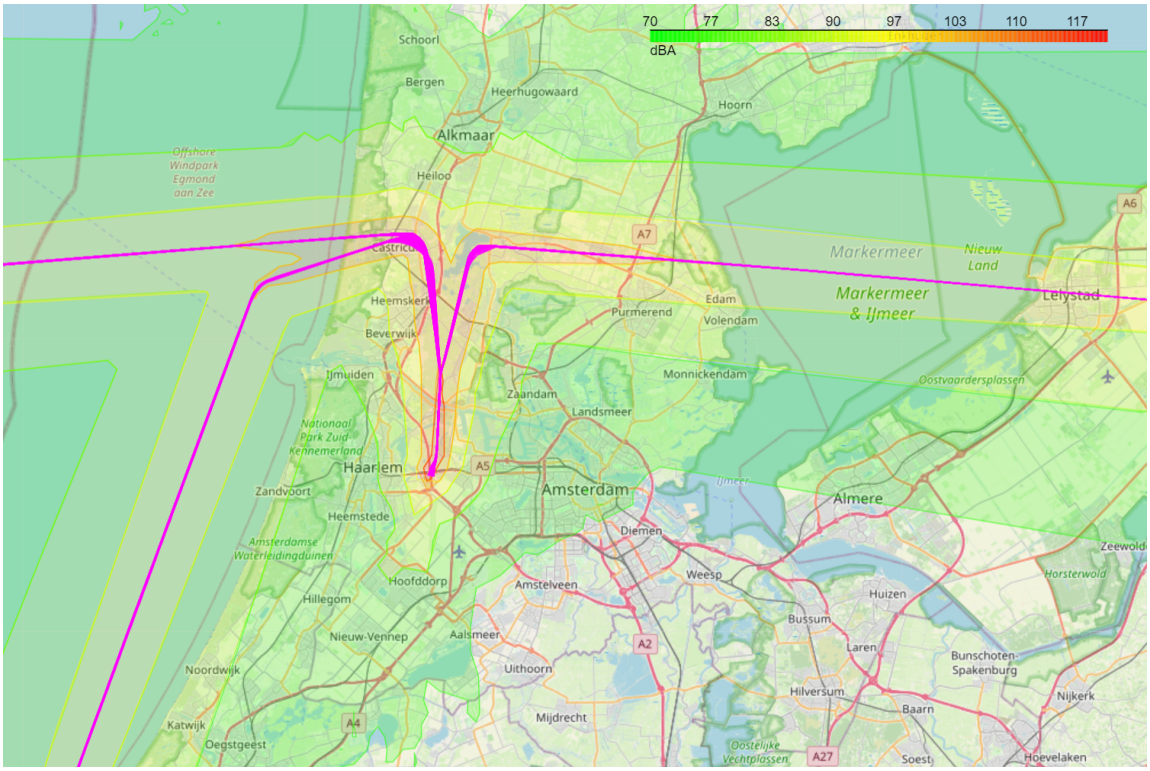

Figure 6.19: Peak Noise Contour for Continuous Descent Approaches with 60 seconds of Estimated Arrival Time Deviation (1σ)

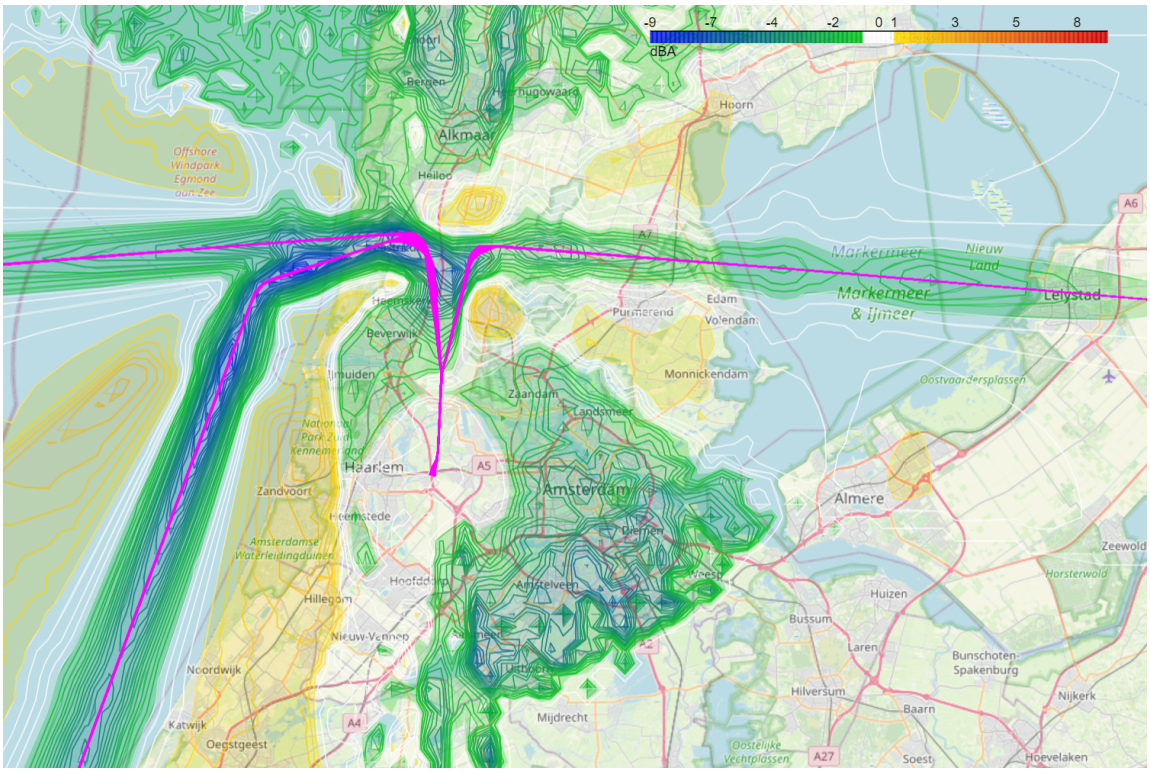

Figure 6.20: Difference between the Peak Noise Contours for Continuous Descent and Stepped Approaches with 60 seconds of Estimated Arrival Time Deviation (1σ)

Negative numbers in Figure 6.20 indicate a reduction in noise when switching from stepped to continuous descent approaches. This contour looks almost exactly the same as that for the L_{24h}. Again, due to the fact that aircraft performing a continuous descent approach fly significantly higher than those performing stepped approaches, noise

underneath the track is significantly lowered but further away from the track, the noise level actually increases slightly. The resulting peak noise areas are shown in Table 6.30.

Table 6.30: Peak Noise Area Comparison for Continuous Descent and Stepped Approaches with 60 seconds of Estimated Arrival Time Deviation (1σ)

	Peak Noise Area [km^2]	
Threshold	80 dB	100 dB
Stepped Approaches	3392	276
Continuous Descent Approaches	3509	156
Difference [-]	3.4%	-43.5%

NUMBER OF PEAKS CONTOUR

Finally, the effect of EAT adherence on the number of peaks contour for stepped approaches is shown in Figure 6.21.

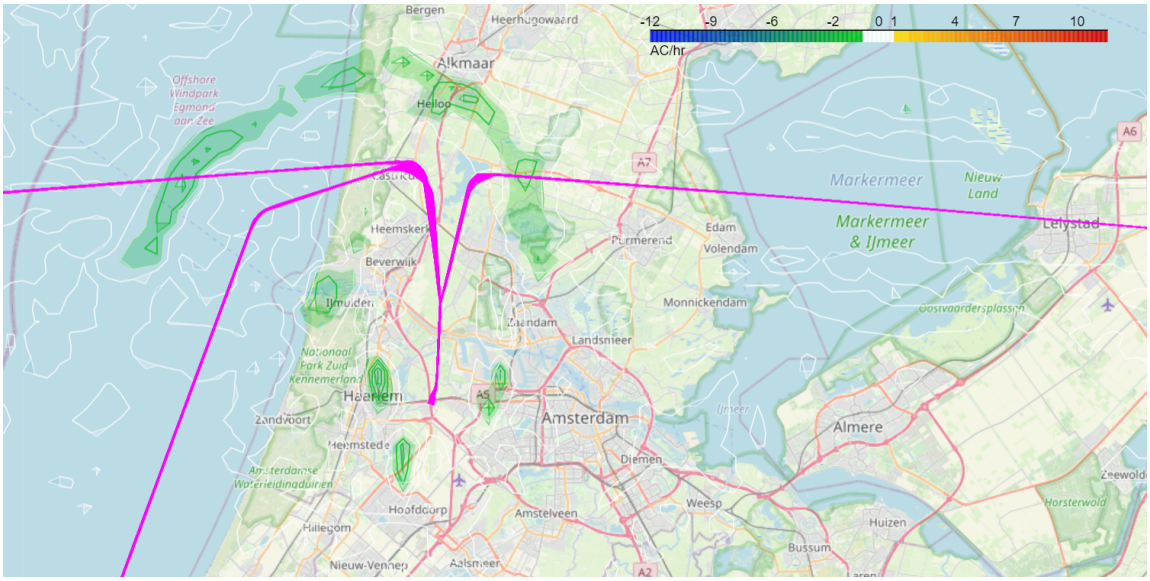

Figure 6.21: Difference between number of peaks contours with EAT deviations of 0 and 240 seconds (1σ)

As Figure 6.21 shows, there is only a very small difference between the two number of peaks maps. It should be noted that this is for stepped approaches, which have the largest difference. As a result, the impact of EAT adherence on the number of peaks over 60dB is assumed to be negligible. Therefore, all further comparisons will be done with the median EAT deviation of 60 seconds.

The number of peaks contour for continuous descent approaches can be seen in Figure 6.22, while the difference between stepped and continuous descent approaches is shown in Figure 6.23.

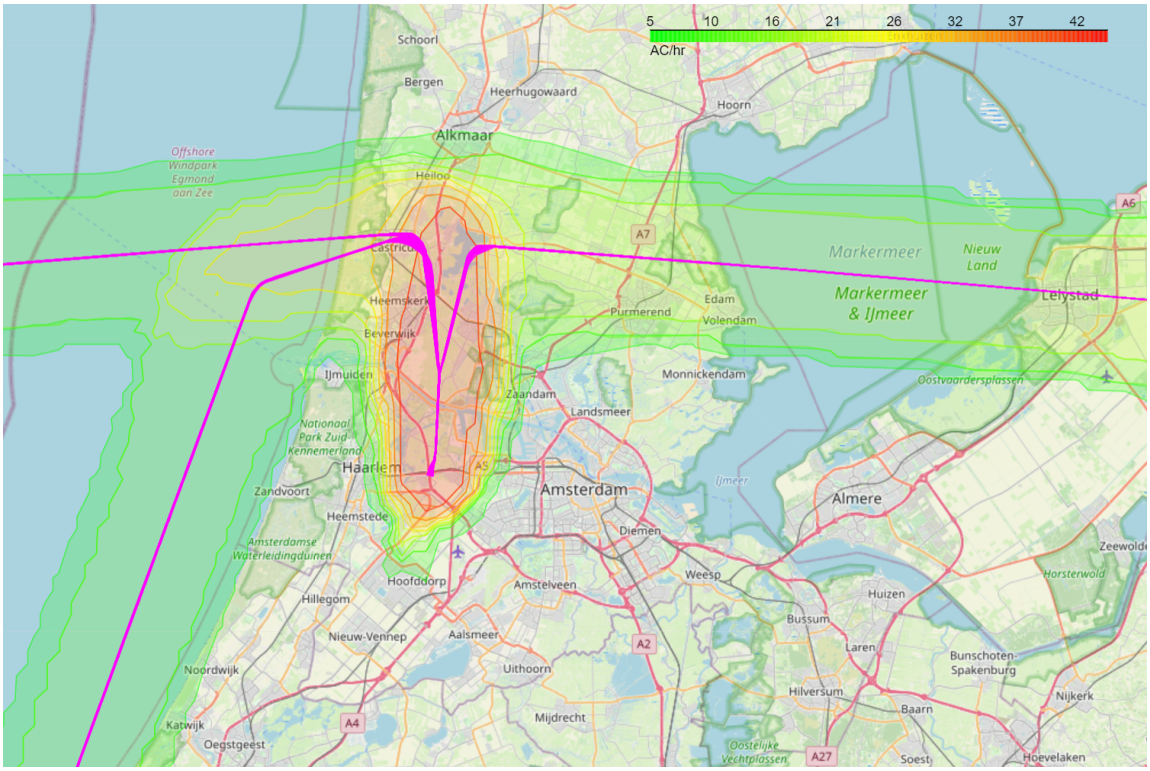

Figure 6.22: Number of Peaks Contour for Continuous Descent Approaches with 60 seconds of Estimated Arrival Time Deviation (1σ)

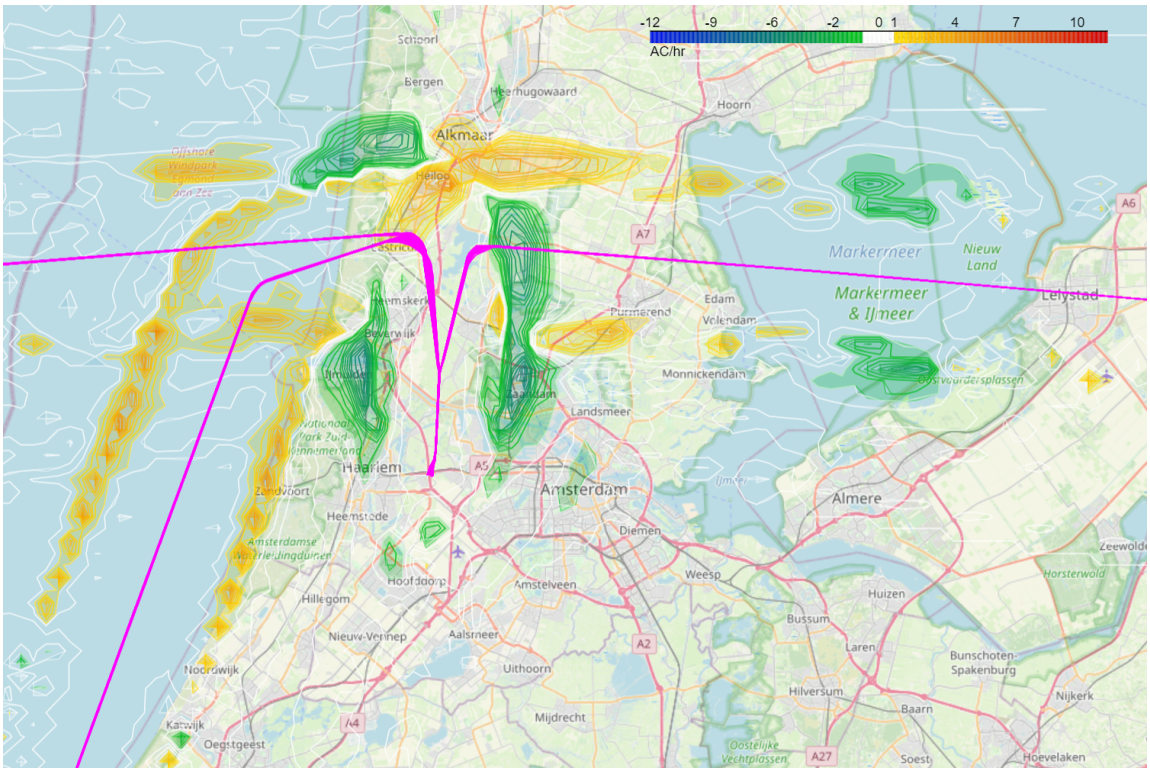

Figure 6.23: Difference between the Number of Peaks Contours for Continuous Descent and Stepped Approaches with 60 seconds of Estimated Arrival Time Deviation (1σ)

Again, a negative value in Figure 6.23 corresponds to a decrease in noise when switching from stepped to continuous descent approaches. The difference in number of peaks is rarely over about 3 peaks over $60dB$ per hour. The main differences can be found towards the edges of the tracks, where the noise level is close to $60dB$. Additionally, the

most significant differences are seen around the final approach, over Ijmuiden and Zaandam. This is caused by the fact that on final, the aircraft from all routes have merged, resulting in a larger number of total peaks per hour so if all noise is reduced by a certain amount, as can be seen in the L_{24h} contour, this is then also where the largest difference is made. The resulting noise areas can be seen in Table 6.31.

Table 6.31: Number of Peaks Area Comparison for Continuous Descent and Stepped Approaches with 60 seconds of Estimated Arrival Time Deviation (1σ)

	Number of Peaks Area $[km^2]$	
Threshold	10 AC/hr	30 AC/hr
Stepped Approaches	2381	222
Continuous Descent Approaches	2333	221
Difference [-]	-2.0%	-0.5%

6.2.4. Controller Taskload

A few measures for controller taskload will be discussed here. Together these give a more general indication of the implications of introducing continuous descent as opposed to stepped approach procedures. First, the number of conflicts will be discussed, this is followed by how often a loss of separation occurs. Finally, the distance at the Closest Point of Approach (CPA) between each pair of aircraft will be discussed. For the latter two results, the final merge and approach are filtered out of the results. This was done because the air traffic controller module regularly fails to ensure proper separation during the final merge. This makes it very difficult to distinguish between the effects of differing the approach procedures and the effects of this limitation. This issue will be discussed in more detail in Chapter 7.

NUMBER OF CONFLICTS

The number of conflicts that are detected give an indication of how often an air traffic controller has to issue a command. Whenever the air traffic controller module in the simulation detects a conflict, it also tries to resolve this by telling the trailing aircraft to slow down. So the number of detected conflicts directly translates to the number of commands issued. The results for the entire route can be seen in Figure 6.24, since there is no significant difference between the results on and off-final. The error bars at 0 and 240 seconds of EAT adherence signify the standard deviation calculated using 5 separate simulation runs.

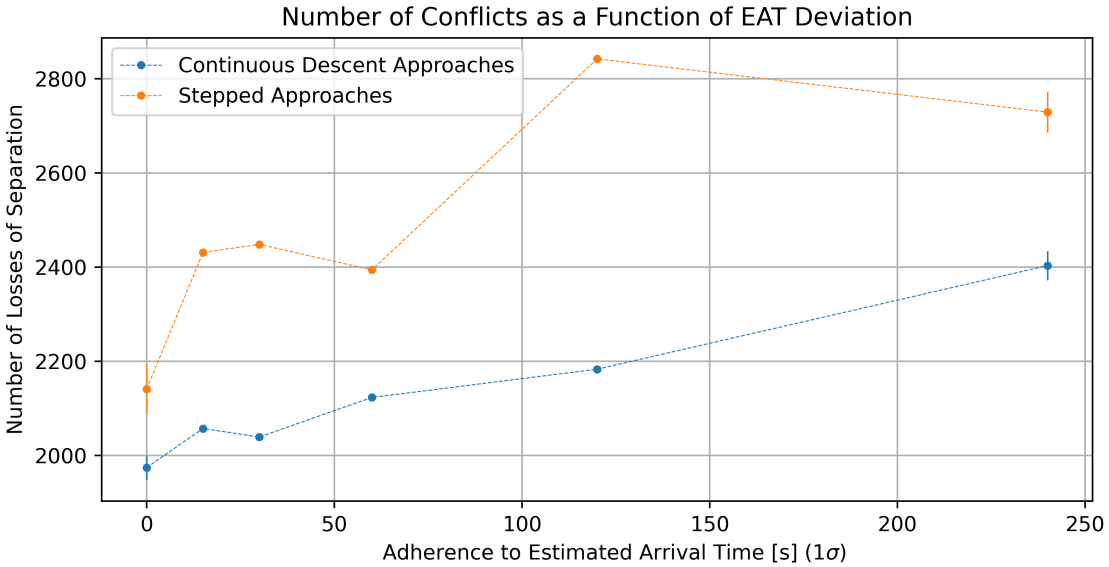

Figure 6.24: Number of Conflicts as a Function of Estimated Arrival Time Adherence

As Figure 6.24 shows, the number of conflicts is significantly lower for continuous descent approaches. The reason for this is that the segments where aircraft descend during stepped approach are relatively steep, when compared to CDAs. During these steep segments, some aircraft start to accelerate slightly. What this means is that if 2 aircraft are at target separation during a horizontal segment and the trailing aircraft starts to accelerate slightly during the next

descent, another conflict occurs. Because an actual inbound traffic sequence is used for this simulation, most aircraft arrive in groups from the same IAF. Due to this, such bouncing conflicts occur relatively often, which inflates the number of conflicts of stepped approaches with respect to that for CDAs. This does not occur to the same extent for CDAs because the maximal flight path angle is shallower here, meaning that fewer aircraft pairs show such behaviour. An real air traffic controller would foresee this and add a little extra separation between aircraft where they suspect such issues might occur or solve it entirely with one command at the end. As such, the difference between stepped and continuous descent approaches can be fully explained by the limits of the air traffic controller module.

NUMBER OF LOSSES OF SEPARATION

Whenever an actual loss of separation occurs in this simulation, that means that only using speed control on this aircraft combination was not enough. This gives an indication of how often path stretching is needed to ensure all aircraft were to land safely. Since this simulation is meant to be exploratory, a more complex air traffic controller module, which could actually decide when to use path stretching and when speed control was enough, was not implemented. It should be noted that a loss of separation is counted here whenever the closest point of approach for an aircraft pair is less than 3 nm, not when the simulation registers a loss of separation since the target separation in the simulation is increased as a function of aircraft speed. This target separation is explained in more detail in Section 5.1.2. The resulting data for the entire tracks without the final merge and approach can be seen in Figure 6.25. When EAT adherence is perfect (0 seconds), the number of losses of separation varies by up to 9 over 10 simulations for both continuous descent and stepped approaches.

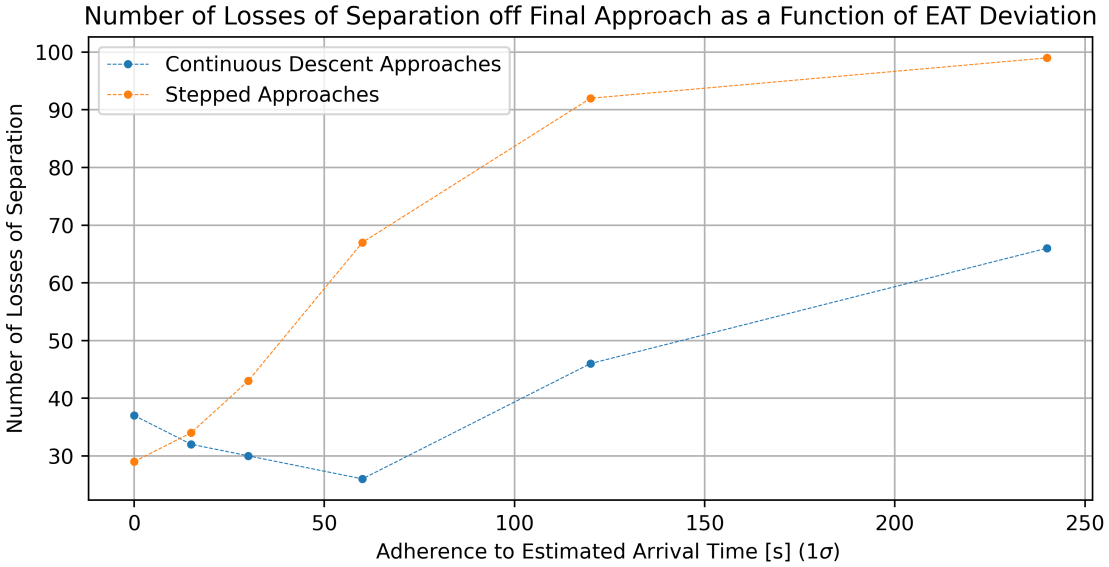

Figure 6.25: Number of Losses of Separation as a Function of Estimated Arrival Time Adherence

There are two ways in which a Loss of Separation (LoS) can occur in these simulations. First, there is an in-sequence LoS, where two aircraft are following the same route segment, but where the trailing aircraft flies faster than the leading aircraft, resulting in a LoS. This can most often be seen during continuous descent approaches since some aircraft, like those of the Airbus A330-series, cannot comply with all speed restrictions throughout the route and thus perform the approach too quickly. The second way in which an LoS can occur is through the merges that are necessary throughout the route. Since the final merge is not included in this simulation, the only point at which these conflicts can occur is when the aircraft arriving from RIVER and SUGOL are merged into one stream. When the EAT adherence is high (0 seconds deviation), this merging is relatively simple since the schedule already ensures separation throughout the approach, with the air traffic controller only needing to resolve small inaccuracies and deviations. As the EAT adherence drops (to 240 seconds of deviation) however, this merge becomes more and more difficult since aircraft might as well arrive at random, with no discernible prior planning. As such, the number of LoSs would be expected to increase as EAT adherence drops (from 0 to 240 seconds).

Both of these effects can also be seen in Figure 6.25. At perfect EAT adherence (0 seconds), the number of LoSs is higher for CDAs. This is caused by the in-sequence LoSs that mainly occur during CDAs. Merging LoSs are still somewhat rare and as such, stepped approaches have relatively few LoSs. As the EAT adherence drops to 60 seconds, two things can happen to the in-sequence loSs during continuous descent approaches. Either the aircraft are placed

closer together, and a loss of separation still occurs (but with reduced separation at the CPA), or the aircraft are placed further apart, in which case there is a chance that the separation at the CPA increases past the minimum separation, resulting in fewer LoSs. As the EAT adherence continuous to drop (to 240 seconds), the second source of LoSs takes over for CDAs, as has already been the case for stepped approaches. The increased merging difficulty starts to result in an increasing amount of losses of separation.

There is one more difference between the stepped and continuous descent profiles that can influence the results of both this and the distance at closest point of approach metrics. While aircraft performing continuous descent approaches are always descending, resulting in less speed control being available to controllers, those performing stepped approaches descend more steeply whenever they are descending. As such, while a stepped approach aircraft is descending, the ATCo has much less speed control over such an aircraft, even when compared to continuously descending aircraft. As it happens, such a descending segment is part of the merge for aircraft arriving from SUGOL. This can be seen in Figure 6.26, where the altitude is represented as the colour. As a result, the ATCo module can only properly control half of the aircraft, making it more difficult to perform the merge safely for stepped approaches. Such a descent segment could be moved away from the merges, but in that case the aircraft either have to descend very early, using more fuel, or very late, making it difficult to descend in time to intercept the ILS and slow down enough to safely land.

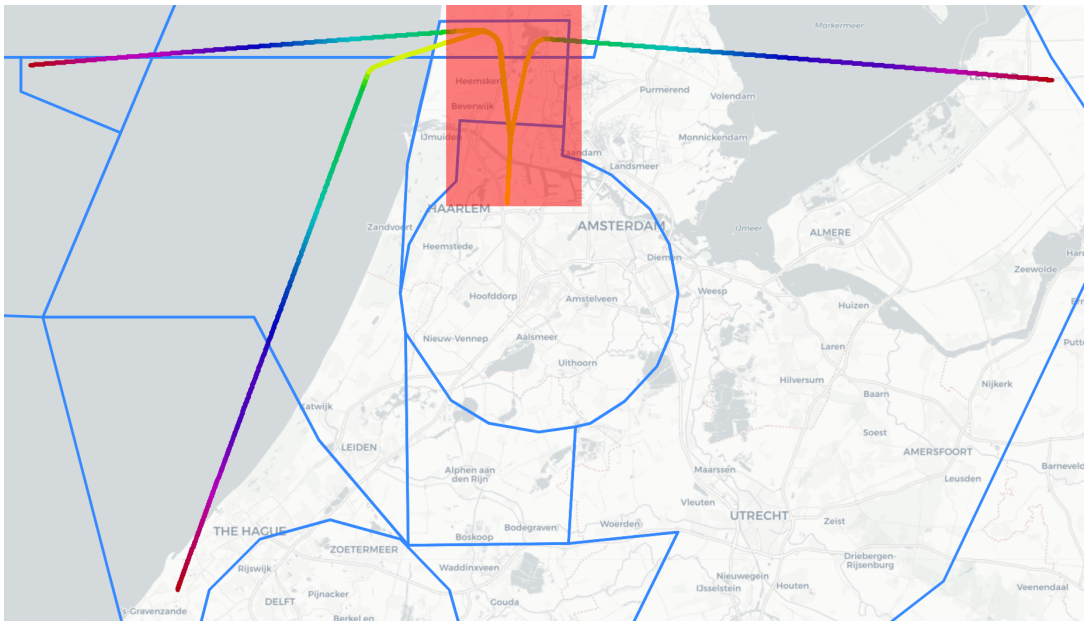

Figure 6.26: Routes to Runway 18R used for Simulation where the Colour represents the Altitude with the Final Merge and Approach Area is Marked in Red

Finally, since the air traffic controller module relies on state-based conflict detection, it does not know the intent of aircraft and as such can't account for it. This causes some difficulties performing the merge between the RIVER and SUGOL aircraft but mainly influences the final merge that is not included in Figure 6.25. While a certain aircraft arriving from RIVER might just go in front of an aircraft arriving from SUGOL if it did not perform the base turn, performing the base turn often causes the controller module to finally notice the impending LoS when it's too late to respond. A real controller would be able to foresee this and act appropriately under normal circumstances, but this could still cause problems during busy times or when unexpected events happen.
While there seems to be a difference in the number of LoSs which is to the advantage of continuous descent approaches, the size of this difference is determined by the limitations of the ATCo module, and the design of the stepped descent profile. While the former is mainly a result of this simulation and the effect of the latter could be reduced through fine-tuning of the profile, both are also inherent problems with stepped descent profiles in a fixed-route environment. Because aircraft cannot be significantly influenced while they are descending and these descend segments have to be placed somewhere, stepped approaches are by definition more complex than continuous descent approaches, where controllers have the same amount of control over their aircraft throughout the entire track.

DISTANCE AT CLOSEST POINT OF APPROACH

The distance the closest point of approach (CPA) gives an indication of why the losses of separation discussed above occur. Aircraft pairs with CPAs near minimum separation shows that the ATCo module tried to ensure separation but

just failed, indicating a slight lack of either foresight or authority. For combinations where the minimum separation is very close to 0, one aircraft overtook the other, essentially flying through it. This is partly caused by some of the aircraft in the sequence being unable to perform the continuous descent approaches within the speed limits, but others are cause by merging problems. Unless stated otherwise, the results shown in this section do not include the final approach. The distribution of the distances at CPA at 0 and 60 second EAT adherence are shown in Figures 6.27 and 6.28. Figures 6.27 and 6.29 include narrow error bars indicating the standard deviation found using 10 simulations of 500 aircraft.

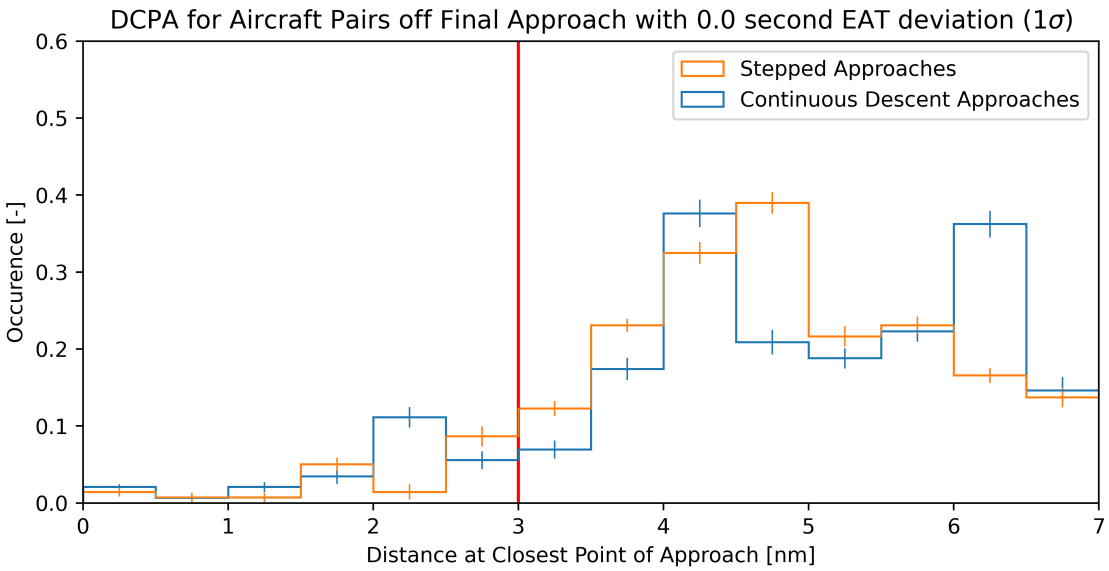

Figure 6.27: Distance at Closest Point of Approach for each Aircraft Pair off Final Approach with 0 second EAT deviation (1σ) with Error Bars

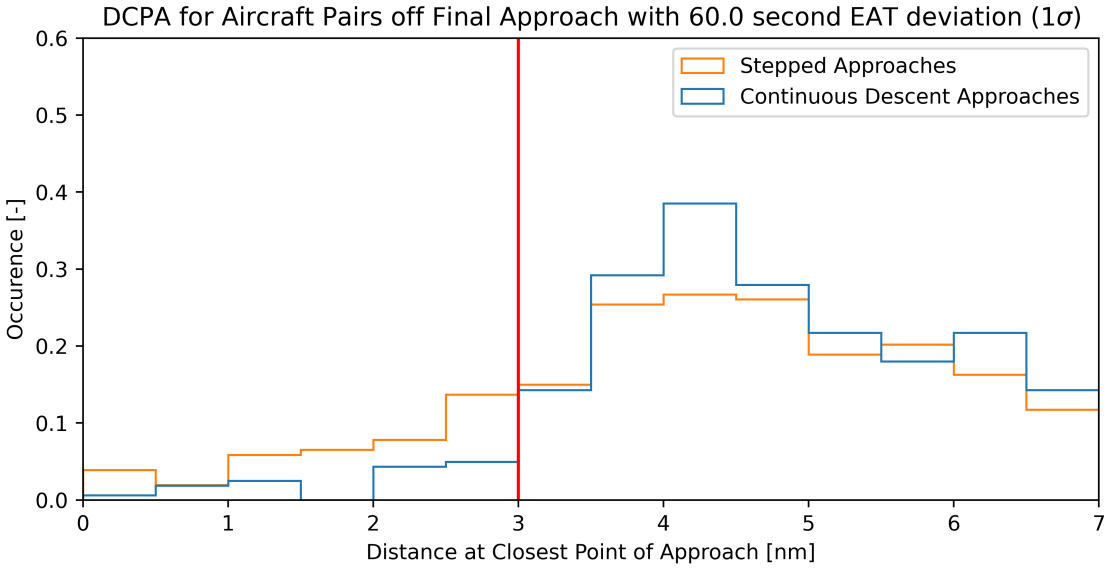

Figure 6.28: Distance at Closest Point of Approach for each Aircraft Pair off Final Approach with 60 second EAT deviation (1σ)

The main peak of minimum separations in figures 6.27 and 6.28 occurs at a little over 4 nm. This is caused by the fact that the target separation is dependent on the aircraft's speed. Since these figures don't include the final merge and approach, the minimum speed during the included segment is around 200 kts. Overall the shape is very similar, with only the second separation peak at around 6 nm for CDAs disappearing as EAT adherence drops. It is already evident that aircraft performing stepped approaches experience more LoSs. This trend continues as as the EAT adherence

drops to 240 seconds.

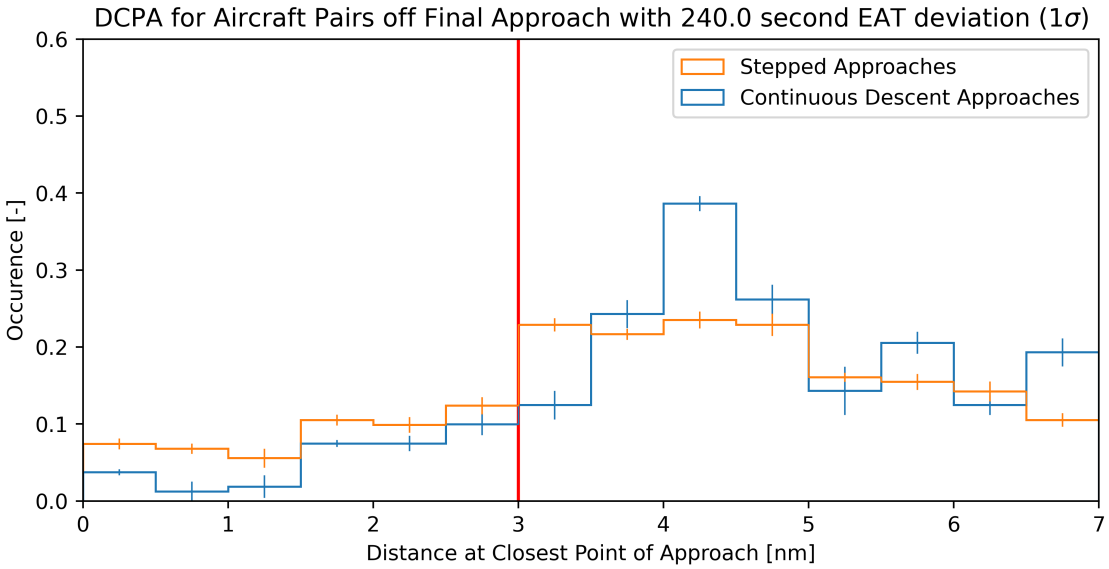

Figure 6.29: Distance at Closest Point of Approach for each Aircraft Pair Off Final Approach with 240 second EAT deviation (1σ) with Error Bars

When looking at the distance at CPA distribution for all aircraft during final, something interesting shows up. Figures 6.30 through 6.32 show the distance at closest point of approach distributions during the final approach segment with 60 and 120 seconds of EAT adherence. These figures show that when the EAT adherence is 60 seconds, the ATCo module already has a more difficult time safely separating aircraft when they're performing stepped approaches resulting in an increase in losses of separation. But when the EAT adherence drops further, the lowest bin starts to occur much more often. This means that during difficult merges, the controller module is completely unable to ensure separation, resulting in aircraft crossing paths at less than 0.5 nm from each other. While, a significant number of aircraft performing continuous descent approaches also have a LoS, the percentage is much lower and the distribution does not show the peak in the lowest bin that it does for stepped approaches, even when the EAT adherence drops further to 240 seconds. This further confirms that merging aircraft which are performing a stepped approach can be more difficult than those performing a continuous descent approach.

Finally, while a significant part of the aircraft pairs experience a loss of separation in this simulation, many also don't come close with a disproportionately large number of aircraft with minimum separations of over 5 nm. This means that there is still space in the final landing sequence to resolve the losses of separation without losing capacity.

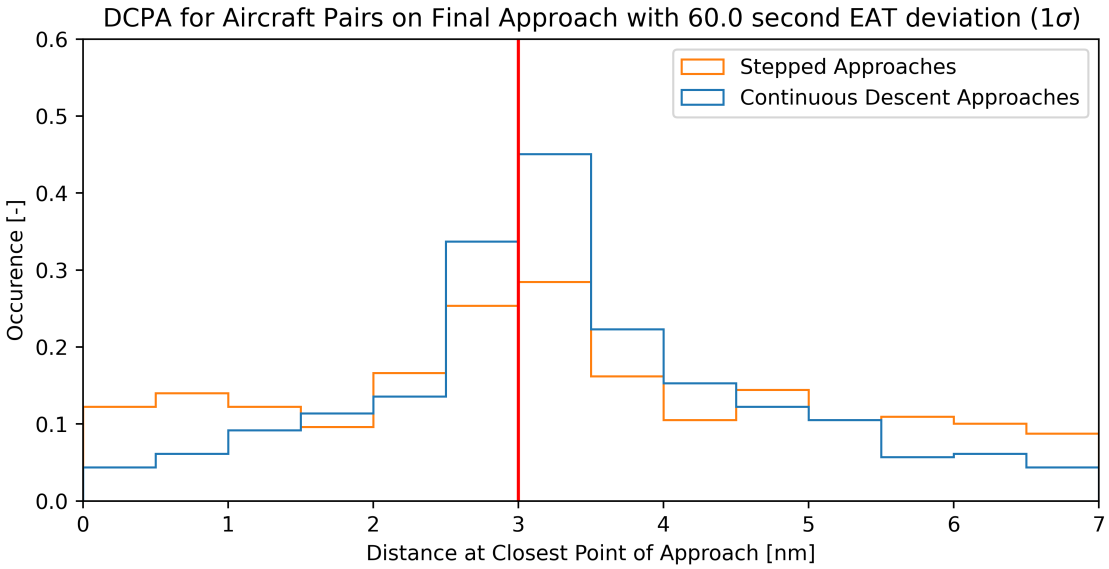

Figure 6.30: Distance at Closest Point of Approach for each Aircraft Pair on Final Approach with 60 second EAT deviation (1σ)

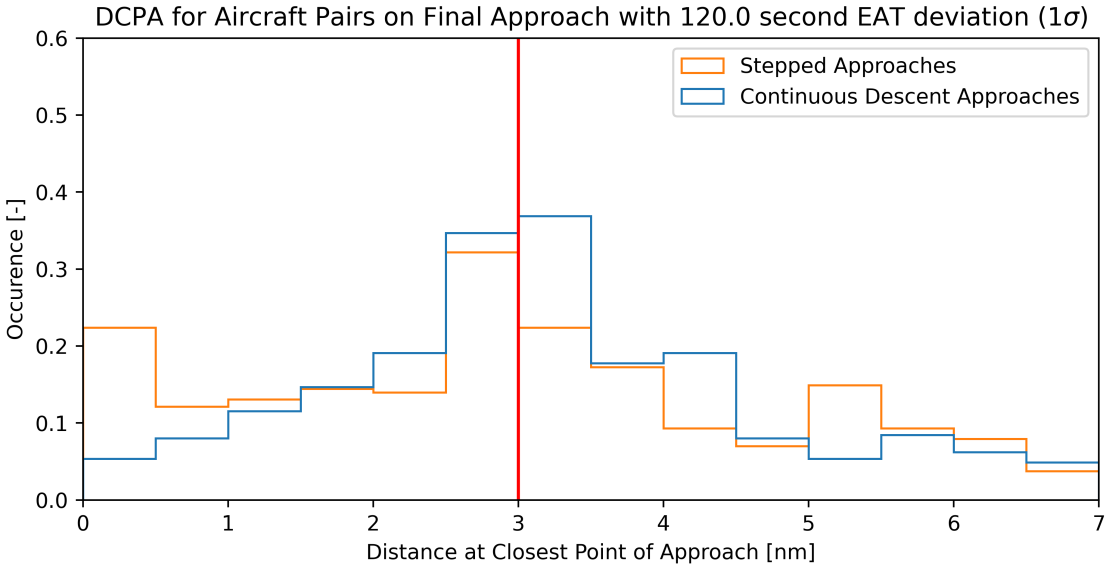

Figure 6.31: Distance at Closest Point of Approach for each Aircraft Pair on Final Approach with 120 second EAT deviation (1σ)

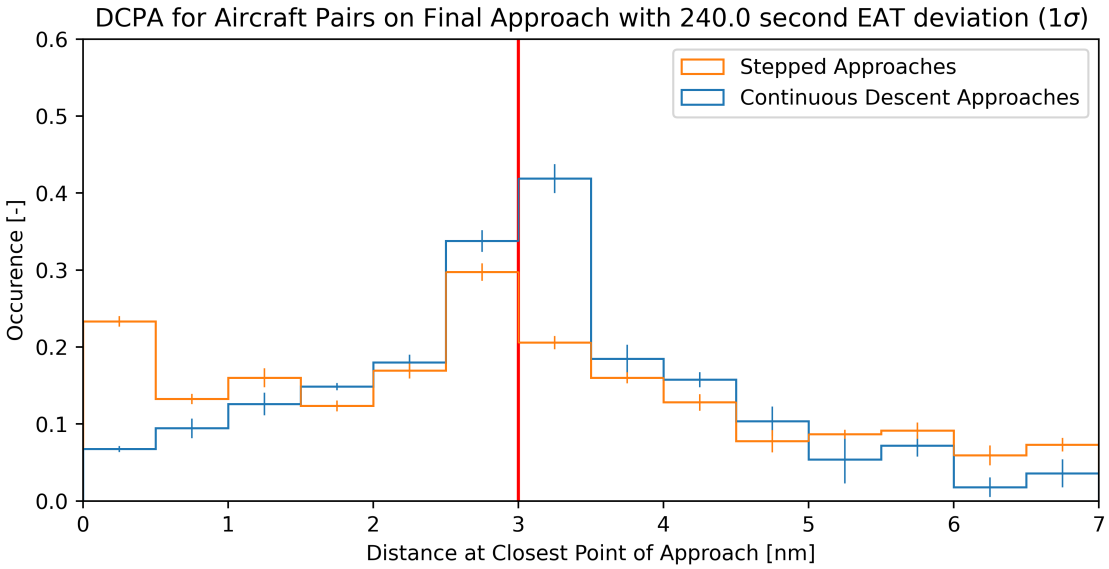

Figure 6.32: Distance at Closest Point of Approach for each Aircraft Pair on Final Approach with 240 second EAT deviation (1σ)

TASKLOAD CONCLUSION

On of the main inaccuracies in this simulation is caused by the air traffic controller module. Due to the fact that the conflict detection is only based on the current state of all aircraft, it does not take the intended path of all aircraft into account. This means that often, the conflict detection does not foresee impending conflicts because they are caused by an aircraft making a turn or an aircraft accelerating slightly due to a descent. An actual air traffic controller would take this into account so a more sophisticated controller module would greatly benefit the accuracy of this simulation. However, since this research is meant to be exploratory, this was considered outside of the scope.

Overall, all metrics show a reduction in taskload when switching from stepped to continuous descent approaches. How big this reduction is depends on a number of factors, not all of which are inherent properties of stepped or continuous descent approaches. For instance, the merging difficulty for stepped approaches could be reduced by ensuring all aircraft are flying horizontally during the merge. While this would likely decrease the taskload for the ATCo, it would also increase the fuel usage, showing a trade-off that will always be part of stepped approaches due to their nature. The inaccuracy in the ATCo module that was explained above, however, also impacts the taskload metrics. Since it's impossible to know which part of the difference shown in the taskload can be attributed to which cause without further research, the conclusion can only state that the data does suggest a reduction in taskload when switching from stepped to continuous descent approaches. In order to quantify the size of this difference, further research is needed.

Finally, Figure 6.31 shows that under the conditions simulated in this research, the needed metering accuracy for stepped approaches is 60 seconds, while continuous descent approaches can handle delivery accuracies of up to at least 240 seconds without showing major problems. What this means is that for stepped approaches, the arrival time distribution of incoming aircraft needs have a standard deviation of under 120 seconds, while a standard deviation of at least 240 seconds can still be dealt with when aircraft are performing continuous descent approaches.

7
Discussion

This document showed the most relevant data and literature with regards to this research on Off-Idle Continuous Descent Approaches (CDA), as well as research into the optimal descent angle during such approaches, and a comparison between fixed-route stepped and continuous descent approaches. In the background chapter the peculiarities of Amsterdam Airport Schiphol, its runway configuration and vectoring procedures, are discussed. In order to capture the impact of CDAs in such an environment, four runways will be used for this research which represent the different directions in which aircraft can land at Schiphol. Additionally, the conceptual difference between the current vectoring approach procedures at Schiphol and the CDA procedures at for instance London Heathrow (LHR) or Los Angeles International (LAX) are discussed.

In the motivation section, different types of constant FPA approaches are explained. While there are a number of relatively complex concepts, this thesis aims to explore a CDA concept that can be implemented quickly, without new airborne infrastructure. This is why the simplest approach type was chosen for this research, the constant geometric Flight Path Angle (FPA) approach. While the fact that this is an off-idle CDA means that it's suboptimal in terms of fuel economy, it can still result in almost 90% of the fuel savings that a fully idle CDA produces [32, 38]. Additionally, such an approach could reduce the flight time by up to 1 minute and the 50 dBA L_{DEN} by up to 28% [8].

While the carbon and noise emissions as well as the flight time have been well documented, the practical implications of implementing such a concept are not well known. For instance, some research states that the needed metering accuracy at the Initial Approach Fix (IAF) is ± 30 seconds while other research finds that ± 45 seconds is still results in feasible solutions [9, 10]. This difference can be explained by the fact that different support systems are available for different studies. On top of that, the needed metering accuracy has yet to be determined for an airspace without any new airborne systems. Additionally, the influence of the FPA on operational aspects that aren't the fuel usage and noise production have not yet been thoroughly investigated.

The main research question of this thesis is:

> "What is the impact of implementing constant FPA CDA routes without adding new airborne systems at Schiphol airport with regard to the capacity, operation robustness and flexibility, noise production, fuel consumption, and controller task load when compared to a conventional descent profile?"

This was done in two parts; first, the FPA that results in the best trade-off between capacity, operational robustness and flexibility, noise production, and fuel consumption needed to be determined. This was then followed by an in-depth comparison of fixed-route stepped and continuous descent approach procedures.

The main trade-off for finding the optimal flight path angle is between operational robustness and environmental impact. While capacity was also taken into account, the impact of flight path angle on the capacity was found to be relatively small with a maximal spread of less than 1 aircraft per hour for each runway. The robustness and flexibility was measured using two metrics; the time authority and the compliance. The time authority quantifies the effect that an air traffic controller can have on the arrival time of an aircraft. The compliance on the other hand quantifies how often a controller can no longer affect the arrival time of aircraft, it finds the percentage of aircraft that can no longer comply with all speed restrictions along the approach path. The emissions of aircraft can be divided into two parts: those resulting from fuel usage and noise emissions. As such the fuel usage is used as an indication of greenhouse gas emissions and air quality impact. The noise impact was split into three parts, but the one that gives the most objective indication of the overall impact of any change in approach procedure is the L_{24h} contour, which is the same as the L_{DEN} contour without applying any penalty for evening and night flights. This is used since the reduction in arriving aircraft that would occur during the evening and night in real life is not modelled. The main trade-off then happens between a 2.3 and a 2.4 degree approach angle. While before this, the minimal time authority and minimal compliance drop by around 5% and 4% per 0.1 degree with respect to the 2.0 degree value, respectively. Increasing the descent angle from 2.3 to 2.4 degrees drops the minimal compliance by 36%. In the meantime, both the fuel usage and the area of the $70dB$ L_{24h} contour continue to drop by around 4% per 0.1 degrees each. At 2.3

degrees the percentage of aircraft that cannot comply with all speed restrictions and as such requires either path stretching or speed brake usage is 17.6% at most. Increasing the FPA any further would result in a tripling of this value, while only decreasing the environmental impact by another 4%. This can also be seen in Table 7.1.

Table 7.1: Summary of the Impact of Changing the Flight Path Angle on Different Metrics

Metric	**Flight Path Angle**		
	2.2 [Deg]	**2.3** [Deg]	**2.4** [Deg]
Time Authority Difference w.r.t. 2.0 Deg	-12.1%	-16.3%	-21.2%
Minimal Compliance	86.3%	82.4%	46.4%
Fuel Usage Difference w.r.t. 2.0 Deg	-8.4%	-12.7%	-17.3%
70 dB L_{24h} Contour Area w.r.t. 2.0 Deg	-7.8%	-12.0%	-15.6%

Because of this 2.3 degrees was found to be the ideal flight path angle, where over 80% of aircraft can comply with all speed restrictions and air traffic controllers have only lost around 15% of their control when compared to that at 2.0 degrees. In the meantime, the fuel usage and noise impact have dropped by almost 13% and 12% with respect to the 2.0 degree values, respectively.

Finally, these 2.3 degree continuous descent approaches were compared to stepped approaches at different levels of schedule adherence to assess the feasibility and advantages of implementing constant flight path angle continuous descent approaches at Schiphol. In this simulation's planning no extra buffer was added between aircraft. This is normally done for fully idle continuous descent approaches because controllers don't have an easy way to ensure separation during such approaches. Here it is assumed that this is not necessary for off-idle CDAs and because of this, there is no significant difference in capacity, whether aircraft are performing stepped or continuous descent approaches. While the median values for the fuel usage of medium aircraft show very little difference between approach types, their mean values do vary significantly. This shows that the fuel usage of lighter medium aircraft doesn't change much between approach methods, while heavier medium aircraft do see a reduction, but still use more fuel than the lightest medium aircraft. This is not the case for heavy aircraft, where almost all aircraft see a significant reduction in fuel usage, resulting in a total average reduction of 14%, independent of EAT adherence when switching from stepped to continuous descent approaches. Noise production is more interesting, however. Due to the fact that aircraft performing CDAs are higher up, their noise can reach further. As a result, the size of the low-decibel contours, like the 60 dB L_{24h} contour, increases by around 1%, while underneath the tracks this extra distance results in a large reduction in noise, reducing the size of the high-decibel contours, like the 100 dB peak noise contour, by up to around 40%. Finally, one of the most important metrics is the controller taskload. This metric shows a decrease in taskload when switching from stepped to continuous descent approaches, which means that not only are additional buffers between aircraft not needed, CDAs seem to be simpler to control as well. The size of the difference cannot be accurately quantified by this simulation since a part of the difference is caused by the limitations of the air traffic controller module. Which part of the difference found is caused by the ATCo module and which is caused by differences in the approach types is not clear and would require further research.

An additional interesting find in the inbound peak simulation is that the controller taskload metrics show that increasing the planning uncertainty past 60 seconds (1σ) for stepped approaches results in a large number of aircraft effectively crashing into each other. This highlights the disadvantage of having a descending segment during a merge, and thus allowing the air traffic controller almost no control over half of the merging aircraft, since these are fixed-route stepped approaches where stopping a descent that is part of the route cannot be done. As a result, for stepped approaches the air traffic controller module completely fails after 60 seconds (1σ) of EAT adherence, while for continuous descent approaches, where such a difficulty was not added, no clear failure point was found. As such, this research found a required metering accuracy on the IAF of 60 seconds for stepped approaches, but no such limitation for continuous descent approaches. In order to assess when an air traffic controller can no longer ensure separation to a high enough degree in more detail, the effect of path stretching and speed brake usage needs to be taken into account, thus requiring further research.

In conclusion, currently at night at Schiphol, fully idle, fixed-route continuous descent approaches are already used. A 150 second buffer is added between arrivals to take profile variations between aircraft into account. This needs to be done because during fixed-route, fully idle CDAs, an air traffic controller has almost no control over aircraft without completely rerouting it. These buffers lower the applicability of fully idle CDAs to such an extent that they can only be used during night-time operations. During this simulation, such a buffer was not included because the continuous descent approaches in this research are off-idle CDAs, where controllers can use speed changes to more easily ensure separation between aircraft. Under these conditions, this simulation shows that the controller taskload

would be lower during CDAs than during stepped approaches. Additionally, as planning accuracy drops, stepped approaches show a significantly higher number of occasions where the air traffic controller module completely fails. As a result, such a buffer is not necessary when off-idle CDAs are used, showing that continuous descent approaches can be performed at busy airports without losing any capacity compared to fixed-route, stepped approaches. By implementing these continuous descent approaches, the areas with the most noise pollution could see average noise energy reductions of close to 9 dB and an average of over 40 kg of fuel per aircraft could be saved resulting in a total yearly fuel saving of around 10,000,000 kg when traffic numbers are back up to what they were in 2019.

8
Conclusion and Future Work

8.1. Conclusion

The main research question of this thesis is:

> "What is the impact of implementing constant flight path angle continuous descent approach routes without adding new airborne systems at Schiphol airport with regard to the capacity, operation robustness and flexibility, noise production, fuel consumption, and controller task load when compared to a conventional descent profile?"

In order to answer this, two simulation were done: The first determined the optimal Flight Path Angle (FPA) for performing the Continuous Descent Approaches (CDA), while the second allowed for the final part of the question to be answered by comparing the CDAs to fixed-route stepped approaches.

In the first simulation, the flight path simulation, showed that changing the FPA does not have a large impact on the capacity. It does have a large impact on the compliance rate, which is the percentage of aircraft that can abide by all speed restrictions, the fuel usage, and the noise performance however. At the optimal flight path angle of 2.3 degrees, the minimal compliance rate at the most challenging wind conditions is 82%, while the fuel usage and area of the high-threshold noise contours have on average reduced by 13% and 12% with respect to their values at 2.0 degrees. Increasing the angle any further would result in a compliance drop of over 40%, while only decreasing the fuel usage and noise production by another 5%, which was deemed not worth it.

The second simulation focused on comparing fixed-route stepped approach to fixed-route continuous descent approaches. Here controller taskload was also taken into account, on top of the previously used metrics of capacity, fuel usage, noise production. In order to take controller taskload into account, the interaction between different aircraft also has to be included in the simulation. In order to take operational robustness into account, this simulation was performed at 5 levels of estimated arrival time (EAT) adherence varying from perfect adherence ($\sigma = 0$ seconds) to terrible adherence ($\sigma = 240$ seconds). From this, it was found that the capacity does not change much between fixed-route stepped and continuous descent approaches. As the EAT adherence becomes worse and reaches a standard deviation of 240 seconds, the number of outliers greatly increases for both approach types indicating that the air traffic controller module has started to fail. While the capacity does not change between the approach types, the fuel usage does. Overall the average fuel consumption reduction when changing from stepped approaches to CDAs is around 13%. This value varies slightly with worsening EAT adherence, as the fuel usage for both approach types increases slightly but at nearly the same rate. The area of high-threshold noise contours do not change significantly with EAT adherence, but they do reduce when switching from fixed-route stepped to fixed-route continuous descent approaches. The $70dB$ L_{24h} contour reduces in size by close to 14% and shows noise reductions of up to 9 dB underneath the track. The 60 dB contour slightly increases in size, however. This is caused by the fact that the aircraft performing a continuous descent approach are at a higher altitude than those that aren't, which causes their noise to reach further and increases the noise slightly when further away from the track. Finally, the controller taskload seems to be significantly lower for continuous descent approaches than for stepped approaches. Part of this is caused by limitation of the air traffic controller module and part by inherent properties of stepped approaches. Determining which part of the difference is caused by which part of the explanation requires further research.

8.2. Future Work

The research presented in this report provides a thorough look at constant flight path angle continuous descent approaches. However, a number of assumptions had to be made in the process. In future research, a number of these could be omitted to ensure more accurate results.

As shown in Figure 5.38, there are some artifacts in the vertical profile that are caused by the Flight Management System (FMS) in BlueSky, which should not be there. Additionally, as stated in Section 5.3.2, the FMS in BlueSky only looks at its next waypoint to determine the vertical speed, even if there is no altitude constraint on it. Having the

FMS look at the entire track to determine its vertical speed would also have a large impact on the fidelity of further simulations.

Another interesting point has already been partly researched by Wu, Green and Jones [38]. While it isn't feasible for airports to quickly change the FPA based on immediate weather information without a significant investment in both research and infrastructure, it would be possible to change the FPA every Aeronautical Information Regulation And Control (AIRAC) cycle based on the expected weather during the upcoming season. According to Wu, Green and Jones, updating the FPA every season could save approximately 0.7 lb per flight, or 82 tonnes of fuel per year [38], although a smaller fuel saving would be expected if it was only updated every AIRAC cycle. They also calculate the amount of fuel that can be saved when calculating the FPA individually for each IAF, which, for a static FPA value all year round results in approximately 0.3 lb per flight [38]. Combining these two methods would result in a fuel saving of 0.9 lb per flight or 100 tonnes per year [38]. It would be very interesting to see the impact of implementing such measures at Schiphol, not just on the fuel usage, but also on the operational robustness and flexibility.

While some additional validation of the weight distribution will be done for this research, this will still be limited to only a few aircraft types from one operator. While the impact of weight estimation error is fairly small, as shown in Section 5.2.1, using more complete data for more aircraft types and from more operators would be a significant advantage. However the biggest improvement could be made by switching from a normal distribution to a more representative, asymmetric distribution.

Additionally, the simplistic approach to route generation could be greatly improved upon. Implementing more representative tracks that go around densely populated areas would result in much more representative thrust and vertical profiles, and noise contours. Additionally, the routes that are currently used for this research do not take departing aircraft or the use of multiple landing runways into account. As it may not always be possible for all arriving and departing aircraft to use their ideal paths and profiles, converting this idealised situation to 4D separated routes is still a challenge and the impact of locally changing the FPA would have to be investigated.

Finally, the main improvement that could be made to this research is to the air traffic controller module. To allow for more accurate calculation of the taskload, two paths can be taken. By either implementing a much more complex air traffic controller module or using a real-time simulation with human air traffic controllers, the intent of each aircraft as well as the performance limitations of aircraft should be taken into account, allowing for the usage of speed brakes and path stretching as needed.

Reference List

[1] Airbus. Aircraft characteristics, airport and maintenance planning. Online; accessed on April 30 2020.

[2] Amsterdam Airport Schiphol (AAS). Gebruiksprognose 2019, 2019. Online; accessed on February 18, 2021.

[3] ATM Airport Performance Meteorology Working Group. Algorithm to describe weather conditions at european airports. Technical report, Eurocontrol, 2011. Online; accessed on Febuary 21, 2020.

[4] M. Bakker. Method and System for Vertical Navigation using Time-of-Arrival Control, November 2012. U.S. Patent 8,311,687 B2.

[5] D.H.T. Bergmans and A.M. Kruger-Dokter. Een nieuwe berekeningsmethodiek voor vliegtuiggeluid in nederland. Technical Report NLR-TP-2010-208, Nederlands Lucht- en Ruimtevaartcentrum (NLR), 2010. Online; accessed on October 30, 2020.

[6] Boeing. Airplane characteristics for airport planning. Online; accessed on April 30 2020.

[7] Bombardier. Airport planning manual. Online; accessed on April 30 2020.

[8] J.P. Clarke, J. Brooks, G. Nagle, A. Scacchioli, W. White, and S. Liu. Optimized Profile Descent Arrivals at Los Angeles International Airport. *Journal of Aircraft*, 50(2):360–369, March 2013. doi: 10.2514/1.c031529.

[9] N. de Gelder, J.M. Rísquez Fernández, M. García Gutiérrez, and M. de las Mercedes Lopéz. Sesar solution pj.01-05 valr for v2. Technical Report D4.1.050, Nederlands Lucht- en Ruimtevaartcentrum (NLR), Oct 2019. Online; accessed on March 12 2020.

[10] R. de Muynck, L. Verhoeff, R. Verhoeven, and N. de Gelder. Enabling Technology Evaluation for Efficient Continuous Descent Approaches. Technical Report NLR-TP-2008-428, Nederlands Lucht- en Ruimtevaartcentrum (NLR), Sept 2008. Online; accessed on February 5 2020.

[11] ECAC.CEAC Doc 29. Report on standard method of computing noise contours around civil airports. Technical report, European Civil Aviation Conference, Dec 2016.

[12] Embraer. Airport planning manual. Online; accessed on April 30 2020.

[13] EUROCONTROL. User manual for the base of aircraft data (bada) revision 3.9. Technical Report EEC Technical/Scientific Report No. 11/03/08-08, EUROCONTROL, Apr 2011. Online; accessed on February 19 2020.

[14] European Civil Aviation Conference (ECAC). Report on standard method of computing noise contours around civil airports 1: Applications guide, 2016. Online; accessed on October 30 2020.

[15] European Civil Aviation Conference (ECAC). Report on standard method of computing noise contours around civil airports 2: Technical guide, 2016. Online; accessed on October 30 2020.

[16] European Civil Aviation Conference (ECAC). Report on standard method of computing noise contours around civil airports 3.1: Reverence cases and verification framework, 2016. Online; accessed on October 30 2020.

[17] Federal Aviation Administration (FAA). Arrival procedures - from standard to tailored arrivals, 2013. Online; accessed on November 25, 2020.

[18] Federal Aviation Administration (FAA). Los angeles international (lax) airport capacity profile, 2014.

[19] Fokker. Fokker 100, information booklet. Online; accessed on April 30 2020.

[20] Gerard Frawley. *The International Directory of Civil Aircraft*. Airlife Publishing Ltd, 2001.

[21] M. A. Heilig. Aircraft noise: Modelling measuring, using aircraft noise measurements for noise model prediction improvement. Master's thesis, Delft University of Technology, July 2020.

[22] G.J.T. Heppe. Appendices van de voorschriften voor de berekening van de geluidsbelasting in lden en lnight voor schiphol, 2012. Online; accessed on October 30, 2020.

[23] Interational Civil Aviation Organisation (ICAO). ICAO Long-Term Traffic Forecasts, 2018. Online; accessed on January 23 2020.

[24] International Civil Aviation Organisation (ICAO). Airport air quality manual, 2011. Online; accessed on September 1, 2020.

[25] K. Izumi. Sensitivity Studies of 4D Descent Strategies in an Advanced Metering Environment. In *1986 American Control Conference*. Institute of Electrical and Electronics Engineers (IEEE), June 1986. doi: 10.23919/acc.1986.4789026.

[26] R. Ledesma and F. Navarro. Continuous Descent Approaches for Maximum Predictability. In *2007 IEEE/AIAA 26th Digital Avionics Systems Conference*. Institute of Electrical and Electronics Engineers (IEEE), October 2007. doi: 10.1109/dasc.2007.4391871.

[27] Luchtverkeersleiding Nederland (LVNL). Aerodrome chart, 2020.

[28] A. Nuic, D. Poles, and V. Mouillet. BADA: An advanced Aircraft Performance Model for Present and Future ATM Systems. *INTERNATIONAL JOURNAL OF ADAPTIVE CONTROL AND SIGNAL PROCESSING*, March 2010. doi: 10.1002/acs.1176.

[29] L. Ren. *Modeling and Managing Separation for Noise Abatement Arrival Procedures*. Phd dissertation, Massachusetts Institute of Technology, Febuary 2007.

[30] L. Ren and J.P. Clarke. Separation Analysis Methodology for Designing Area Navigation Arrival Procedures. *Journal of Guidance, Control, and Dynamics*, 30(5):1319–1330, September 2007. doi: 10.2514/1.27067.

[31] W. Roberson and J.A. Johns. Fuel conservation strategies: Descent and approach, 2010. Online; accessed on September 1, 2020.

[32] J. Robinson III and M. Kamgarpour. benefits of continuous descent operations in high-density terminal airspace considering scheduling constraints. American Institute of Aeronautics and Astronautics (AIAA), September 2010. doi: 10.2514/6.2010-9115.

[33] Amsterdam Airport Schiphol. Nomos online, 2020.

[34] D. Tipps, D. Skinn, J. Rustenburg, T. Jones, and D. Harris. Statistical loads data for the boeing 777-200er aircraft in commercial operations. Technical Report DOT/FAA/AR-06/11, Department of Transportation (DoT), Federal Aviation Administration (FAA), Nov 2006. Online; accessed on January 25 2021.

[35] K. Tong, E. Schoemig, D. Boyle, J. Scharl, and A. Haraldsdottir. Descent Profile Options for Continuous Descent Arrival Procedures within 3D Path Concept. In *2007 IEEE/AIAA 26th Digital Avionics Systems Conference*. Institute of Electrical and Electronics Engineers (IEEE), October 2007. doi: 10.1109/dasc.2007.4391872.

[36] E. Turgut, O. Usanmaz, M. Cavcar, T. Dogeroglu, and K. Armutlu. Effects of Descent Flight-Path Angle on Fuel Consumption of Commercial Aircraft. *Journal of Aircraft*, 56(1):313–323, January 2019. doi: 10.2514/1.c033911.

[37] M. Wu and S. Green. Analysis of Fixed Flight Path Angle Descents for the Efficient Descent Advisor. Technical Report NASA/TM–2011–215992, National Aeronautics and Space Administration (NASA), nov 2011. Online; accessed on January 29 2020.

[38] M. Wu, S. Green, and J. Jones. Strategies for Choosing Descent Flight-Path Angles for Small Jets. *Journal of Aircraft*, 52(3):847–866, May 2015. doi: 10.2514/1.c032835.